

Deliverable D7 :

Modelling Sequential
Biosphere Systems
under Climate Change
for Radioactive
Waste Disposal

EC-CONTRACT : FIKW-CT-2000-00024

Continuous climate evolution scenarios over western Europe (1000km scale)



Work package 2: **Simulation of the future evolution of the biosphere system using the hierarchical strategy**

RESTRICTED

'All property rights and copyrights are reserved. Any communication or reproduction of this document, and any communication or use of its content without explicit authorization is prohibited. Any infringement to this rule is illegal and entitles to claim damages from the infringer, without prejudice to any other right in case of granting a patent or registration in the field or intellectual property.'



Foreword

The BIOCLIM project on modelling sequential BIOSphere systems under CLIMATE change for radioactive waste disposal is part of the EURATOM fifth European framework programme. The project was launched in October 2000 for a three-year period. The project aims at providing a scientific basis and practical methodology for assessing the possible long term impacts on the safety of radioactive waste repositories in deep formations due to climate and environmental change. Five work packages have been identified to fulfil the project objectives:

Work package 1 will consolidate the needs of the European agencies of the consortium and summarise how environmental change has been treated to date in performance assessments.

Work packages 2 and 3 will develop two innovative and complementary strategies for representing time series of long term climate change using different methods to analyse extreme climate conditions (the hierarchical strategy) and a continuous climate simulation over more than the next glacial-interglacial cycle (the integrated strategy).

Work package 4 will explore and evaluate the potential effects of climate change on the nature of the biosphere systems.

Work package 5 will disseminate information on the results obtained from the three year project among the international community for further use.

The project brings together a number of representatives from both European radioactive waste management organisations which have national responsibilities for the safe disposal of radioactive waste, either as disposers or regulators, and several highly experienced climate research teams, which are listed below.

- Agence Nationale pour la Gestion des Déchets Radioactifs (Andra), France – **J. Brulhet, D. Texier**
- Commissariat à l’Energie Atomique/ Laboratoire des Sciences du Climat et de l’Environnement (CEA/LSCE) France – **N. de Noblet, D. Paillard, D. Lunt, P. Marbaix, M. Kageyama**
- United Kingdom Nirex Limited (NIREX), UK – **P. Degnan**
- Gesellschaft für Anlagen und Reaktorsicherheit mbH (GRS), Germany – **A. Becker**
- Empresa Nacional de Residuos Radioactivos S.A. (ENRESA), Spain – **A. Cortés**
- Centro de Investigaciones Energeticas, Medioambientales y Tecnológicas (CIEMAT), Spain – **A. Aguero, L. Lomba, P. Pinedo, F. Recreo, C. Ruiz**
- Universidad Politecnica de Madrid Escuela Tecnica Superior de Ingenieros de Minas (UPM-ETSIMM), Spain – **M. Lucini, J.E. Ortiz, T. Torres**
- Nuclear Research Institute Rez, plc - Ustav jaderného výzkumu Rez a.s. (NRI), Czech Republic – **Czech Republic – A. Laciok**
- Université catholique de Louvain/ Institut d’Astronomie et de Géophysique Georges Lemaître (UCL/ASTR), Belgium – **A. Berger, M.F. Loutre**
- The Environment Agency of England and Wales (EA), UK – **R. Yearsley, N. Reynard**
- University of East Anglia (UEA), UK – **C. Goodess, J. Palutikof**

BIOCLIM is supported by a Technical Secretariat provided by Enviros Consulting Ltd, with other technical support provided by Quintessa Ltd and Mike Thorne and Associates Ltd.

For this report, deliverable 7 (D7) of the BIOCLIM project, the main contributors are the climate modelling groups (CEA/LSCE, UCL/ASTR) (contact persons: M. Kageyama (masa@lsce.saclay.cea.fr) and M.F. Loutre (loutre@astr.ucl.ac.be)).

Amongst all the results presented in this report, only the simulations of future climates were obtained within the BIOCLIM project (Section 4.). Results described in section 3. are given to describe and identify the strengths and weaknesses of the models. Please quote the BIOCLIM project when using results from section 4. and directly quote the papers referenced in section 3. for that section. Public should be aware that BIOCLIM material is working material.



Content List

1 - Introduction and objectives	6
2 - Model description	7
2.1. - Climate models	7
2.1.1 - MoBidiC	7
2.1.2 - CLIMBER	11
2.2. - Ice sheet models	12
2.2.1 - Gallée et al model	12
2.2.2 - GREMLINS	13
2.3. - Coupling	13
2.3.1 - MoBidiC + ice sheet model	13
2.3.2 - CLIMBER + GREMLINS	14
3 - Evaluation	16
3.1. - Equilibrium experiments	18
3.1.1 - Control experiment : present climate	18
3.1.2 - 6 kyr BP	23
3.1.3 - Last glacial Maximum	25
3.1.4 - 126 kyr BP	30
3.2. - Transient experiments	33
3.2.1 - Last Interglacial (126-115 kyr BP)	33
3.2.2 - Deglaciation with MoBidiC	36
3.2.3 - Last glacial-interglacial cycle with MoBidiC	37
4 - Bioclim experiments for the next 200 kyr	43
4.1. - Brief description	43
4.2. - The natural scenario – A4a	44
4.2.1 - Ice sheets	45
4.2.2 - Surface temperature	46
4.2.3 - Vegetation	50
4.2.4 - Precipitation, evaporation and snow cover	51
4.3. - Simulation "B3"	53
4.3.1 - Ice sheets	54
4.3.2 - Surface temperature	55
4.3.3 - Vegetation	58
4.3.4 - Precipitation, evaporation and snow cover	59
4.4. - Simulation "B4"	62
4.4.1 - Ice sheets	63
4.4.2 - Surface temperature	63
4.4.3 - Vegetation	66
4.4.4 - Precipitation, evaporation and snow cover	67
5 - Uncertainties and limitations	70
5.1. - Uncertainties on the CO ₂ scenarios	70
5.2. - Model and experimental setup limitations	74
6 - Summary	75
7 - References	78
8 - APPENDIX 1	85



1. Introduction and objectives

The overall aim of BIOCLIM is to assess the possible long term impacts due to climate change on the safety of radioactive waste repositories in deep formations. This aim is addressed through the following specific objectives:

- Development of practical and innovative strategies for representing sequential climatic changes to the geosphere-biosphere system for existing sites over central Europe, addressing the timescale of one million years, which is relevant to the geological disposal of radioactive waste.
- Exploration and evaluation of the potential effects of climate change on the nature of the biosphere systems used to assess the environmental impact.
- Dissemination of information on the new methodologies and the results obtained from the project among the international waste management community for use in performance assessments of potential or planned radioactive waste repositories.

A key point of the project is therefore to develop strategies for representing sequential long-term climatic changes by addressing time scales of relevance to geological disposal of solid radioactive wastes. The integrated strategy, which first step is described in this deliverable (D7), consists of building an integrated, dynamic climate model, to represent all the known important mechanisms for long term climatic variations. The time-dependent results will then be interpreted in terms of regional climate using rule-based and statistical downscaling approaches. Therefore, the continuous simulation of the climate evolution of the next 200 000 years selected for study is a major objective of the BIOCLIM project. This requires models that account for the simultaneous evolution of the atmosphere, biosphere, land-ice and

the ocean. To be able to perform several 200 000-year-long transient climate simulations, the models have to include all these components, but also need to be simple enough to run fast. Therefore, climate models of intermediate complexity have been chosen to complete this part of the BIOCLIM project.

In the present deliverable, we report on the results of two such models, MoBidiC (Louvain-la-Neuve) and CLIMBER-GREMLINS (LSCE). The overall objective of the work presented here is the simulation of the climate of the next 200 000 years for three different CO₂ scenarios [Ref.1]. However, both models used for this work have been either modified for the project (MoBidiC) or developed within the project (CLIMBER-GREMLINS). Therefore their performance, and the modifications and developments needed to be documented, especially as far as their ability to reproduce past and different climates is concerned. Therefore, a large section of the present deliverable is devoted to the evaluation of the models through past climate simulations.

The deliverable is structured as follows: first, a brief description of the models is given. In the second section, results from the models for past climate situations are presented. The third section deals with the future climate simulations devised for the BIOCLIM project: for each CO₂ scenario, the results of the two models are compared.

It is emphasized that the model results, especially those for CLIMBER-GREMLINS, should be regarded as illustrations of possibilities rather than absolute predictions of climate evolution. The novel approach to long-term climate change adopted in BIOCLIM is based on research tools under continuing development, notably, the CLIMBER-GREMLINS model.



2. Model description

2.1. - Climate models

Two climate-ice sheets models, MoBidiC and CLIMBER-GREMLINS, have been used for the present work. Both climate models are Earth system models of intermediate complexity (EMIC), thus allowing multi-millennial simulations. The ice sheet model is rather simple in MoBidiC, while it is quite

complete in CLIMBER-GREMLINS. Both models account for atmosphere-ocean-vegetation-ice-sheet interactions. The vegetation model is the same in both models, its output can therefore be useful to compare the effects of climate changes in both models.

2.1.1 - MoBidiC

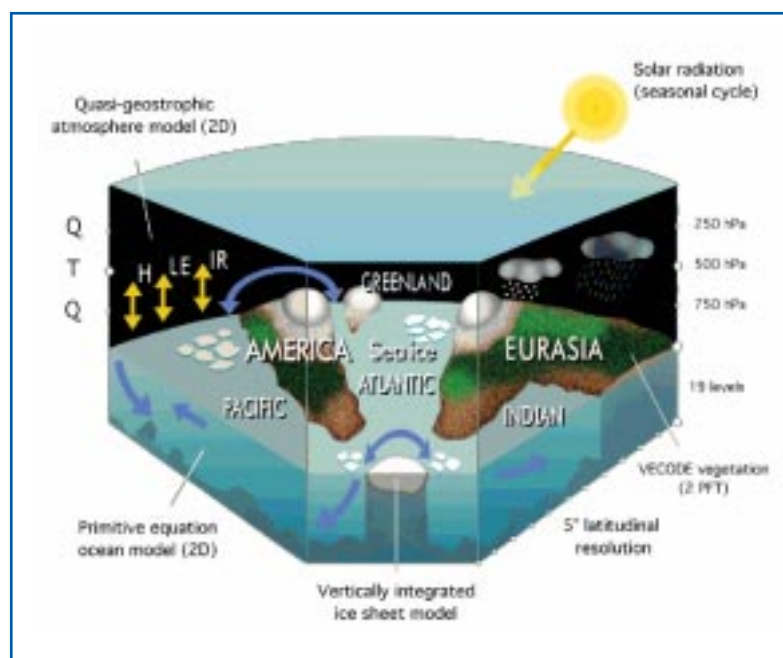


Figure 1: Schematics of the MoBidiC model

General description

MoBidiC (Figure 1) comprises most of the components of the climatic system (atmosphere dynamics, the deep ocean, the continental biosphere, the ice sheets and their underlying bedrock and finally the ocean carbon cycle). However each of these components is represented in a simplified way when compared with more detailed state-of-the art models. The advantage of this approach

is to reduce the computing time required for long simulations while explicitly taking into account the transient interactions between the different components governing climatic change. In this way, climatic mechanisms, such as feedbacks, can be identified and their relative importance in the long-term evolution of climate can be quantified through sensitivity studies.

MoBidiC is made of :

A zonally averaged atmosphere. It is based on the quasi-geostrophic formalism¹ with two layers on the vertical. The model predicts the time evolution of the quasi-geostrophic potential vorticity at 250 and 750 hPa, which in turn allows prediction of the temperature at 500 hPa as well as the zonally averaged zonal wind at 250 hPa and 750 hPa. The surface wind is estimated assuming a linear extrapolation of the zonally averaged vorticity to the surface. In the intertropical areas, the model is improved by an explicit representation of the advection of heat, momentum and moisture by the mean meridional circulation. The meridional resolution is 5 degrees.

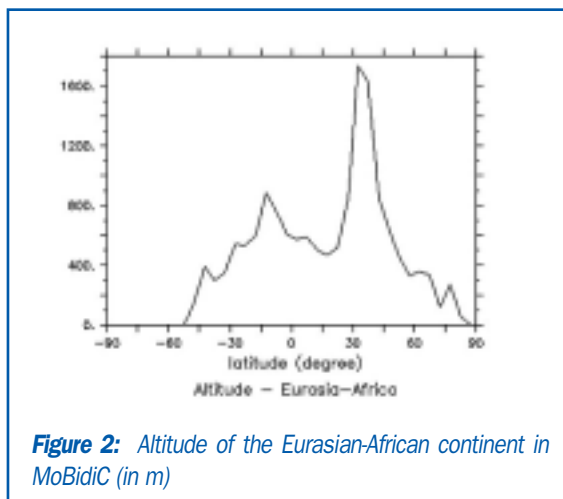


Figure 2: Altitude of the Eurasian-African continent in MoBidiC (in m)

An energy balance of the surface based on a sectorial approach. The energy balance of the surface is computed for each latitudinal band, and up to 13 sectors representing the different continents and oceans, with a distinction between snow-free, snow-covered, ice-covered surfaces over the continent, and ice-free and ice-covered surfaces over the ocean. The altitude of the Eurasian sector is given on Figure 2. This scheme allows prediction of the time evolution of the surface temperature as well as the area and thickness of snow. For each sector, the surface radiative balance is achieved by resorting to an explicit radiative transfer scheme for shortwave and longwave radiation over the entire vertical column divided in 15 levels. Clouds are represented by a single effective layer. The seasonal and meridional cloudiness distribution is prescribed.

The zonally averaged precipitation is derived from the zonally averaged evaporation and the vertically integrated water-vapour meridional transport assuming a steady state approximation for the global water-vapour content. It is computed in this way for each time step and each zonal band and then distributed over the continents and oceans with ratios derived from the statistics by Jaeger [Ref.3]. An additional correction is applied over the ice sheets to take into account the desert-altitude effect [Ref.4]. Runoff is implicitly represented by multiplying the precipitation over the oceans such that the freshwater budget over the oceans is zero.

A dynamic ocean model. In each oceanic sector (the Atlantic, the Pacific and the Indian Oceans), the zonally averaged, primitive equations of fluid motion are solved with a resolution of 5 degrees in latitude and 19 unevenly spaced levels in depth. The formalism is the rigid-surface layer approach as developed by Bryan [Ref.5] with improved numerical treatment (i.e., implicit resolution along the vertical). This numerical treatment allows the use of more efficient recently developed computational techniques such as an implicit convection scheme and parameterisation of the downsloping current along the Antarctic shelf.

A sea-ice model. The sea-ice model is basically the O-layer model of Semtner [Ref.6] that allows prediction of the evolution of ice thickness as a function of the local thermodynamic balance of the sea-ice. This model includes a parameterisation of the fractional area of leads and of meridional advection with a prescribed ice velocity.

A dynamical model of the continental biosphere. This model predicts, over each continent and for each latitude band, the time evolution of the sub-grid scale fraction of forest, grass and desert as a function of annual mean precipitation and the local growing-degree-days (GDD) index (cumulated sum of the local surface air temperature expressed in Celsius degrees, for days when this temperature is positive). This model includes an explicit calculation of the carbon balance, such that it could be included in the framework of a climate model predicting the time evolution of CO₂.

1) Geostrophism formalism assumes that velocity is parallel to contours of geopotential of an isobaric surface. This is a good first approximation for the atmosphere dynamics in case of large horizontal scale, slowly evolving flow and away from the equator (see textbook for more details, e.g. Ref.2)

A dynamical biogeochemical model in the ocean. A series of tracers, such as dissolved organic carbon, dissolved inorganic carbon, alkalinity and phosphorous are included in the ocean. The source-sink functions for these tracers take into account the net primary production of dissolved and particulate organic matter (assuming phosphorous as a biolimiting nutrient), recycling of organic matter in the deep ocean, and the cycling of biogenic carbonates in the ocean. This model can be used to predict the time evolution of the CO₂ partial pressure at the ocean surface and hence subsequently to compute the CO₂ exchanges between the ocean and the atmosphere.

The time step of the model is two days, except for the

ice sheet model for which it is one year. The model is externally forced by astronomical variations of insolation. Although CO₂ is part of the climate system, its atmospheric concentration is prescribed and thus considered as an external forcing. The seasonal and meridional cloudiness distribution is prescribed from present-day observations. The longitudinal profile of the different ice sheets is prescribed. The longitudinal extent of the continents and oceans, and the altitude of the continents in the model are taken from the ETOPO5 [Ref.7] dataset. The distribution over the oceans and the continents of the zonally averaged precipitation is based on statistics from Jaeger [Ref.3].

variable	unit
Surface temperature	°C
Sector area	m ²
Vegetation (tree, grass desert fraction)	
Reflected solar radiation (top of atm.)	W.m ²
Upward infrared radiation (top of atm.)	W.m ²
Net solar radiation at the surface	W.m ²
Downward solar radiation at the surface	W.m ²
Net infrared radiation at the surface	W.m ²
Upward IR radiation at the surface	W.m ²
Downward IR radiation at the surface	W.m ²
Sensible heat flux	W.m ²
Latent heat flux	W.m ²
Surface albedo	
Total precipitation	mm.day ¹
Surface evaporation	mm.day ¹
SEA ICE	
Sea-ice area	m ²
Sea-ice compactness	
Sea-ice thickness	m
Snow thickness above the sea ice	m
Heat flux at the bottom of the sea-ice	W.m ²
Heat flux at the sea-ice surface	W.m ²
Sea-ice surface temperature	°C
Temperature of the ocean under the sea-ice	°C
OCEAN	
Sea surface temperature	°C
Sea surface salinity	psu ¹
Mixed layer thickness	m
Surface heat fluxes (IR, Solar, Latent, Sensible)	W.m ²
Ocean stream function	Sv= 10 ⁶ m ³ s ⁻¹
Meridional heat flux	W
Meridional fresh water flux	Sv

variable	unit
SNOW FIELD	
Snow thickness	m
Snowfall (w.e.)	mm.day ¹
ATMOSPHERE	
Eastward wind speed at 750hPa	m.s ⁻¹
Eastward wind speed at 1000hPa	m.s ⁻¹
Northward atm. Turbulent heat transport	W
Latent heat meridional flux	W
Northward Hadley heat transport	W
Northward total heat transport	W
Planetary albedo	
Solar radiation absorbed by the atmosphere	W.m ²
Net vertical heat fluxes at the surface	W.m ²
Net vertical heat fluxes on the oceans	W.m ²
ICE SHEET	
Ice volume	km ³
Ice accumulation over the ice sheets	cm.year ¹
Ice ablation over the ice sheets	cm.year ¹
Net ice accumulation over the ice sheets	cm.year ¹
Ice-sheet altitude	m
Ice-sheet thickness	m
Bedrock altitude	m
Ice sheet extent	

Tableau 1: List of variables available from MoBidiC. Spatial resolution is 5 deg in latitude, zonally or sectorially (13 surface types) averaged. Time step of the computation is 2 days but variables are given as monthly or annual mean

Improvements

Improving the numerical schemes in the ocean circulation model. In their ocean model, Hovine and Fichet [Ref.8] used Bryan's [Ref.5] leap-frog scheme for the advection-diffusion equations of tracers (temperature, salinity and other possible tracers) and velocity fields. Such a 2-time step scheme presents the advantage of being stable and showing little diffusivity. However, both the atmospheric and sea-ice components of the model are based on a one time-step numerical discretisation. It is therefore almost impossible to calculate the exchanges of momentum, heat and freshwater between, on the one hand, the ocean and, on the other hand, the sea-ice and atmospheric components in a conservative way. It was therefore necessary to fundamentally reconsider the numerical discretisation of the equations of the ocean model. The following rules have been adopted: diffusion and advection of tracers is fully implicit in the vertical and fully explicit in the horizontal (North-South direction). The spatial resolution of vertical advection is centred. Along the horizontal, a second-order, Lax-Wendroff scheme has been adopted as a compromise between the centred scheme (unstable in explicit treatment) and the too-diffusive upwind scheme. As far as velocity is concerned, the temporal resolution of the baroclinic mode is based upon an implicit treatment of vertical advection (centred), viscosity and Coriolis terms, whereas horizontal diffusion and advection are fully explicit. Finally, the baroclinic mode is solved in a fully explicit way²⁾. The convection scheme has been revisited. Taking advantage of the numerical stability provided by the implicit treatment of vertical advection and diffusion, it was decided to adopt the implicit convection scheme. When gravitational instability is detected, the local vertical diffusivity is enhanced to $10 \text{ m}^2\text{s}^{-1}$, i.e., 5 orders of magnitude larger than the regular value, such that the vertical column is fully mixed in one time step. This method is much faster than usual convection schemes, as discussed in Goosse and Fichet [Ref.11].

Finally, two subgrid scale parameterisations have been implemented. The first is the parameterisation of the gravity-driven downsloping current designed by Campin and Goosse [Ref.12]. Its principle is the following: when the density of water on the Antarctic shelf break is higher than that of the neighbouring deep water column, a downsloping current flows from the shelf and along the slope until it reaches a level where the local potential density equals that of the downsloping flow. An upward return flow maintains the conservation of mass and heat. The intensity of this current is linearly related to the horizontal gradient between the two adjacent grid elements of the shelf break, the coefficient of proportionality being prescribed (coefficient γ). In MoBidiC, the value of γ is 10 seconds, which is toward the higher end of the range of values tested by Campin and Goosse [Ref.12]. Similar schemes are now used in several ocean general circulation models (e.g., Ref.13) and allow for a better representation of deep water mass formation. The second parameterisation represents the sub-polar gyre in the northern North Atlantic [Ref.14]. A constant southward transport (typically $1.0 \text{ Sv} = 10^6 \text{ km}^3\text{s}^{-1}$) is set up between 50 and 75°N, and is compensated for by a northward re-turn path. This transport only affects the tracers in the first 50 m., i.e. the first depth level in the ocean model. Though original, the design of this parameterisation is to a large extent based on the work and advice of A. Ganopolski (pers. communication, Ref.15). The goal of this parametrisation is to compensate for the lack of horizontal barotropic transport inherent in the 2-D formalism of the ocean model. In practice, it mainly impacts on the northward transport of salt which, in turn, results in improved representation of the salinity and temperature characteristics of North Atlantic Deep Water.

Refining the Hadley cell parametrisation. The quasi-geostrophic formalism used in the atmospheric component neglects the advection by the divergent component of the wind. This approximation is

2) For more details about numerical discretization, the reader is referred to standard textbooks. Hirsch [Ref.9], for example, describes the explicit and implicit temporal discretization (p. 271) and the spatial upwind and Lax-Wendroff advection schemes (pp. 272 and 308). The implicit treatment of the Coriolis force is achieved in a convenient way by considering the East-West and North-South components of horizontal velocity as the real and imaginary parts, respectively, of a complex number [Ref.10].

reasonable outside the tropics, but it is not acceptable in intratropical areas where a large fraction of heat, water-vapour and momentum is transported by the mean meridional circulation (the Hadley cells). To compensate for this shortcoming, Gallée et al. [Ref.4] superimposed on the quasi-geostrophic model a parameterisation of the heat transport based on the earlier theoretical developments on the intertropical circulation by Held and Hou [Ref.16], subsequently adapted by Peng et al. [Ref.17]. Contrary to the northern hemisphere model of Gallée, MoBidiC includes an interactive hydrological cycle. Furthermore, the surface zonal winds are used to calculate the wind driven circulation in the ocean. The parameterisation of Gallée et al. had therefore to be generalised to calculate the vertically integrated transport of moisture and momentum consistently with the original theory of Held and Hou [Ref.16]. A full description of these parameterisations and the associated parameters is given in Crucifix et al. [Ref.18]. They considerably improve the representation of the Ekman cells in the ocean, such that both heat and salt transports are more compatible with estimates based on observations.

Introducing the VECODE vegetation model. VECODE [Ref.19] is a vegetation model particularly well adapted for EMICS. It has been fully implemented in MoBidiC and advantageously replaces Harvey's parameterisation [Ref.20] of the taiga-tundra fraction formerly used in Gallée et al. [Ref.4]. VECODE is based on a dynamical set of equations, essentially derived from ecological observations, aimed at representing control of climate on vegetation at the global scale. For each grid point, the sub-grid fractions of trees, grass and desert are predicted as functions of the annual mean precipitation and the growing-degree-day index³. VECODE also includes a calculation of the carbon balance. An important advantage of this model is that it is dynamic, i.e., the biome distribution evolves towards its potential equilibrium with a characteristic time that accounts for the characteristic life-time of the biomass. The latter is calculated by the carbon cycle component of the model. For example, the characteristic time of northern boreal forest is typically 80 – 100 years.

2.1.2 - CLIMBER

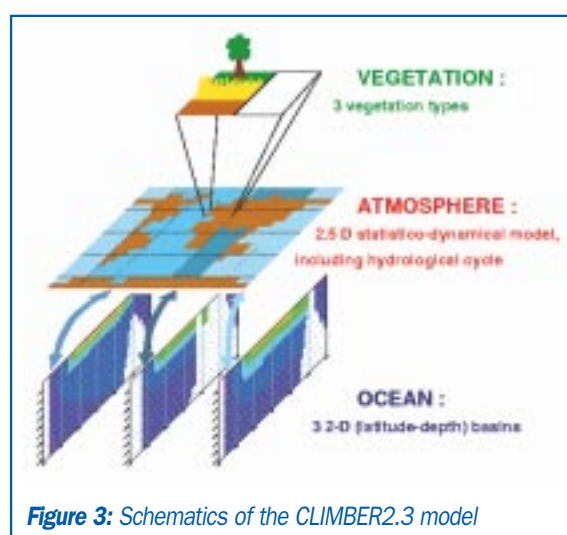


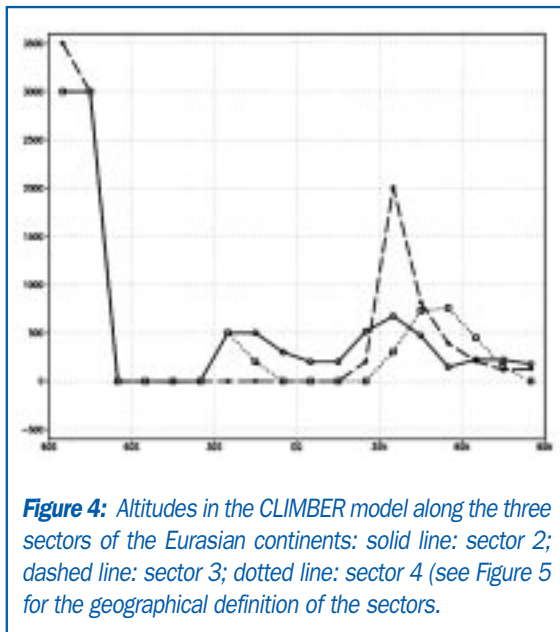
Figure 3: Schematics of the CLIMBER2.3 model

General description

CLIMBER2.3 [Ref.21] (Figure 3) is a climate model of “intermediate complexity”. It has a coarse longitudinal-latitude grid: each atmospheric grid box is 51° in longitude and 10° in latitude. It includes a 2.5-dimensional dynamical-statistical atmosphere model; a multi-basin, zonally averaged ocean model including a sea ice model; a terrestrial vegetation model and a surface parameterization scheme based on BATS [Ref.22]. The altitudes along the three sectors of the Eurasian continent are shown on Figure 4.

The surface albedo and energy fluxes are calculated separately for different land types (forest, grassland, desert or bare soil) which can be covered by snow.

3) The growing-degree-days index (GDDO) is defined as the annual sum of the continental surface air temperature for days during which this temperature exceeds 0°C. In this way, both summer temperature and the length of the growing season (i.e. number of days of positive temperature) are taken into account.



The snow albedo is calculated accounting for snow temperature and age, as well as zenith angle. The albedo of forest covered by snow is a function of the water equivalent snow depth and forest roughness. The vegetation model VECODE is based on a continuous bioclimatic classification [Ref.19]; it describes vegetation as a composite of simple plant functional types (trees and grasses). This VECODE module is the same as the code that has been implemented in MoBidiC. Equilibrium tree fraction is parameterized as a function of climate expressed as a sum of degree-days and annual precipitation. Thanks to its coarse spatial resolution, CLIMBER-2 can be used for the simulation of climate system dynamics over several millennia. The model sensitivity to a doubling of atmospheric CO₂ concentration is 2.5°C with prescribed vegetation cover; with interactive vegetation cover it is 2.6°C.

Improvement

In our coupling to the ice sheet model, a number of modifications have been introduced in CLIMBER. However, these modifications essentially consist of computing additional variables necessary for the

coupling to the ice sheet model. Throughout the process of the development of the coupling, we have deliberately avoided changing the parameterisations of CLIMBER.

2.2. - Ice sheet models

2.2.1 - Gallée et al model

MoBidiC includes up to 5 ice sheets, representing the ice sheets of North America, Greenland and Eurasia in the northern hemisphere, and Eastern and Western Antarctica in the southern hemisphere. The ice sheet model consists of the vertically integrated equations of motion, assuming that the ice sheet behaves in a perfect plastic manner along the east-west direction, which requires a double-parabolic zonal profile. The meridional advection of ice

is parameterised as a function of the fourth power of the meridional gradient of the ice sheet altitude. The model predicts the time evolution of the zonal summit thickness as a function of the local ablation / accumulation balance with a resolution of 0.5 degrees in latitude. The model of the lithosphere used is based on the assumption of local damped isostasy, with parameters independently calibrated to insure consistency with explicit 3D geophysical models.

2.2.2 - GREMLINS

The ice-sheet model used in the present work is the GREnable Model of Land Ice of the Northern hemisphere developed in the Laboratoire de Glaciologie et de Géophysique de l'Environnement [Ref.23]. It is a three dimensional, thermomechanical ice-sheet model that predicts the evolution of the geometry (extension and thickness) of the ice and the coupled temperature and velocity fields. This model deals only with grounded ice and not with ice shelves. The equations are solved on a Cartesian grid (45 km x 45 km) corresponding to 241 x 231 grid points in the Northern Hemisphere. The evolution of the ice sheet surface and geometry is a function of surface mass balance, velocity fields, and bedrock position. The isostatic adjustment of bedrock in response to the ice

load is governed by the reaction of the lithosphere and the asthenosphere, characterized by a time constant of 3000 years. The temperature field is computed both in the ice and in the bedrock by solving a time-dependent heat equation. Changes in the ice thickness with time are a function of the ice flow, the surface mass balance and the basal melting. The ice flow results both from internal ice deformation and basal sliding and the surface mass balance is the sum of accumulation and ablation. The accumulation term is computed by CLIMBER and the ablation term is computed using the positive degree day method which is based upon an empirical relation between air temperatures and melt processes.

2.3. - Coupling

2.3.1 - MoBidiC + ice sheet model

The first version of MoBidiC originally presented by Tulkens [Ref.24] did not include the ice sheet component used by Gallée et al. [Ref.25] and Dutrieux [Ref.26]. It therefore had to be implemented again, with some adaptations: in contrast to Gallée's [Ref.4] climate model, MoBidiC includes ocean dynamics. It was therefore necessary to design a run-off scheme in order to account for the possible impact of ice sheet meltwater on ocean salinity and, consequently, on the thermohaline circulation. Given the sectorial structure of the ice sheet model, a fundamental difficulty is to represent the meridional boundaries of the drainage basins. To this end, it has been assumed that the meltwater flow calculated in a given latitude band is distributed between different drainage basins (e.g., Hudson Bay, the Gulf of Mexico, the St. Lawrence River) on the basis of prescribed, constant ratios. For the deglaciation experiment, these ratios have been inferred from the reconstruction by Teller [Ref.27] for the pre-Younger Dryas (21 -13 kyr BP) period. This runoff scheme and more technical details are given in Crucifix and Berger [Ref.28]. Iceberg calving

had to be explicitly computed to include it in the freshwater balance of the ocean. When, at a given latitude, the longitudinal extent of the ice sheet reaches the limits of the continental platform, lateral discharge leads to iceberg calving in the adjacent ocean. Icebergs are then assumed to melt throughout the year in the latitudinal band where they have been released [Ref.28]. The formulation of isostasy has been revisited. The present formulation is the classical damped local isostasy (e.g. Ref.29) with, as an original concept, effective asthenosphere density and relaxation time. The concept of effective parameters was derived by comparing the results of model calculations with local damped isostasy with those of a 3-D geophysical model of the lithosphere and the asthenosphere [Ref.30] for typical ice-load scenarios of duration 20, 40 and 100 kyr [Ref.31]. The values selected for the effective relaxation time and density of the asthenosphere are the parameters giving the best results with respect to the 3-D geophysical model.

2.3.2 - CLIMBER + GREMLINS

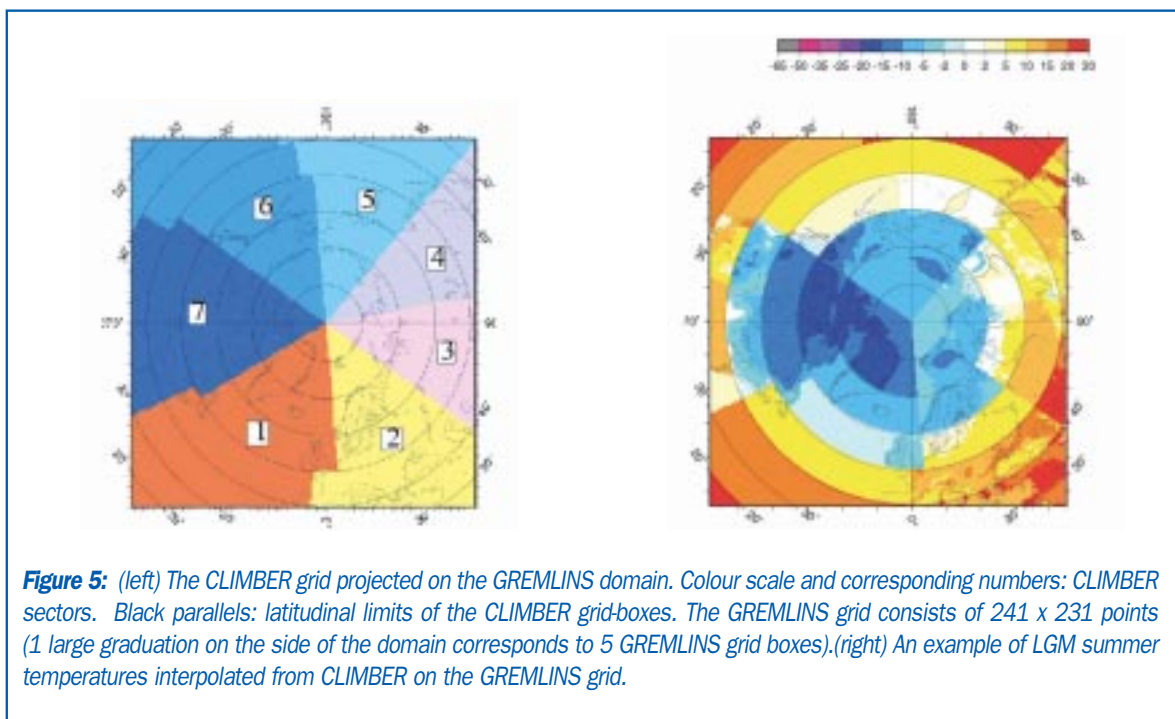
Previous work on the coupling between this ice-sheet model and a climate model included asynchronous coupling between GREMLINS and the LMD Atmospheric General Circulation Model (AGCM). The coupling used here is built on this experience. Values of the following variables are exchanged between CLIMBER and GREMLINS:

- mean annual temperature, summer temperature and annual precipitation are computed in CLIMBER and passed to GREMLINS
- a new land-ocean distribution, the fraction of land covered by ice-sheets and a new topography are computed in GREMLINS and passed to CLIMBER. In the computation of this land-ocean distribution, we take into account the global sea-level change given to the model for the past simulation (SPECMAP stack). For the future simulation, no change in global eustatic sea level was given to the model.

The main difference between the coupling procedure developed for the AGCM and the present one is that the present one uses absolute fields, and not fields relative to a simulated climate for the present. The latter approach corrected the biases of the AGCM. However,

it is not very satisfactory and we chose to avoid relying on relative values.

The very different horizontal resolutions of the models means that we are faced with a downscaling problem when passing the variables computed by CLIMBER to GREMLINS. This is summarised in Figure 5. To solve this downscaling problem, we have adopted the following approach: we have chosen to recompute the three variables that are to be passed to the ice-sheet model for a fixed number (15) of vertical levels, in exactly the same way as it is done in each of the CLIMBER grid-boxes. This involves re-computing the energy budget for each of the 15 vertical levels. This approach is justified by the fact that the vertical profiles (of temperature, snowfall) are generally far from linear. In the particular version used for the BIOCLIM project (Version 9.4 with no horizontal interpolation) the snowfall passed to GREMLINS is computed by the interpolation of a vertical profile computed by CLIMBER. We do not use, as in previous versions, the total precipitation and the recomputed temperature to deduce snowfall for the ice-sheet model.



In the version of the model that has been used for the BIOCLIM project, there is no horizontal interpolation when fields computed in CLIMBER are passed to GREMLINS. For each point on the GREMLINS grid, we only consider the vertical profile of the CLIMBER grid box in which the GREMLINS point is (we do not take into account vertical profiles of neighbouring points) and

compute the value of the variables at this point taking its altitude into account using a simple linear interpolation of the CLIMBER vertical profile (see an example of an interpolated summer temperature on Figure 5). This coupling can be seen as being perfectly coherent with the CLIMBER grid.



3. Evaluation

Several simulations (Table 2) covering a few thousand of years were performed using both CLIMBER and MoBidiC to evaluate the ability of both models to simulate past climates. First, some snapshot simulations were performed. These allow comparisons with existing General Circulation Model experiments, in particular with the results from the Paleoclimate Modelling Intercomparison Project (PMIP) (Ref.32 for instance).

The experiments performed for validation and inter-model comparison, are:

- A snapshot experiment for the present-day climate.
- The snapshots of extreme climate during the last glacial-interglacial cycle, i.e. the Last Interglacial (126 kyr BP), Last Glacial Maximum (21 kyr BP), Holocene Climate Optimum (6 kyr BP)
- For the transient experiments, the designs are sometimes a little different and will be detailed for each experiment in the relevant section. However, the different experiments are:
 - The Last Interglacial (126ky BP-115ky BP).
 - The Last Deglaciation (21ky BP - 0)
 - The Last Glacial Cycle (126ky BP - 0). This last

experiment is used to set up the rules for downscaling from models of intermediate complexity to the regional scale [Ref.33].

Before using the climate model for past and future climate simulation, the control simulation is performed to check the ability of the model to simulate the present-day climate and the interactions between the different parts of the climate system. Then other characteristic and extreme epochs are identified. The interglacial simulations are not too much different. They can help to gain a deeper understanding of the mechanisms leading to the simulated changes. They are also a test of the stability of the model. The LGM represents an example of extreme cold climate. It allows a better understanding of how the ice age boundary conditions can influence climate change. At last transient simulations are performed. Indeed the climate system is actually never at equilibrium. It is thus important to identify the strength and weaknesses of the model on longer time intervals, as well as to evaluate their ability to simulate the transient behaviour of the climate system.

Experiment	Model	Forcing
<u>Equilibrium</u> Present	MoBidiC and CLIMBER-GREMLINS	Solar Forcing : present CO ₂ concentration : 280 ppmv
Sensitivity (2xCO ₂)	MoBidiC : CLIMBER-GREMLINS	2.0°C 2.6°C
6 kyr BP	MoBidiC and CLIMBER-GREMLINS	Solar Forcing : 6 kyr BP CO ₂ concentration : 267 ppmv
21 kyr BP (LGM)	MoBidiC CLIMBER-GREMLINS	Solar Forcing : 21 kyr BP CO ₂ concentration : 200 ppmv Fixed ice sheet - as in LLN 2-D NH at 21 kyr BP Solar Forcing : 21 kyr BP CO ₂ concentration : 200 ppmv Interactive NH ice sheets - initial values as in ICE-4G reconstruction
126 kyr BP	MoBidiC CLIMBER-GREMLINS	Solar Forcing : 21 kyr BP CO ₂ concentration : 261 ppmv Fixed ice sheets : 1/2 Greenland + today Antarctica Solar Forcing : 21 kyr BP CO ₂ concentration : 261 ppmv
<u>Transient</u> Last Interglacial	MoBidiC CLIMBER-GREMLINS	Initial conditions : equilibrium at 126 kyr BP and CO ₂ concentration = 261 ppmv Fixed ice sheets : 1/2 Greenland + today Antarctica Solar Forcing : computed for 126 - 115 kyr BP CO ₂ concentration : 261 ppmv Initial conditions : end of equilibrium simulation at 126 kyr BP (see above) Solar Forcing : computed for 126 - 115 kyr BP Interactive NH ice sheets CO ₂ concentration : Vostok record
Deglaciation	MoBidiC	Initial conditions : equilibrium at 21 kyr BP and CO ₂ concentration = 200 ppmv (see equilibrium above) Solar Forcing : computed for 21 kyr BP to today CO ₂ concentration : [Ref.34 ; Ref.35] Interactive ice sheets + routing of meltwater
Last glacial- interglacial cycle	MoBidiC	Initial conditions : equilibrium at 126 kyr BP and CO ₂ concentration = 261 ppmv (see equilibrium above) + less active THC than in the equilibrium above Solar Forcing : computed for 126 kyr BP to today CO ₂ concentration : Vostok record Interactive ice sheets + routing of meltwater
Holocene [Ref.18]	MoBidiC	Initial conditions : equilibrium at 9 kyr BP and CO ₂ concentration = 261 ppmv Solar Forcing : computed for 9 kyr BP to today CO ₂ concentration : [Ref.35]

Table 2: List the different experiments performed with MoBidiC and CLIMBER-GREMLINS

3.1. - Equilibrium experiments

Annual mean surface temperature

Exp.	MoBidiC			CLIMBER-GREMLINS		
	Global	NH	SH	Global	NH	SH
Present	14.6	14.9	14.3	13.9	14.0	13.8
6 kyr BP	14.7	15.1	14.3	13.6	13.8	13.5
21 kyr BP	13.1	12.7	13.5	10.3	9.1	11.4
126 kyr BP	14.7	15.2	14.3	14.0	14.0	13.9

Annual mean sea-surface temperature

Exp.	MoBidiC			CLIMBER-GREMLINS		
	Global	NH	SH	Global	NH	SH
Present	17.9	19.4	16.8	16.7	16.4	17.0
6 kyr BP	17.8	19.3	16.7	16.6	16.3	16.8
21 kyr BP						
126 kyr BP	17.9	19.4	16.8	16.8	16.4	17.1

Table 3: summary table for the different snapshot experiments performed with MoBidiC and CLIMBER Zonally averaged annual mean surface temperature and annual mean sea-surface temperature

3.1.1 - Control experiment : present climate

The reference state is an equilibrium obtained using today's orbital parameters, a solar constant of 1368 Wm^{-2} and a CO_2 concentration of 280 ppmv (pre-industrial value; Ref.36).

- For MoBidiC, at equilibrium the simulated global annual mean surface temperature is 14.6°C (14.9°C for the Northern Hemisphere and 14.3°C for the Southern Hemisphere) and the global annual mean sea-surface temperature is 17.9°C (19.4°C for the Northern Hemisphere and 16.8°C for the Southern Hemisphere) (Table 3).
- For CLIMBER-GREMLINS, the simulated global annual

mean surface temperature is 13.9°C (14.0°C for the Northern Hemisphere and 13.8°C for the Southern Hemisphere) and the global annual mean sea-surface temperature is 16.7°C (16.4°C for the Northern Hemisphere and 17.0°C for the Southern Hemisphere). So the temperatures simulated by CLIMBER-GREMLINS are generally a little colder than those simulated by MoBidiC, especially in the northern hemisphere (Table 3).

The comparison between this reference state and modern observations (see [Ref.18] for MoBidiC and [Ref.21] for CLIMBER-GREMLINS) shows that both MoBidiC and CLIMBER-GREMLINS satisfactorily capture

the large scale features of climate. The seasonal cycle of the zonally averaged surface temperature (Figure 6) compares favourably with data although there is a cold bias in the northern polar regions for MoBidiC. MoBidiC

also overestimates surface temperatures in the 30-50°N latitude band and in the equatorial regions. On the other hand, CLIMBER presents a small cold bias in the tropics.

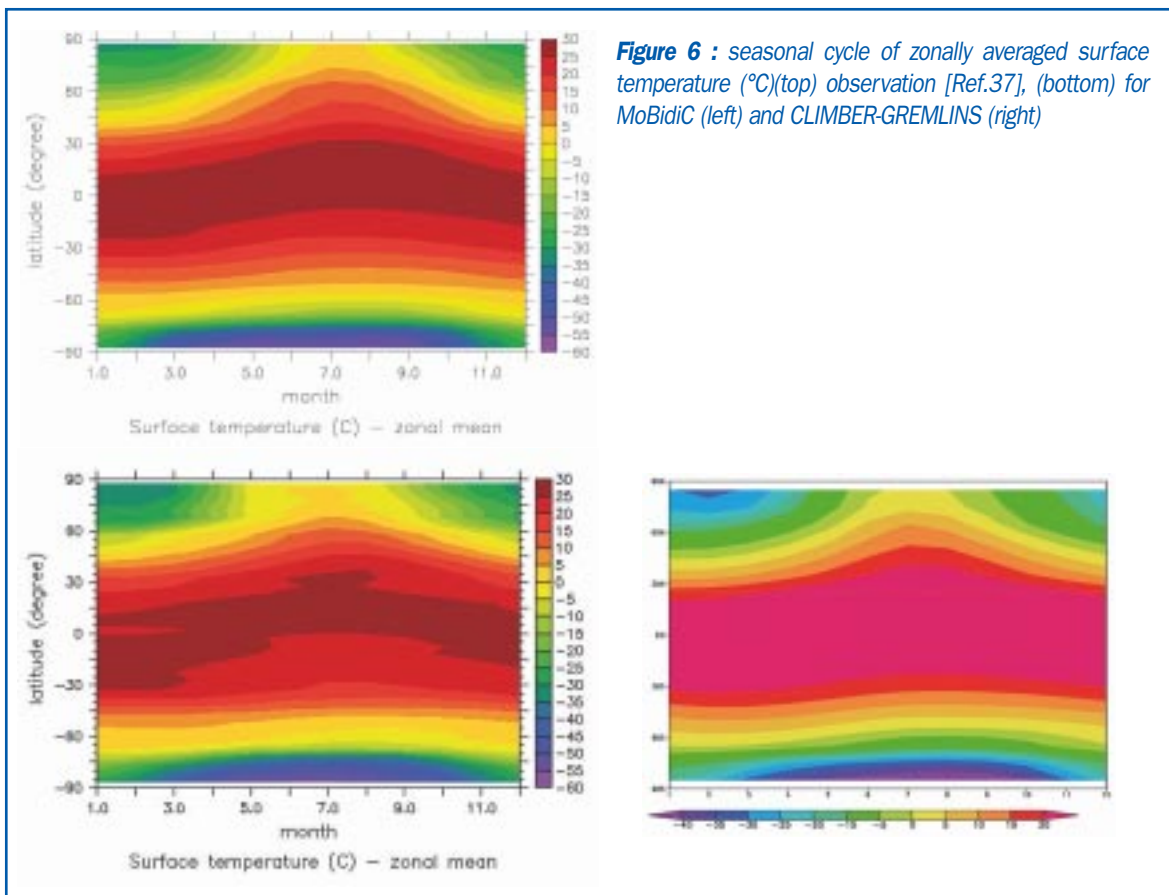


Figure 6 : seasonal cycle of zonally averaged surface temperature (°C)(top) observation [Ref.37], (bottom) for MoBidiC (left) and CLIMBER-GREMLINS (right)

As far as the ocean is concerned, the models capture the main features of the annual mean sea surface temperatures (SST) (Figure 7 and Figure 8) and sea-surface salinities (SSS) Figure 8). Inspection of deep-ocean temperature and salinity also shows that the large-scale distribution of water masses is correct (Figure 9). The modelled southward transport of North Atlantic Deep Water (NADW) at 27.5°S amounts to 11.5 Sv (1 Sv=10⁶m³/s) in MoBidiC and to 10.8 Sv in CLIMBER-GREMLINS. The models successfully reproduce the formation of both NADW and Antarctic Bottom Water (AABW) in the ocean and the seasonal cycle of sea-ice in both hemispheres (see schematic of North Atlantic Water Masses, Figure 10). In MoBidiC, the main deficiency is the absence of convection in the Atlantic Basin north of 60°N, which produces a surface

cold bias in the northern polar regions, mainly in winter (locally up to 5°C). Moreover, the model overestimates salinity and temperature (by about 0.4 psu and 1°C, respectively) of NADW. It also underestimates the salinity gradient between tropical and equatorial areas. The equatorial sea surface is too cold by 1 to 2°C. The CLIMBER ocean model shares many similarities with the MoBidiC one, in particular because such 2D models produce too flat a thermocline in the tropics. The latitudinal gradients are therefore underestimated in CLIMBER also. Since convective sites cannot be represented accurately in a 2D ocean model, the deep waters forming in the Atlantic are also too warm and salty because they are formed at a lower latitude than in actual case (see Figure 9).

⁴ The southward transport of NADW at 27.5S is a measure of the amount of water actually flowing out of the Atlantic Basin

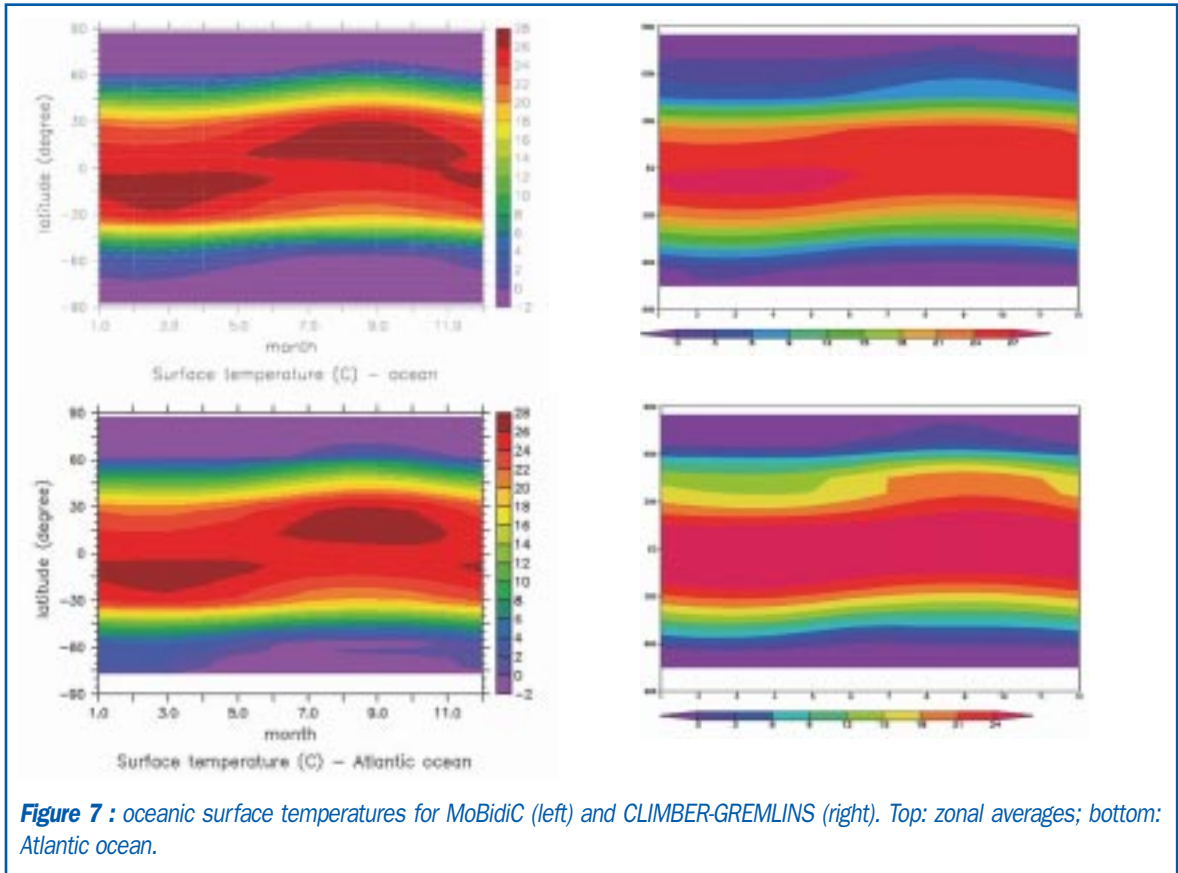


Figure 7 : oceanic surface temperatures for MoBidiC (left) and CLIMBER-GREMLINS (right). Top: zonal averages; bottom: Atlantic ocean.

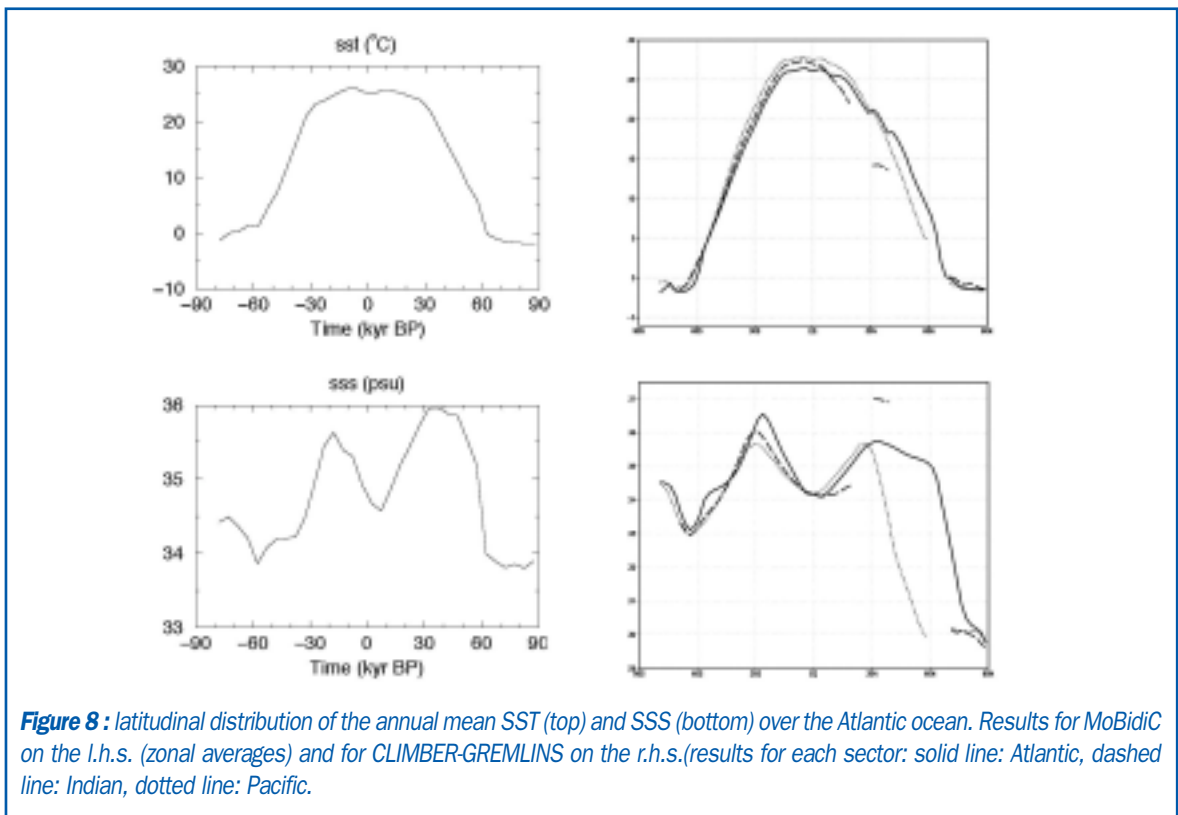


Figure 8 : latitudinal distribution of the annual mean SST (top) and SSS (bottom) over the Atlantic ocean. Results for MoBidiC on the l.h.s. (zonal averages) and for CLIMBER-GREMLINS on the r.h.s. (results for each sector: solid line: Atlantic, dashed line: Indian, dotted line: Pacific).

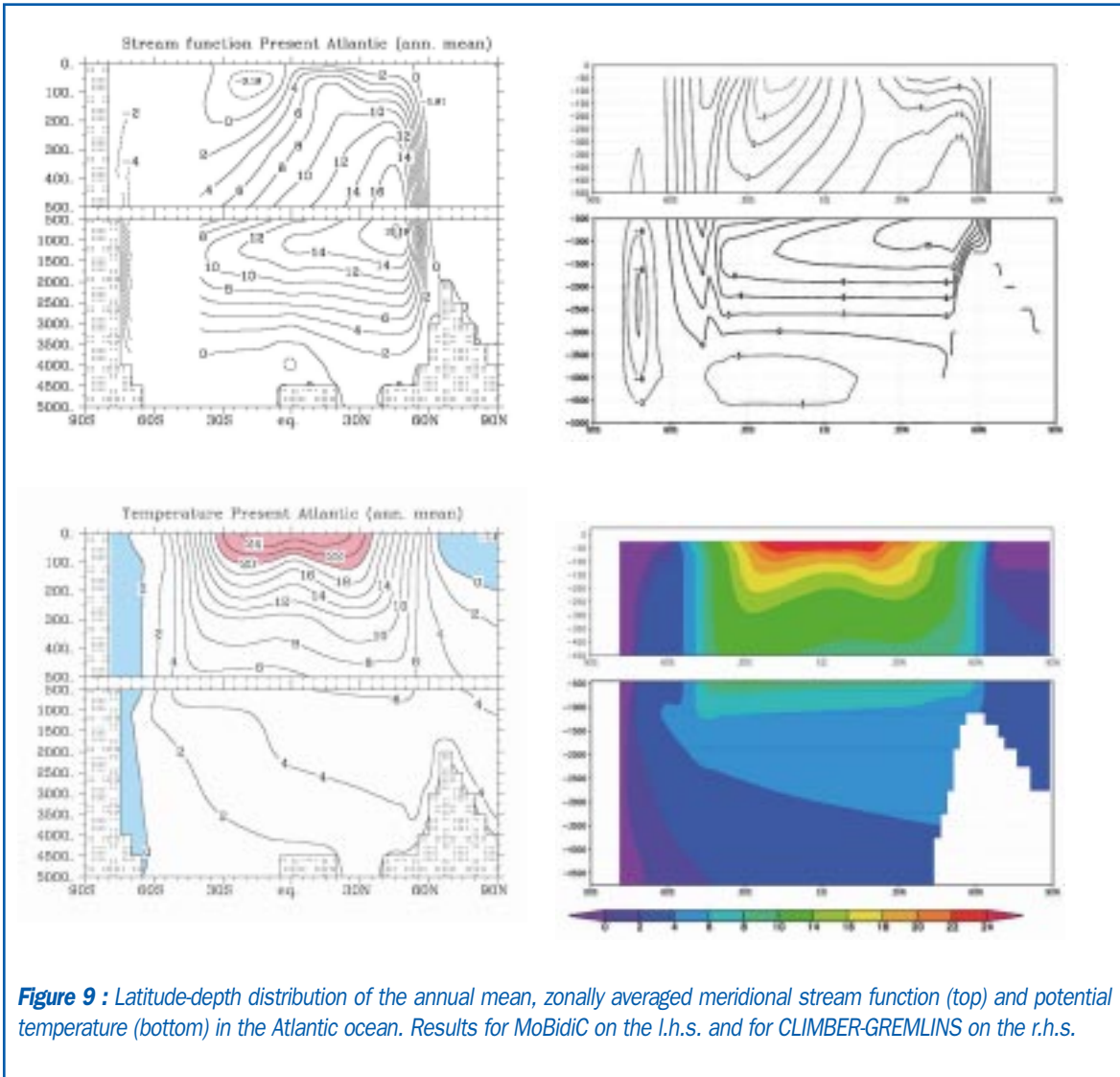
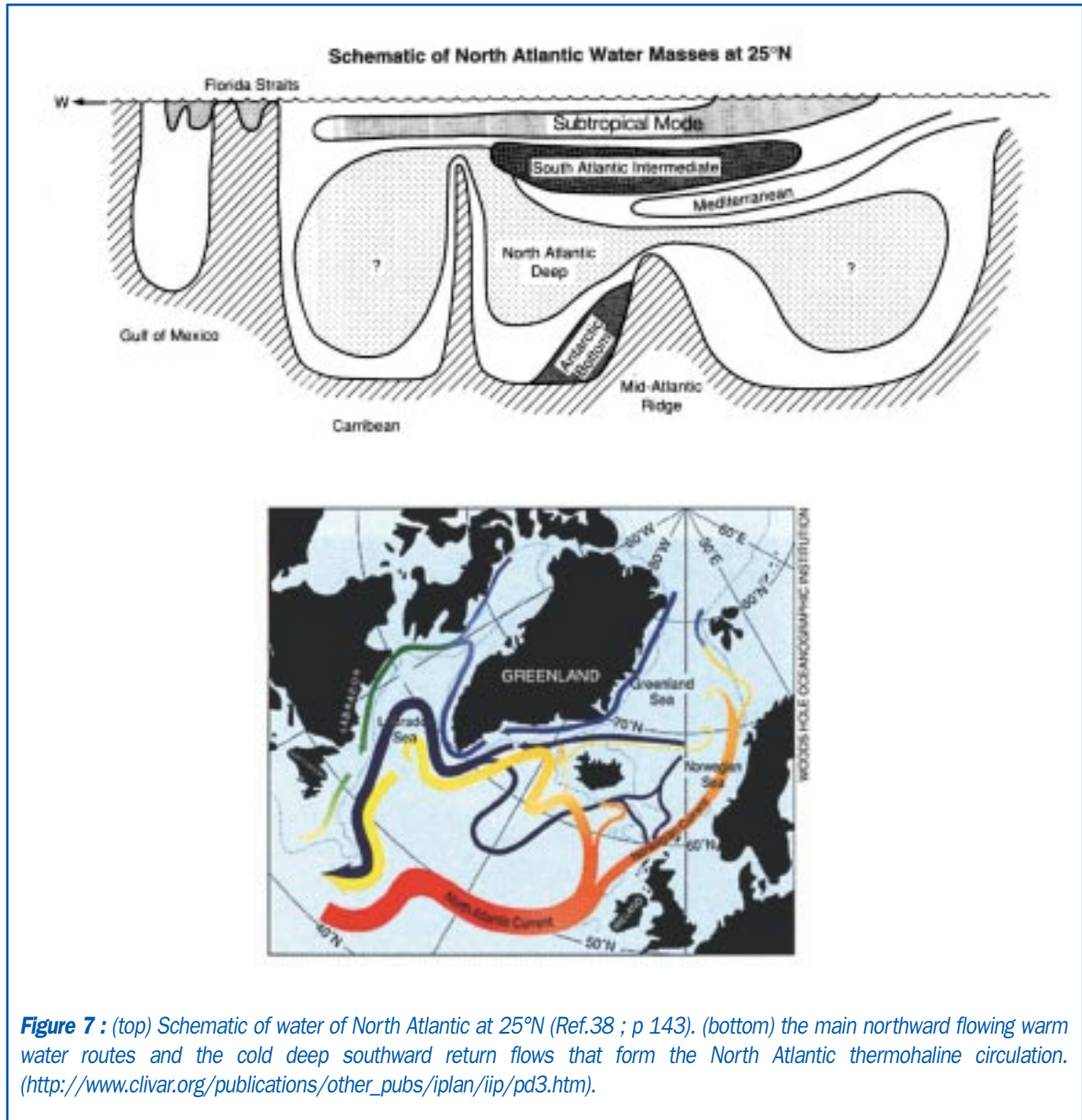


Figure 9 : Latitude-depth distribution of the annual mean, zonally averaged meridional stream function (top) and potential temperature (bottom) in the Atlantic ocean. Results for MoBidiC on the l.h.s. and for CLIMBER-GREMLINS on the r.h.s.



The response of MoBidiC to a doubling of atmospheric CO₂ concentration is an increase in temperature reaching 2.0°C at equilibrium. The changes in thermohaline circulation are small. The export of NADW at 27.5°S is virtually the same level at double the CO₂ concentration as in the control. The CLIMBER model sensitivity to CO₂ doubling is 2.6°C,. NADW production decreases significantly during the transient CO₂ experiments, but stabilizes to near control values at the imposed 2xCO₂ equilibrium. According to IPCC, near the Earth's surface, the global average warming due to

doubling CO₂, as deduced from GCM, lies between +1.5°C and +4.5°C. This estimate is unchanged from the first IPCC Assessment Report in 1990 and the SAR [Ref.39 ; Ref.40 ; Ref.36]. MoBidiC is thus towards the lower end of the IPCC range, whereas CLIMBER-GREMLINS is in the middle of the range of values for atmospheric GCMs.

For MoBidiC, sensitivity experiments to freshwater perturbation show that both active ($\psi = 12.4$ Sv) and inactive ($\psi = 0$ Sv) North Atlantic circulation are

compatible with the unperturbed pre-industrial forcing. Actually, a peculiarity of MoBidiC is that it presents other stable states compatible with the pre-industrial forcing. These states can be identified by suppressing, one by one, the northernmost convective sites in the

North Atlantic Ocean. No equivalent experiment has been performed at LSCE for CLIMBER-GREMLINS yet although Ganopolski et al [Ref.41] identified multiple stable states in a slightly different version of CLIMBER.

3.1.2 - 6 kyr BP

The model is run to equilibrium under 6 kyr BP orbital forcing (eccentricity=0.018682, longitude of perihelion = 0.87°, obliquity = 24.105°; Ref.42) and a CO₂ concentration of 267 ppmv [Ref.35].

- For MoBidiC at equilibrium, the simulated global annual mean surface temperature is 14.7°C (15.1°C for the Northern Hemisphere and 14.3°C for the Southern Hemisphere) and the global annual mean sea-surface temperature is 17.8°C (19.3°C for the Northern Hemisphere and 16.7°C for the Southern Hemisphere) [Ref.18] (Table 3).
- For CLIMBER-GREMLINS, at the equilibrium the simulated global annual mean surface temperature

is 13.6°C (13.8°C for the Northern Hemisphere and 13.5°C for the Southern Hemisphere) and the global annual mean sea-surface temperature is 16.6°C (16.3°C for the Northern Hemisphere and 16.8°C for the Southern Hemisphere). These mean values are very similar to the values for the control experiment and again CLIMBER-GREMLINS simulates slightly colder temperatures than MoBidiC (Table 3).

The seasonal and latitudinal distribution of the insolation at the top of the atmosphere is characterised by an increase of solar radiation during the warm season (May to August) in the Northern Hemisphere and during the southern spring season (September to December) in the Southern Hemisphere (Figure 11).

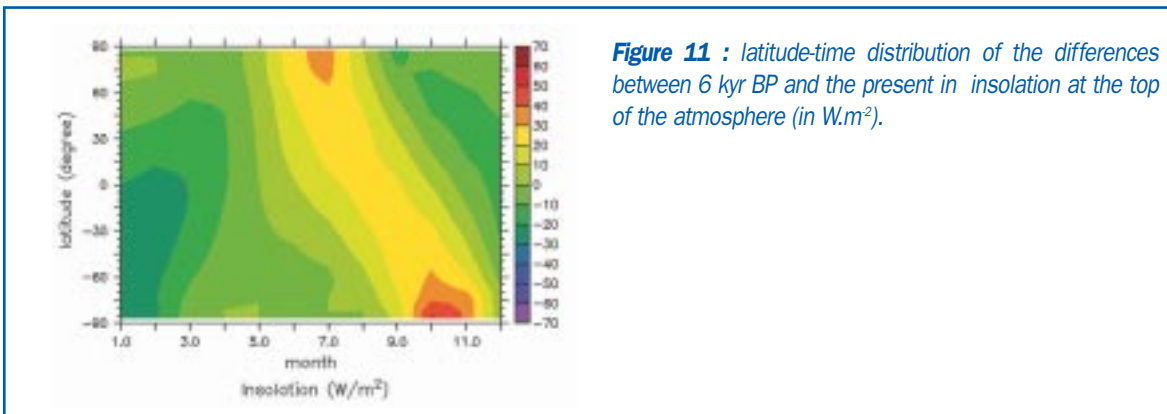


Figure 11 : latitude-time distribution of the differences between 6 kyr BP and the present in insolation at the top of the atmosphere (in W.m²).

North of 60°N MoBidiC simulates a warming throughout the year (Figure 12), up to 5°C in spring, and about 2°C in autumn and winter. The spring and summer warming is mostly related to the continental warming due to vegetation change and change in the snow field extent. This temperature change and the importance of the vegetation are in qualitative agreement with both data and model [Ref.43]. South

of 60°N, vegetation changes are smaller and have less impact on the climate than in the higher latitudes. Hence, surface continental temperature deviations from the present reproduce roughly the insolation anomalies with a lag of about one month. Like the continental surface temperature, the sea-surface temperature (SST) reproduces roughly the insolation anomalies with a lag of about 3 months, except north

of 60°N. At these northern latitudes, the decrease in sea-ice area is responsible for a warming in late winter and early spring. In annual mean, the Arctic sea-ice area is reduced by 10%.

CLIMBER-GREMLINS, on the other hand, simulates

surface temperatures that follow the insolation forcing, but with a lag of 2 to 3 months. Contrary to MoBidiC, the model simulates very little changes in sea ice (not shown) or in vegetation cover (Figure 13) and there is no signature of any feedback from these components in the temperature anomalies of Figure 12.

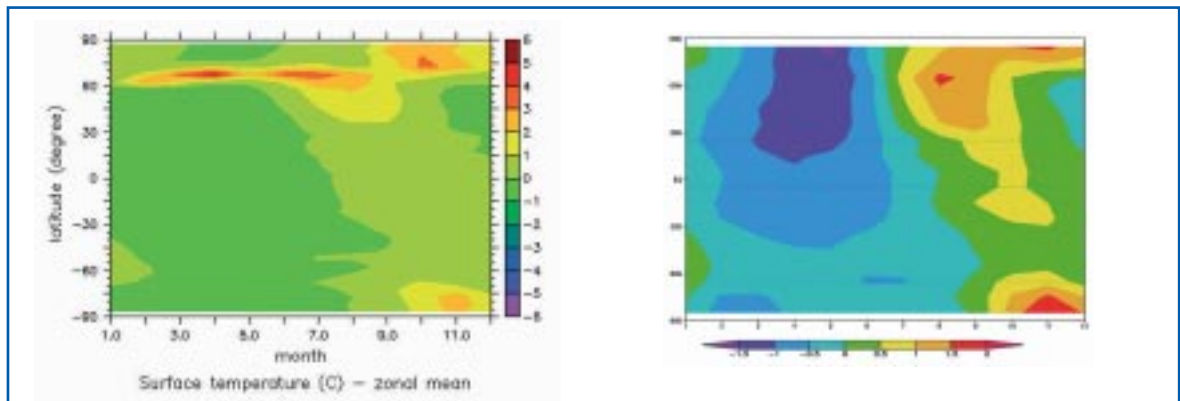


Figure 12 : Latitude-time distribution of the differences between 6 kyr BP and the present in the simulated zonally averaged surface temperature (in °C). Results for MoBidiC on the l.h.s. and for CLIMBER-GREMLINS on the r.h.s. The colour scales are different for the two models.

In MoBidiC, the 6 kyr BP climate is characterised by a northward displacement of the boreal treeline with respect to today (Figure 13). This treeline shift is mostly due to a warmer and longer growing season at 6 kyr BP. On the other hand, in CLIMBER-GREMLINS no vegetation change is simulated over Eurasia.

Paleoreconstruction suggested a shift in the treeline [Ref.44 ; Ref. 45], smaller than simulated by MoBidiC. Vegetation-GCM coupled models suggested an expansion of the boreal forest of less than a factor 1.2 [Ref.46] whereas it is about 1.3 in MoBidiC.

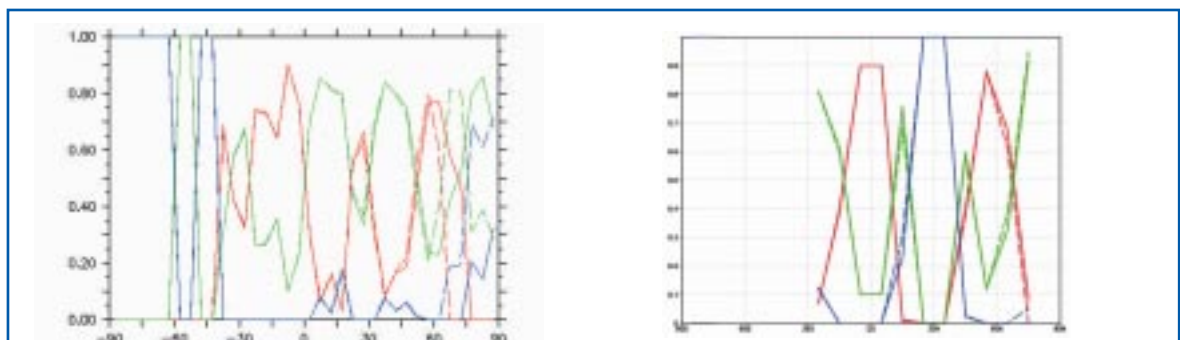
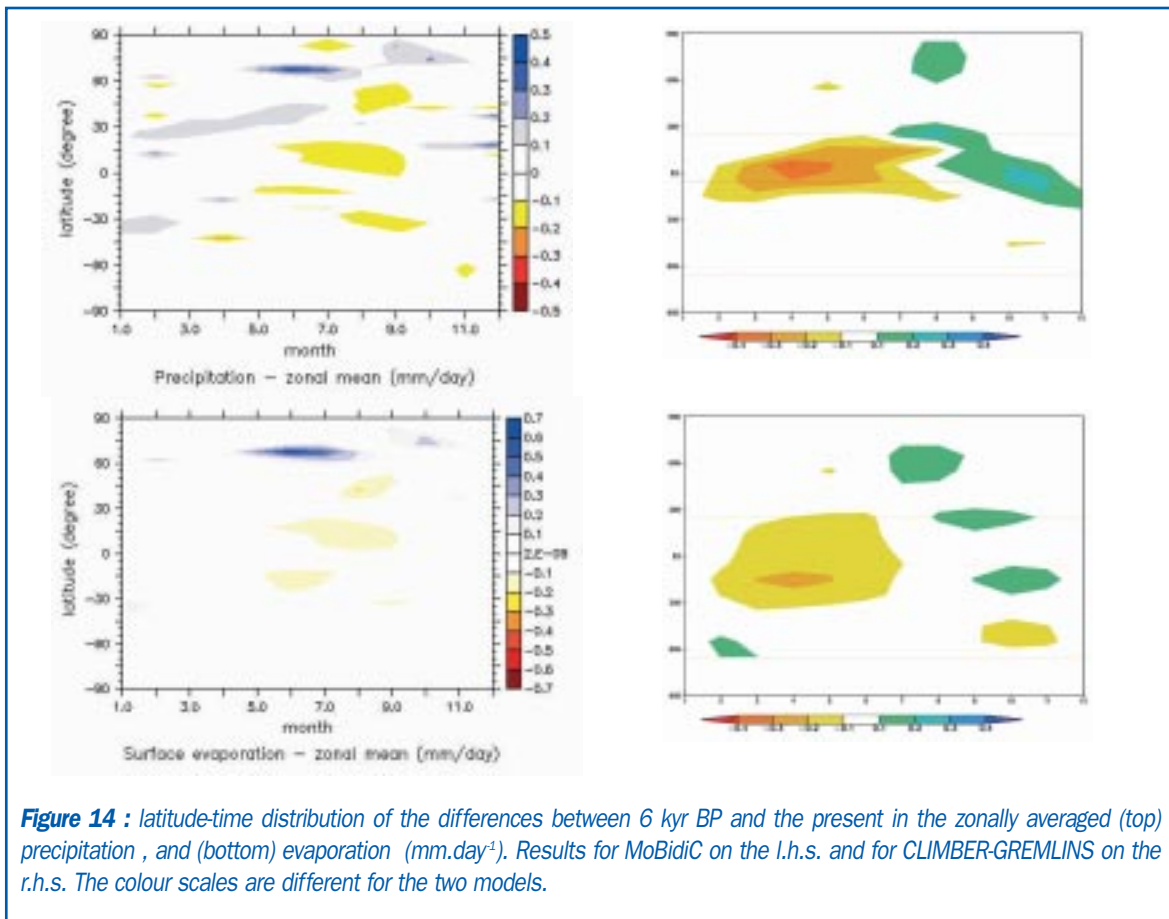


Figure 13 : Latitudinal distribution of the tree (red), grass (green) and desert (blue) fraction over Eurasia and Africa for 6 kyr BP (full line) and the present (dashed line). Results for MoBidiC on the l.h.s. and for CLIMBER-GREMLINS on the r.h.s.

In MoBidiC, the changes in zonally averaged precipitation between 6 kyr BP and today are small. They amount to less than $0.001\text{mm}\cdot\text{day}^{-1}$ in the annual mean north of 60°N . The increase is larger in summer (up to $0.3\text{mm}\cdot\text{day}^{-1}$ in June at 60°N). This increase in precipitation corresponds to an increase in evaporation

over the oceans in the cold season and over the continents during the warm season. In CLIMBER-GREMLINS, the simulated changes of precipitation are very small as well and occur mainly in the tropics, where they closely follow the temperature changes, via effects on evaporation (Figure 14).



3.1.3 - Last Glacial Maximum

For the glacial climate the model is run under 21 kyr BP orbital forcing (eccentricity = 0.018994, longitude of perihelion = 114.42° , obliquity = 22.949° ; Ref.42) (Figure 15) and a CO_2 concentration of 200 ppmv.

- For MoBidiC, the topography of the North American, Eurasian and Greenland ice sheets is set at 21 kyr BP according to the simulation by the LLN 2-D NH climate model [Ref.25]. The North American and Eurasian ice sheets extend south to within the

latitude band $50\text{-}55^\circ\text{N}$. The Antarctic ice sheet is as today.

- For CLIMBER-GREMLINS, the model starts with the ICE-4G reconstruction from Peltier (Ref.47 ; see Figure 16) and the same coupling procedure as the one applied in the BIOCLIM simulations was followed. The model was run for 5000 years. The experiments for the two models are therefore slightly different. Here we focus on the ocean-atmosphere states during those two experiments.

The orbital parameters are very close to their present-day values. The eccentricity is only slightly larger, the perihelion occurs only a few days later than now and the obliquity is a bit smaller. Consequently the seasonal and latitudinal distribution of the insolation is not very different from the present-day one. Positive anomalies occur in Autumn and Winter in the Northern Hemisphere and in the first part of the year in the Southern Hemisphere. However the largest anomalies reach only $+4.2 \text{ W.m}^{-2}$ in December at $40\text{-}45^\circ\text{N}$ and -13.6 W.m^{-2} in November at the South Pole.

- For MoBidiC, at equilibrium, the simulated global annual mean surface temperature is 13.1°C (12.7°C for the Northern Hemisphere and 13.5°C for the Southern Hemisphere) (Table 3).
- For CLIMBER-GREMLINS, after 5000 years of simulation (after which the climate is in equilibrium but the ice sheets are still slowly growing), the simulated global annual mean surface temperature

is 10.3°C (9.1°C for the Northern Hemisphere and 11.4°C for the Southern Hemisphere), thus significantly colder than for MoBidiC (Table 3).

GCMs show global mean cooling at the LGM of the order of 4°C [Ref.48 ; Ref.49], in line with estimates from proxy records (5°C quoted by Ref.50). CLIMBER-GREMLINS simulates LGM global annual temperature decrease at the LGM of the same order of magnitude. However, these values are larger than the temperature anomalies simulated by MoBidiC. The cooling simulated by the GCMs is stronger in the Northern Hemisphere. Moreover it can even be larger at the regional scale. The LMD-LMCE model has simulated a cooling of from 5°C to 8°C in Southwestern Europe, and from 15°C to 20°C near the European ice sheet [Ref.51]. Climatic reconstruction over Europe suggests a cooling of 10 to 13°C at the LGM compared to today [Ref.51]. This cooling can reach 20°C over the former Soviet Union [Ref.52] but it is reduced in the tropical region, from 2 to 6°C [Ref.53].

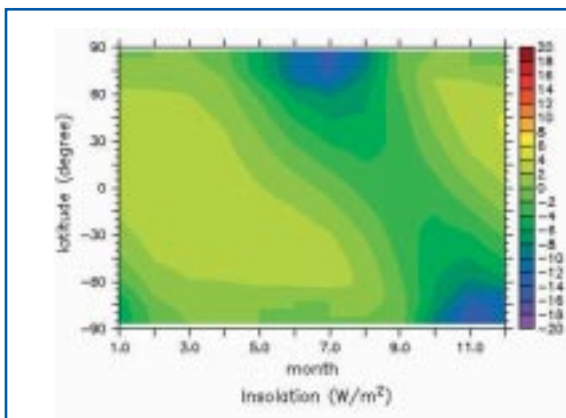


Figure 15 : latitude-time distribution of the differences between 21 kyr BP and the present in insolation at the top of the atmosphere (in W.m^{-2})

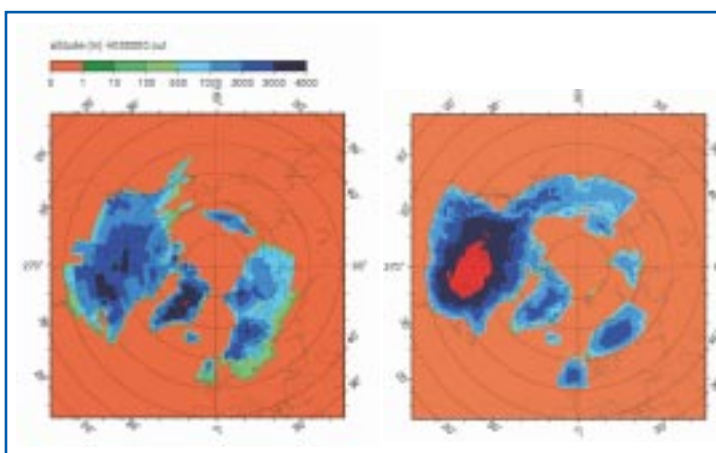


Figure 16 : (left) Thickness of the ice sheets given as initial conditions to CLIMBER-GREMLINS for the Last Glacial Maximum simulation: ICE-4G reconstruction, Peltier (1994). (right) thickness of the ice sheet at the end of the 5000-year-long simulation.

For MoBidiC, the simulated ocean (Figure 17, top) is characterised by a southward shift of the northern boundary of the convection zone (from 60°N in the present-day simulation to 55°N in this glacial simulation). The modelled southward transport of NADW at 27.5°S is also reduced to 9.1 Sv compared to the present-day simulated value of 11.51 Sv. For the Atlantic Ocean, the surface temperatures are cooler, the NADW becomes shallower and warmer and the deepest water masses experience a cooling, when compared to the present-day simulated Atlantic Ocean. The global annual mean sea-surface temperature is

17.0°C (18.3°C for the Northern Hemisphere and 16.1°C for the Southern Hemisphere). For CLIMBER-GREMLINS, the NADW circulation is enhanced due to the stronger thermal gradient. Since deep waters are still formed at high latitudes, deep waters are cooling significantly. For hydrological parameters (the freshwater bypass) which are slightly different from present day ones representing the changes in the geometry of the Canadian Archipelago (see Ref.41), a second state, with a weaker thermohaline circulation, is obtained with CLIMBER.

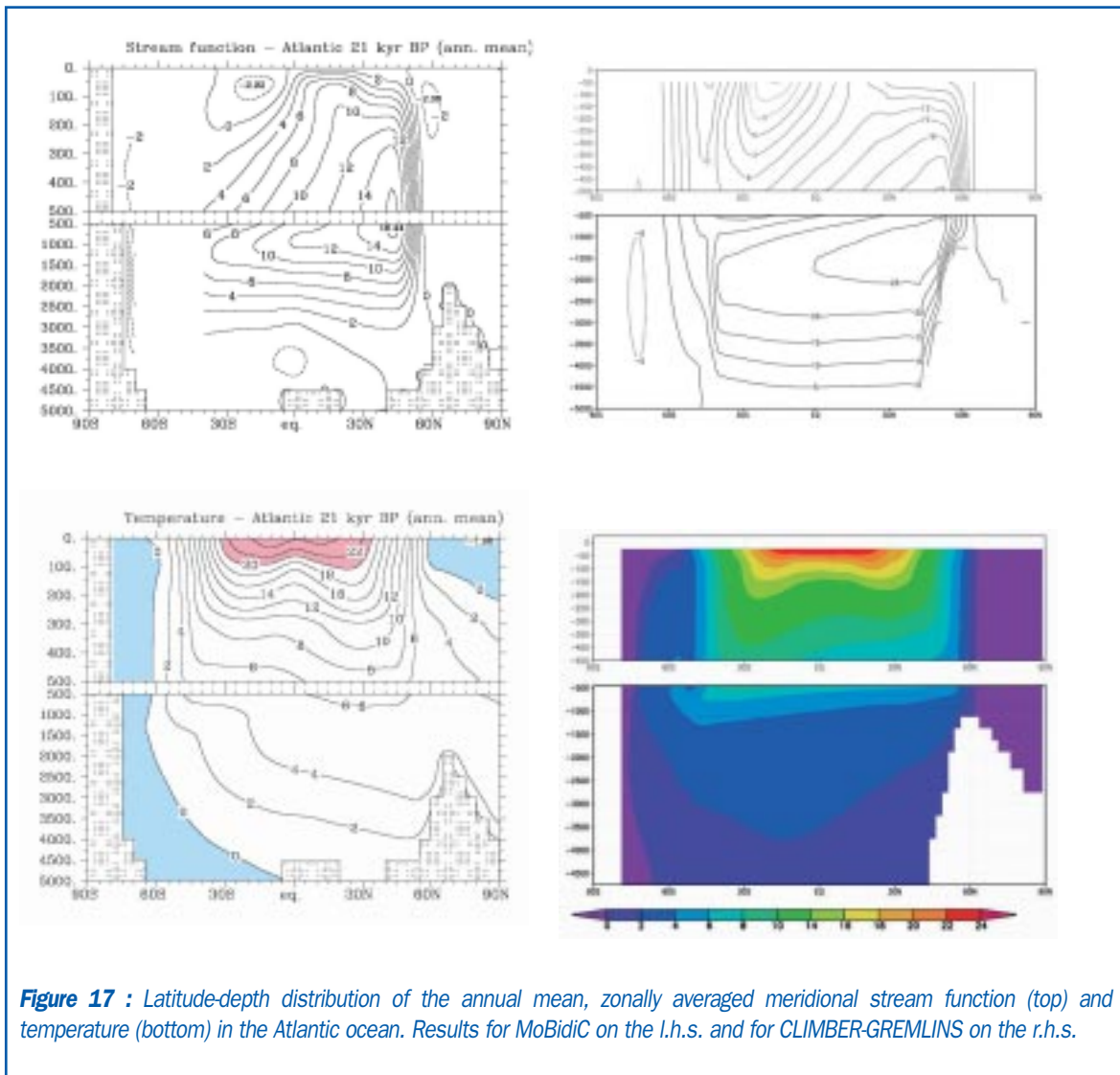


Figure 17 : Latitude-depth distribution of the annual mean, zonally averaged meridional stream function (top) and temperature (bottom) in the Atlantic ocean. Results for MoBidiC on the l.h.s. and for CLIMBER-GREMLINS on the r.h.s.

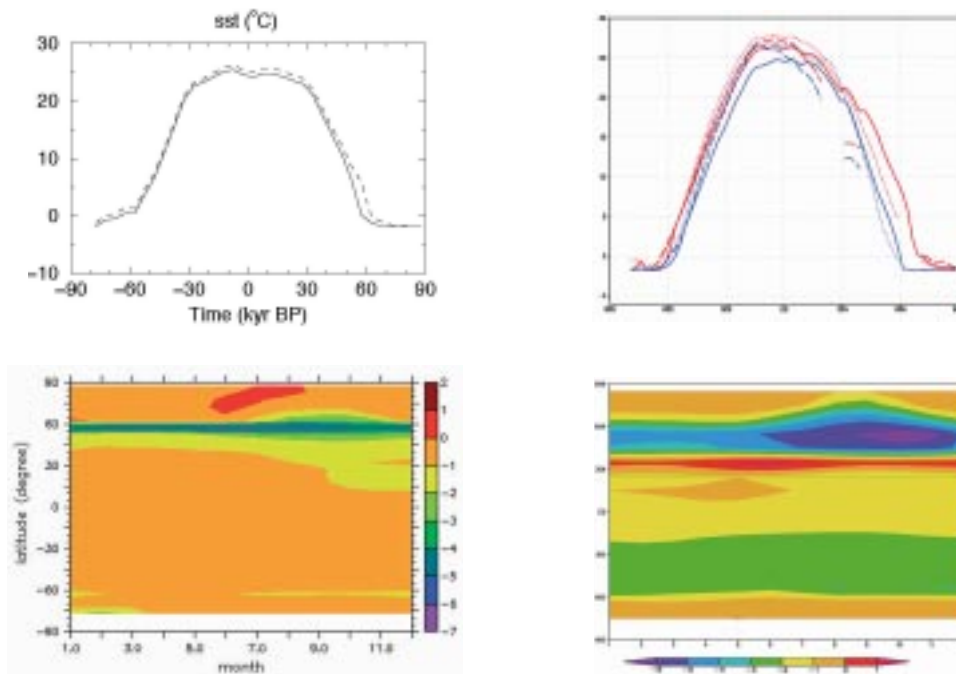


Figure 18 : latitudinal distribution of the anomaly (vs. the control experiment) of the annual mean SST. Results for MoBidiC on the left, for CLIMBER-GREMLINS on the right. Top; 21 kyr BP in full line and reference simulation in dashed line (for CLIMBER, LGM in blue and reference in red for the 3 ocean basins: full line= Atl., dotted = Pac., dashed = Indian). Bottom: seasonal cycle of the Atlantic ocean sea-surface temperature.

The SST cooling in MoBidiC (Figure 17) is greater in higher northern latitudes, related to the presence of large ice-sheets and the increase in sea-ice extent. The summer Arctic (perennial sea ice) area increased by $6.0 \times 10^6 \text{ km}^2$. In annual mean, the Arctic sea-ice area increased by 25%. The southward boundary of the Atlantic sea ice shifted from 55°N in the reference simulation to 50°N in the glacial simulation.

Surface temperatures experience a moderate cooling in the equatorial and tropical latitudes (up to 3°C) and a stronger cooling in the high northern latitudes in MoBidiC. This cooling was up to 13.3°C in July at $60\text{-}65^\circ\text{N}$. This strong cooling is related to a more southward extent of the sea ice compared to the reference simulations, to the presence of the Northern Hemisphere ice sheets (Eurasian and Laurentide), and

also to a change in vegetation in the northern latitudes. The treeline in Eurasia shifted southward by more than 600 km compared to the reference case and the Eurasian continent is almost entirely desert northward of 60°N .

There is an overall reduction of the precipitation compared with today in MoBidiC (Figure 21). This decrease is of the order of 0.04 mm.day^{-1} in annual mean on average south of 50°N . However, it is much larger north of 50°N (0.4 mm.day^{-1} on average in annual mean). The maximum deviation from present-day simulated values is reached in July at $60\text{-}65^\circ\text{N}$ ($-1.08 \text{ mm.day}^{-1}$). Eurasia is characterised by a very strong decrease of precipitation during summer (in the latitude band $40\text{-}60^\circ\text{N}$). The zonal mean evaporation shows a pattern similar to the precipitation one.

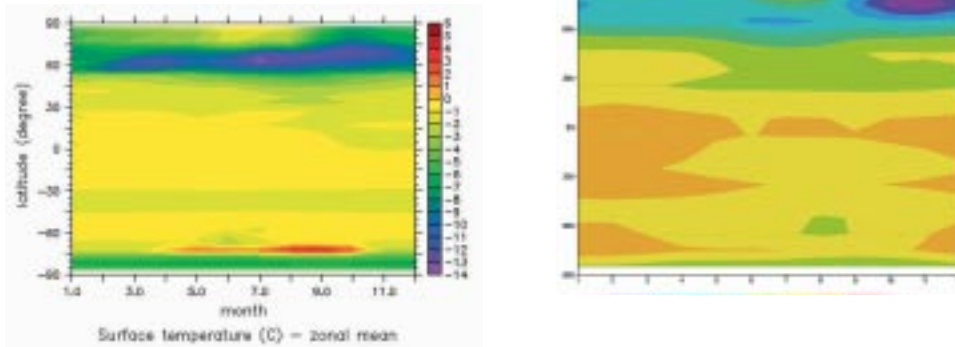


Figure 19 : latitude-time distribution of the differences between 21 kyr BP and the present of the simulated zonally averaged surface temperature (in °C). Results for MoBidiC on the left, for CLIMBER-GREMLINS on the right.

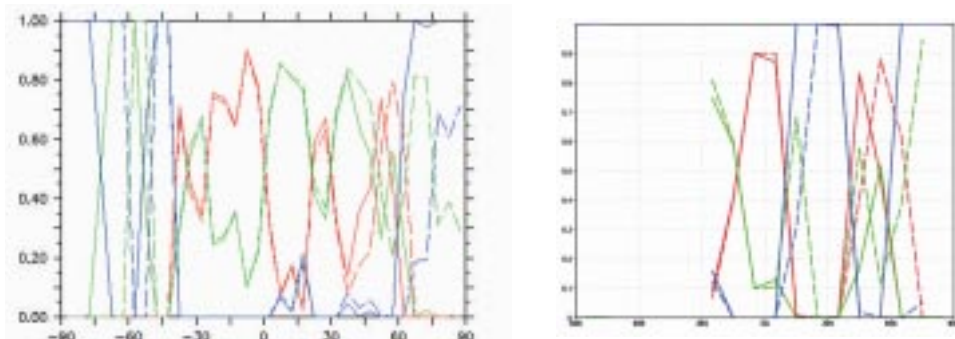


Figure 20 : latitudinal distribution of the tree (red), grass (green) and desert (blue) fraction over Eurasia and Africa for 21 kyr BP (full line) and the present (dashed line). Results for MoBidiC on the left, for CLIMBER-GREMLINS (2nd sector, i.e. West European sector) on the right.

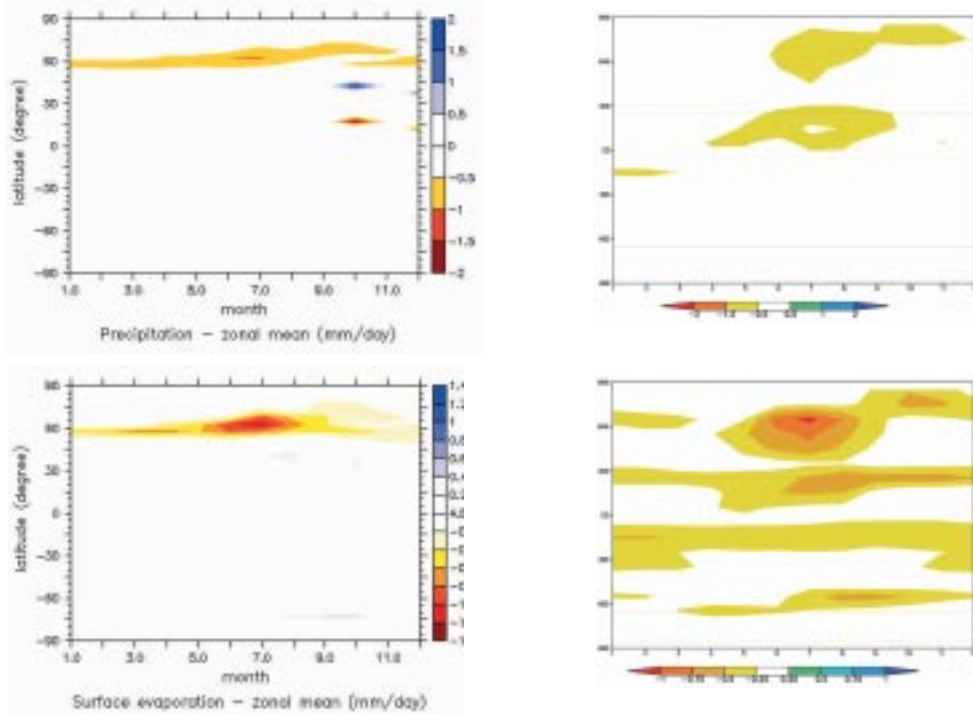


Figure 21 : latitude-time distribution of the differences between 21 kyr BP and the present in the zonally averaged (top) precipitation, and (bottom) evaporation (mm/day). Results for MoBidiC on the left, for CLIMBER-GREMLINS on the right.

3.1.4 - 126 kyr BP

The models have been run under 126 kyr BP orbital forcing (eccentricity = 0.039710, longitude of perihelion = 291.24°, obliquity = 23.928°; Ref.42) (Figure 22) and a CO₂ concentration of 261 ppmv until equilibrium. The orbital parameters are not very different from those at 6 kyr BP. Obliquity is very slightly smaller but it is larger than the present-day value. The perihelion occurs between the June solstice and the September equinox, closer to the June Solstice, at 126 kyr BP. It was at the September equinox at 6 kyr BP. The major difference appears with the eccentricity, which is much larger at 126 kyr BP than at 6 kyr BP.

- For MoBidiC, at equilibrium the simulated global annual mean surface temperature is 14.7°C (15.2°C for the Northern Hemisphere and 14.3°C for the Southern Hemisphere) and the global annual

mean sea-surface temperature is 17.9°C (19.4°C for the Northern Hemisphere and 16.8°C for the Southern Hemisphere) [Ref.18] (Table 3).

- For CLIMBER-GREMLINS, at the equilibrium the simulated global annual mean surface temperature is 14.0°C (14.0°C for the Northern Hemisphere and 13.9°C for the Southern Hemisphere) and the global annual mean sea-surface temperature is 16.8°C (16.4°C for the Northern Hemisphere and 17.1°C for the Southern Hemisphere). Again, these annual mean values are not very different from the ones computed for the present day situation, and CLIMBER-GREMLINS temperatures are slightly colder than those from MoBidiC. These relatively small temperature anomalies in annual mean hide much larger ones in seasonal averages (Table 3).

The seasonal and latitudinal distribution of the insolation at the top of the atmosphere is characterised by an increase of solar radiation during the warm season (April to August) in the Northern Hemisphere and during the local spring season (August to December) in the Southern Hemisphere (Figure 22, left). The positive deviation from present-day values

occurs earlier in the year at 126 kyr BP than at 6kyr BP. The major difference is in the amplitude of the deviation. The deviation from the present-day value is much larger at 126 kyr BP than at 6 kyr BP. This is due to the larger eccentricity value at 126 kyr BP than at 6 kyr BP.

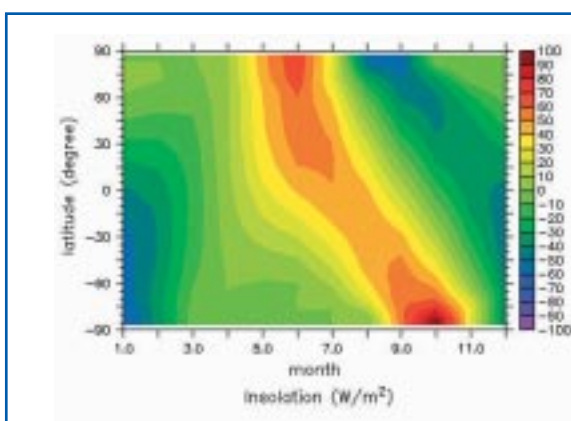


Figure 22 : latitude-time distribution of the differences between 126 kyr BP and the present in insolation at the top of the atmosphere (in W/m^2).

North of $60^{\circ}N$, MoBidiC simulated a warming throughout the year, up to $7^{\circ}C$ in June, and about $3^{\circ}C$ in autumn and winter (Figure 23). The spring and summer warming is mostly related to the continental warming due to vegetation change and change in snow field extent. South of $60^{\circ}N$, the surface temperature deviation from the present reproduces roughly the insolation anomaly pattern with a lag of about one month. Sea-surface temperatures (SST) reproduce roughly the insolation anomalies with a lag of about 3 months. In polar latitudes, larger spring and summer insolation accelerates the melting of sea ice. Therefore, the summer Arctic sea-ice area is reduced by $5.2 \times 10^6 km^2$. In annual mean the Arctic sea-ice area is reduced by 15%.

anomalies throughout the year follow the insolation changes with a lag of 2 to 3 months. The maximum anomalies are larger than for the mid-Holocene, especially during summer and autumn when they can reach $4^{\circ}C$. At very high latitudes in the Arctic Ocean there are signs of sea ice feedback having an impact on surface temperatures, with a warming of the ocean concomitant with less sea ice at the end of the year. This does not have an influence on mid latitudes, in which the temperature anomalies follow the insolation forcing.

The behaviour of CLIMBER-GREMLINS in presence of the insolation forcing of 126 kyr BP is very similar to the 6 kyr BP (mid-Holocene) case: the temperature

Paleodata for France [Ref.54] suggested that the first part of Eemian (roughly corresponding to 126 kyr BP) was probably 1 to $2^{\circ}C$ warmer than the present. For Central England, Eemian and present temperature are similar. Lehman et al [Ref.55] suggest that subtropical Atlantic SSTs were $22.6^{\circ}C$, i.e. $0.2^{\circ}C$ cooler than the present-day value.

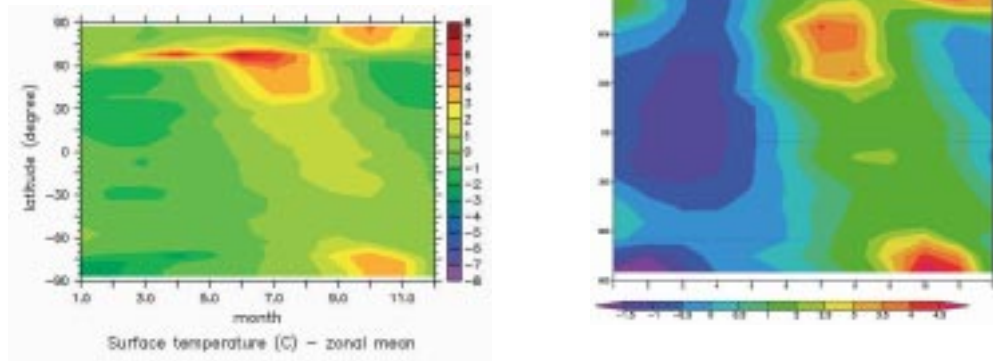


Figure 23: latitude-time distribution of the differences between 126 kyr BP and the present in simulated zonally averaged surface temperature (in °C). Results for MoBidiC on the left, for CLIMBER-GREMLINS on the right.

The 126 kyr BP climate is characterised by an important northward displacement (of the order of 1500 km) of the boreal treeline in MoBidiC with respect to today (Figure 24). This displacement is simulated

both by MoBidiC and CLIMBER-GREMLINS. It follows the lengthening of the growing season as shown by the temperature anomalies.

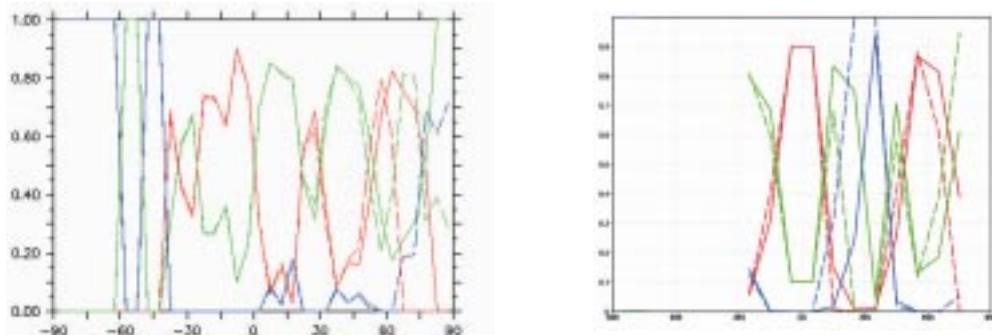


Figure 24: Latitudinal distribution of the tree (red), grass (green) and desert (blue) fraction over Eurasia and Africa for 126 kyr BP (full line) and the present (dashed line). Results for MoBidiC on the left, for CLIMBER-GREMLINS on the right.

In MoBidiC, the increase of zonally averaged precipitation at 126 kyr BP compared to today reaches 0.77 mm.day^{-1} in June at $65\text{-}70^\circ\text{N}$ (Figure 25). However it amounts to less than $0.064 \text{ mm.day}^{-1}$ in annual mean north of 60°N . This increase in precipitation corresponds to an increase in evaporation over the oceans in the cold season and over the continents during the warm season. In CLIMBER-GREMLINS, the anomalies in precipitation and evaporation are a little

larger than in MoBidiC, but they are not very large (maximum of the order of mm.day^{-1}). As for the mid-Holocene simulation, these changes in precipitation and evaporation appear to closely follow the temperature anomalies. One could then interpret the changes in precipitation as caused by more local recycling, which is favoured by a larger evaporation, itself explained by a higher temperature.

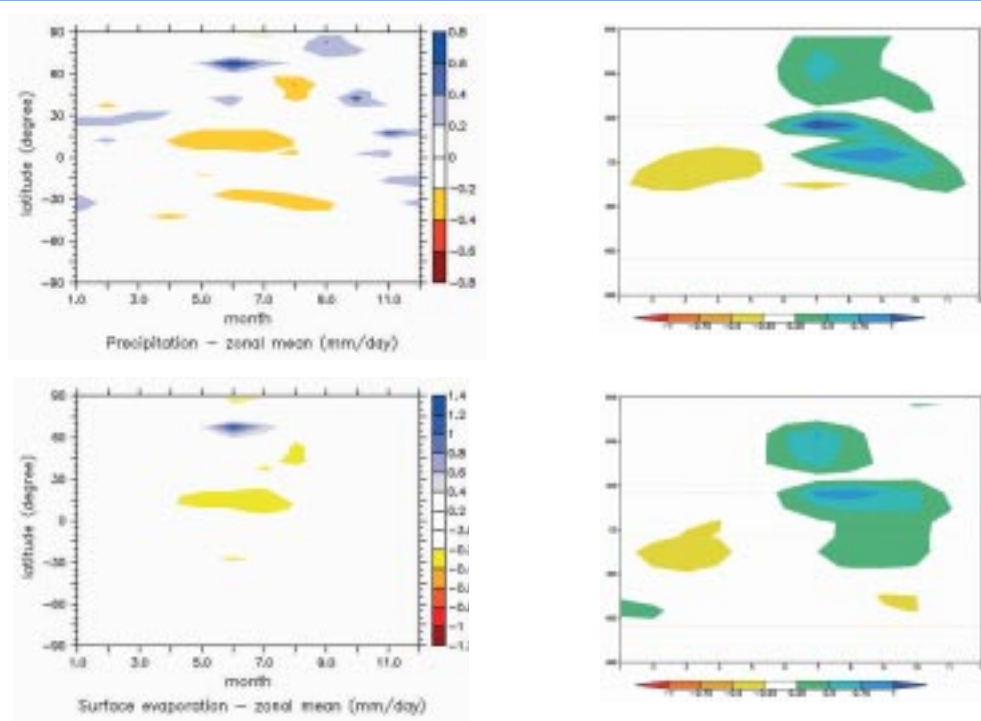


Figure 25 : latitude-time distribution of the differences between 126 kyr BP and the present in the zonally averaged (top) precipitation, and (bottom) evaporation (mm/day). Results for MoBidiC on the left, for CLIMBER-GREMLINS on the right.

3.2. - Transient experiments

Correctly simulating past climate at particular times is a first test, but in the perspective of the BIOCLIM experiments it was also essential to evaluate if the models were able to simulate climate transitions. Here we report simulations of the last interglacial, the last deglaciation and the last glacial-

interglacial cycle. All experiments were performed with MoBidiC in the framework of previous studies. However, it was not possible to carry out all experiments with CLIMBER-GREMLINS.

3.2.1 - MoBidiC

Last Interglacial (126-115 kyr BP) with MoBidiC

A transient experiment covering the Eemian (126 – 115 kyr BP) has been performed with MoBidiC [Ref.31]. The initial conditions are determined by starting the model from its reference state and running it until it reaches the equilibrium with the

boundary conditions prevailing at 126 kyr BP, i.e. insolation computed for 126 kyr BP and the CO₂ concentration set equal to 261 ppmv. Moreover, the Greenland Ice Sheet is reduced to half of its present-day volume and the Antarctic Ice Sheet is as today. For

the transient run, only the orbital forcing is considered, the CO₂ record of Vostok [Ref.57] showing little clear trend between 126 and 115 kyr BP. The change in astronomical forcing results from the contributions of a decrease in obliquity and an increase in the climatic precession. In terms of insolation at the top of the atmosphere, the decrease in obliquity causes a decrease in insolation in the summer hemisphere (the Northern Hemisphere in June and the Southern Hemisphere in December). The increase in climatic precession produces a decrease in June insolation (in both hemispheres) at the benefit of December insolation. Combined, precession and obliquity caused a substantial weakening of the seasonal contrast at high latitudes. The insolation at the June solstice north of 60°N decreases by roughly 100 W.m² from 126 to 115 kyr BP whereas the insolation at the December solstice increased by less than 25 W.m² over the same period (Figure 26). North of 60°N, annual mean continental temperatures decrease by 5°C and SSTs decrease by 0.3°C. Both winter and summer decrease but the largest changes occur in summer, with up to 14°C over the continents and 1°C over the oceans. Most of the cooling occurs between 122 and 120 kyr BP. The simulated temperature changes are in pretty good agreement with those estimated from pollen data for southwestern Europe [Ref.58].

Throughout the Eemian, the decrease of summer insolation at high latitudes causes, in the model, a cooling of the continent that, in turn, causes a gradual southward shift of the boreal treeline (by 1400 km) (Figure 26). This shift is one of the fundamental components of the response of the climate system to the orbital forcing during interglacial periods. This shift of the vegetation belts explains about 60% of the annual mean cooling of the continent between 60 and 90°N [Ref.31]. The contribution of the continental biosphere to the continental cooling is maximum in spring. Given these large impacts, boreal vegetation turns out to be, in MoBidiC, one of the key components involved in the glacial inception (about 118 kyr BP, Ref.59). The large amplitude of the response to vegetation is due to the positive feedback loop that takes place between the treeline shift and surface temperature [Ref.60 ; Ref.20]. Changes in vegetation distribution affect mainly snow albedo and impact mainly on winter and spring temperatures, whereas the

vegetation distribution is essentially sensitive to summer temperatures. The length of the snow cover season is the factor that closes the amplifying feedback loop. Indeed, as a lower tree fraction cools down the surface in spring, thaw is delayed. Consequently, the snow-free season is shorter, which is unfavourable to tree growth. This mechanism is particularly effective in MoBidiC.

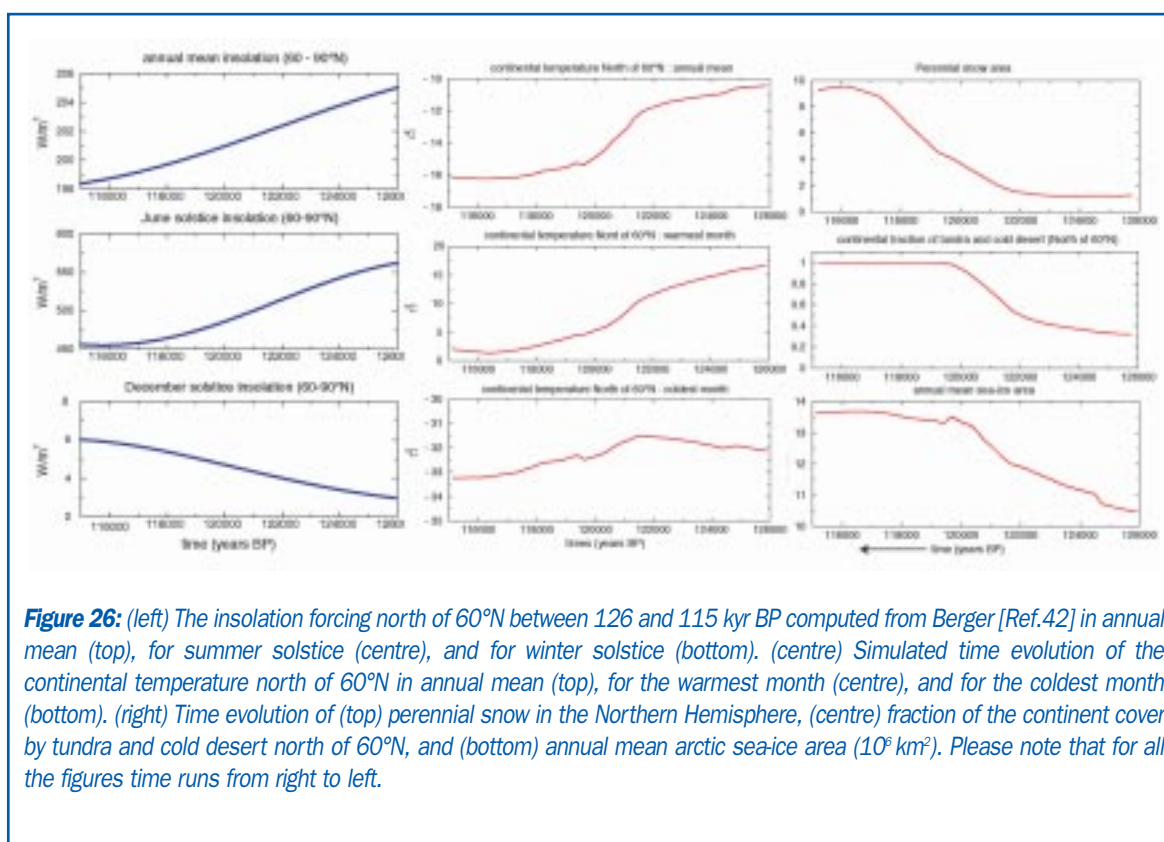
Qualitatively speaking, the results of our simulations are compatible with the palaeodata reconstructions [Ref.61 ; Ref.62 ; Ref.63]. However, the data for Eemian are not accurate enough to enable us to be conclusive. Based on intercomparison between several EMICs, it appears likely that MoBidiC is over sensitive to the vegetation-temperature feedback loop [Ref.19].

Moreover, although the astronomical forcing varies slowly, the transition from taiga-dominated to tundra-dominated vegetation cover is quite fast. This transition takes place in 2000 years, between 120 and 118 kyr BP. Paleodata indicate that the Eemian climate may have passed through an episode of rather rapid cooling such as shown by the simulation undertaken here. For example, from seven pollen cores from France and Poland, [Ref.61] concluded that winters abruptly cooled by about 6 to 10°C around 4 to 5 kyr after the beginning of the Eemian. Likewise, the pollen record from the Tagus abyssal plain (off the Iberian margin) analysed by Sanchez Goñi et al. [Ref.58] exhibits a shift from warm conditions to a colder and wetter climate around 119 kyr BP. For the ocean, the SST reconstructions by Cortijo et al. [Ref.62] suggest a decrease by 2.5°C of the northern North Atlantic August temperature between approximately 124 and 120 kyr BP (dates inferred from benthic δ¹⁸O data), whereas temperature at lower latitudes remained more stable or even experienced a slight increase.

The general circulation of the ocean did not experience any fundamental reorganisation throughout the Eemian and the simulated circulation is similar to that observed today. This result is well supported by reconstructions based on biogeochemical tracers [Ref.65 ; Ref.66]. However the model simulates a 5 % decrease of the export of NADW during the Eemian, but such a trend is too weak to cause any significant variation of the heat balance of the climatic system at the global scale.

Moreover, the response of the ocean-sea-ice system strengthens the effects of summer insolation on the continent. This can be explained by the fact that insolation decreases significantly in spring, which

delays sea-ice melting in spring and early summer. Continental snow melting is therefore delayed as well, so that the summer cooling trend is further enhanced.



Last Interglacial (126-115 kyr BP) with CLIMBER-GREMLINS

The experiment was started from the end of the 126 kyr BP equilibrium simulation. It was run for 11 000 years under orbital forcing (see previous section) and Vostok estimates of atmospheric CO₂ concentrations. Here we briefly give some results for this simulation.

The ice volume (Greenland ice only at the beginning of the simulation) decreases at the beginning of the simulation, before starting to grow again after 1 500 years. The Laurentide ice sheet starts to build up at around 120 kyr BP, on the Canadian archipelago as well as on the Canadian Rockies.

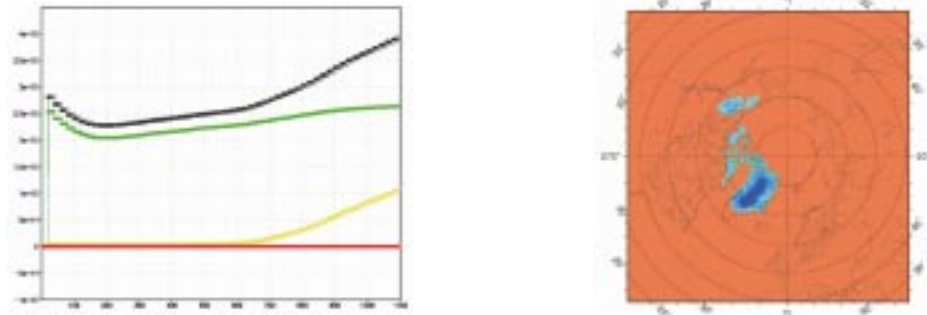


Figure 27: (left) ice volumes simulated by CLIMBER-GREMLINS in the 126-115 kyr BP simulation. Total volume in black, Greenland in green, Laurentide in yellow, Fennoscandia in red (x-axis $\times 10$: years of simulation). (right): thickness of the ice sheet at the end of the simulation, in meters.

Summer temperature, annual precipitation and forest fraction all decrease over the Eurasian latitude belt of 50-60°N, which should favour the start of a glaciation there. However the temperatures remain much too

warm, even at latitudes more to the north, to allow for a permanent snow cover. This drawback of the model requires further investigation.



Figure 28: Summer temperature, annual precipitation and forest fraction over the latitude band 50-60°N over Eurasia in the CLIMBER-GREMLINS last interglacial simulation. X-axis: year of simulation in kyr.

3.2.2 - Deglaciation with MoBidiC

The fully coupled model, including the ice sheets, was used to simulate the deglaciation [Ref.28]. Starting from the glacial conditions (see section 3.1.3 on 21 kyr BP simulation), the model is run with astronomical forcing and prescribed evolution of the CO₂ concentration between 21 kyr BP and today [Ref.34 ;

Ref.35]. North America is divided into four drainage basins corresponding to the meltwater routes towards the Hudson Strait, the Arctic Ocean, the St. Lawrence River and the Mississippi River [Ref.27]. Meltwater from the British Isles and continental Europe (south of 50°N in the model) is released into the Atlantic through the

English Channel. Meltwater from Fennoscandia (north of 55°N in the model) is routed to the Barents Sea. The model reproduces the gradual melting of the ice sheets between 21 kyr BP and 8 kyr BP. The Eurasian continental ice volume decreases gradually until complete melting at about 11 kyr BP. The complete melting of the American ice sheet occurs at about 8 kyr BP, and Greenland does not exhibit significant variations. Even in full glacial conditions, some melting occurs at the southern edge of the ice sheets, which is compensated for by a southward ice flow from accumulation areas. As deglaciation progresses, the ablation zone shifts gradually northward, generating melt water that is routed to the Barents Sea (from 14.7 kyr BP) the Hudson Strait (from 14.0 kyr BP) and the Arctic (from 11.6 kyr BP). Sensitivity studies show that this melting is primarily a consequence of the astronomical forcing, no melting occurring with orbital parameters fixed at those of 21 kyr BP.

A series of simulations including a parameterisation to account for Heinrich event 1 (HE1 : 18,000 - 14,700 kyr BP) were also carried out. For that purpose, a gradual flattening of the American and Eurasian ice sheets was prescribed, which mimics the instability of the ice sheets, related to sea-level increase. This flattening causes an intensification of iceberg calving, providing freshwater into the North Atlantic Ocean [Ref.28 ; Ref.67]. The HE1 is simulated as either a two-step or a three-step calving sequence. The first pulse starts at 17.7 kyr BP, originating from Eurasia. The second pulse, from the North American ice sheet, takes place

between 17.35 and 15.6 kyr BP. Possibly, there is a late European pulse. The model simulates the following sequence in response to HE1: (1) the thermohaline circulation is drastically reduced as soon as HE1 starts, causing a sharp cooling in the Northern Atlantic and a smooth warming in the southern hemisphere, (2) circulation restarts abruptly at the end of HE1, producing an intense warming in both hemispheres, (3) along with this warming, the melting of the North American and Eurasian ice sheets is enhanced, producing a freshwater discharge in the North Atlantic, with a small impact on the Atlantic salinity and thermohaline circulation, (4) a few decades after the post-Heinrich warm event, both the southern Atlantic and Antarctica enter a prolonged cold period caused by the active thermohaline circulation, finally (5), about 1500 years later, meltwater flowing into the North Atlantic through the Hudson Strait and the Barents Sea causes a gradual vertical stratification of the Northern Atlantic. This is in agreement with climate records during HE1. At that time, data are indeed suggesting (1) a reduction of the NADW outflow [Ref.68 ; Ref.69 ; Ref.70 ; Ref. 71 ; Ref.72 ; Ref. 73], (2) a cooling in Greenland [Ref.74], (3) a cooling and freshening in the northern North Atlantic [Ref.75], and (4) a warming of the tropical and southern Atlantic [Ref.73] that can probably be associated with concomitant warm and wet conditions reported in tropical South America [Ref.77 ; Ref.78 ; Ref.79]. For a full discussion about the agreement between data and simulation, see Crucifix and Berger [Ref.28].

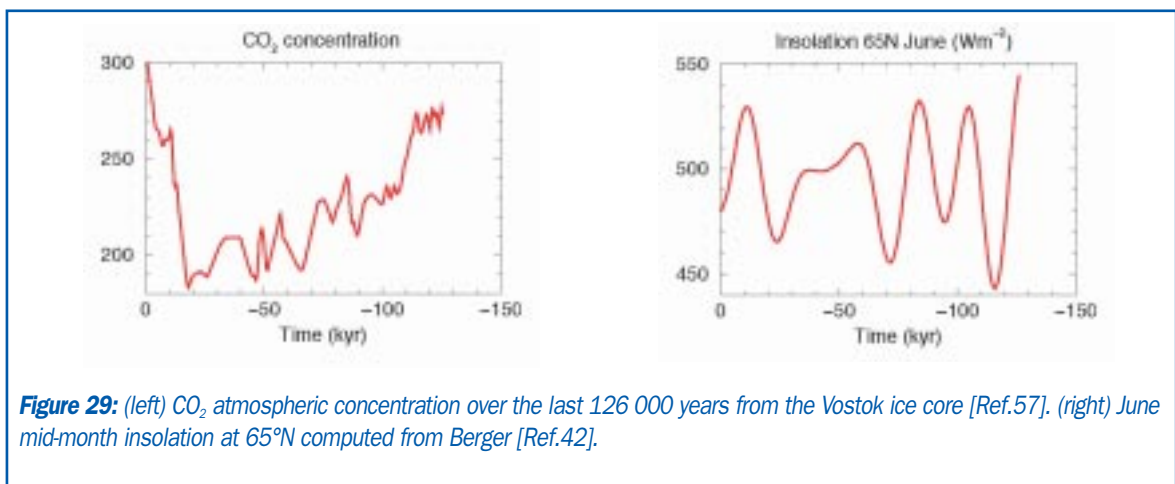
3.2.3 - Last glacial-interglacial cycle with MoBidiC

The initial conditions for the transient experiment are slightly different from the equilibrium state described in section 3.1.4 . The initial state for the ocean (IG2) is characterised by a NADW export of 9.3 Sv. and the northern boundary of the convection zone in the Atlantic is situated at 52.5°N. In this transient experiment, all the components (atmosphere, ocean, vegetation, ice sheets) of the model are interactive. Over the last 126 kyr, the atmospheric CO₂ concentration varies according to Petit et al. [Ref.57]

(Figure 29). During the last interglacial (126-113 kyr BP) it varies very slightly around a mean value of 270 ppmv. Then it decreases with a general trend of 0.8 ppmv/kyr. However the variability superimposed on this trend is large, several tens of ppmv in a few thousand years. The concentration reaches a minimum value of ~180 ppmv at the last glacial maximum, some 18 kyr BP. This minimum is followed by a fast increase (5 ppmv/kyr) towards the present-day value. The model is also forced by insolation changes, computed according to Berger

[Ref.42], at every time step (2 days) and for each latitude in the model (5° zonal resolution). As often done, the insolation at 65°N at the June solstice (Figure 29) is considered as a guideline. It oscillates with a

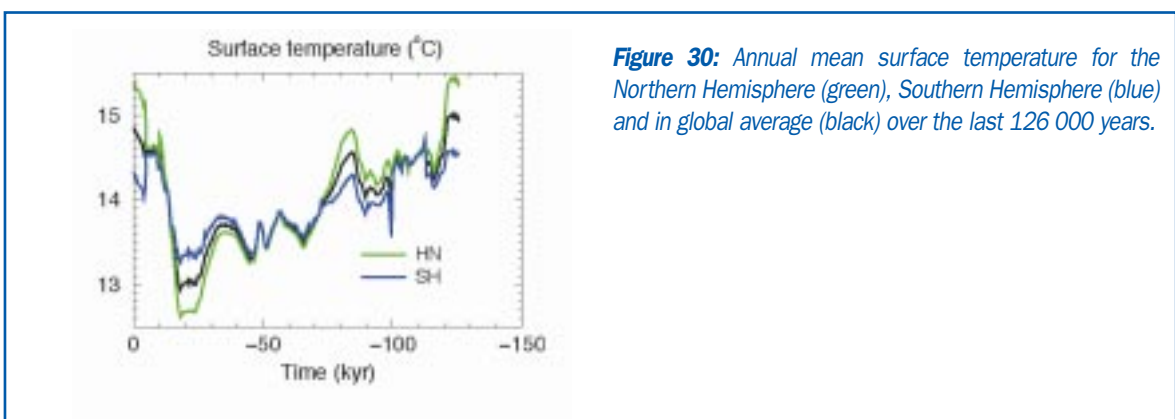
quasi-period of 23 kyr, between 440 and 550 Wm⁻². The amplitude of the variations is largest at the beginning of the transient simulation.



Surface temperature

The simulated annually averaged surface temperature (Figure 30) experiences variations of up to 2.1°C in global mean. These variations are larger for the

Northern Hemisphere (2.8°C) and lower for the Southern Hemisphere (1.5°C). However, larger variations may occur in higher latitudes.



In the latitude band 50-60°N, the annual mean surface temperature of the Eurasian continent increases by 3.7°C between 25 kyr BP and the present (Figure 31). Moreover, the amplitude of the variations is much larger in monthly mean than in annual mean. For example, the temperature increase between 24 and 11 kyr BP is

8.5°C in July whereas its decrease between 30 and 17 kyr BP is 1.6°C in January. The seasonal contrast between January and July reaches up to 40°C in the 50-60°N latitude band over the Eurasian continent. However, over the ocean this seasonal contrast is much smaller. It remains smaller than 9°C in the

50-60°N latitude band over the last glacial-interglacial cycle. This difference between continent and ocean is clearly related to the ocean heat capacity. Moreover, different feedbacks (albedo-temperature feedback,

vegetation-temperature feedback, ice sheets feature-snow fall feedback, ...) can also dampen or amplify the temperature response.

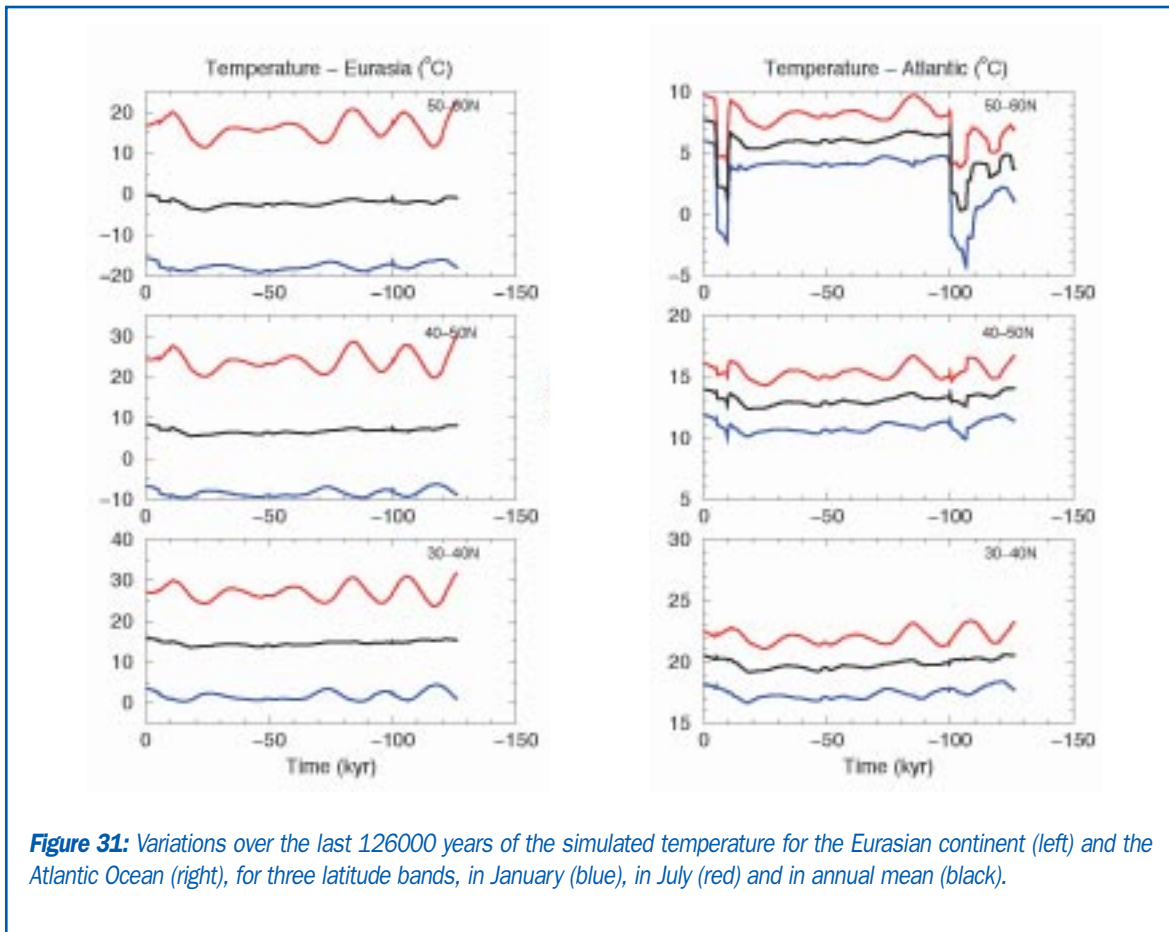


Figure 31: Variations over the last 126000 years of the simulated temperature for the Eurasian continent (left) and the Atlantic Ocean (right), for three latitude bands, in January (blue), in July (red) and in annual mean (black).

The high northern latitudes of the Atlantic Ocean exhibit abrupt temperature change of large amplitude at around 100 kyr BP and 10 kyr BP (Figure 31). Both events are characterised by a rapid cooling of 4 to 5°C followed by a period of slow warming, although temperatures remain low. The temperature then increases again rapidly by 6-7°C. In both cases, the

export of NADW is reduced by ~5 Sv (Figure 32). These events are also characterised by a southern shift of the convection zone in the Atlantic and a cooling of the upper and intermediate water of the Atlantic Ocean. The total area and volume of Arctic sea ice also increase during this event (by 2×10^6 km² and 12×10^3 km³, respectively).

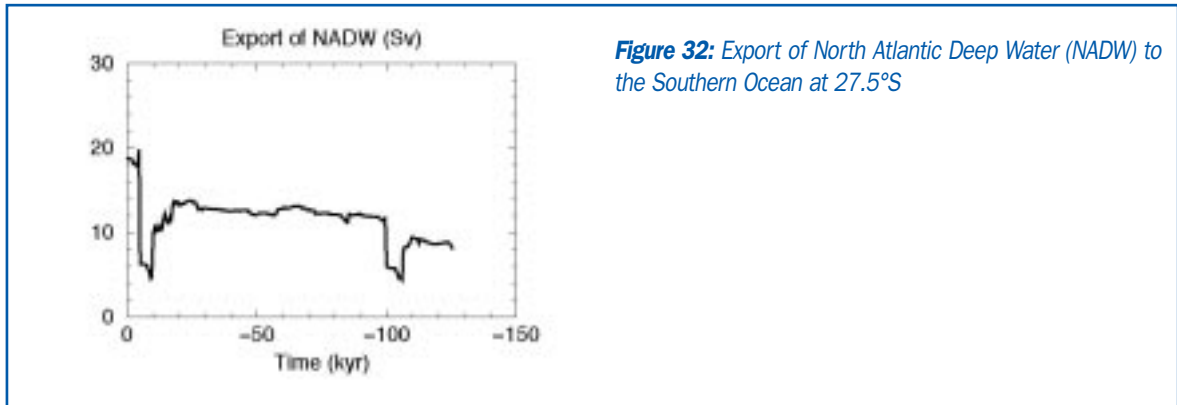


Figure 32: Export of North Atlantic Deep Water (NADW) to the Southern Ocean at 27.5°S

Vegetation

Vegetation is simulated as experiencing large changes during the last glacial-interglacial cycle (Figure 33). In the model, vegetation is dependent on temperature (GDD0 = cumulated continental temperature above 0°C) and precipitation. In the high latitudes (higher than 60°N) vegetation is mostly constrained by temperature whereas in the lower latitudes precipitation plays an important role. For example, there is a clear correlation between vegetation characteristics and annual mean

precipitation in the 50-60°N band, although the amplitude of precipitation change is small. In this latitude band, the amplitude of the variations in vegetation is very large. Between 84 and 76 kyr BP the forested area in this region underwent an increase of 14%, i.e. 1.4×10^6 km². On the other hand, the vegetation change in the 30-40°N band is much smaller.

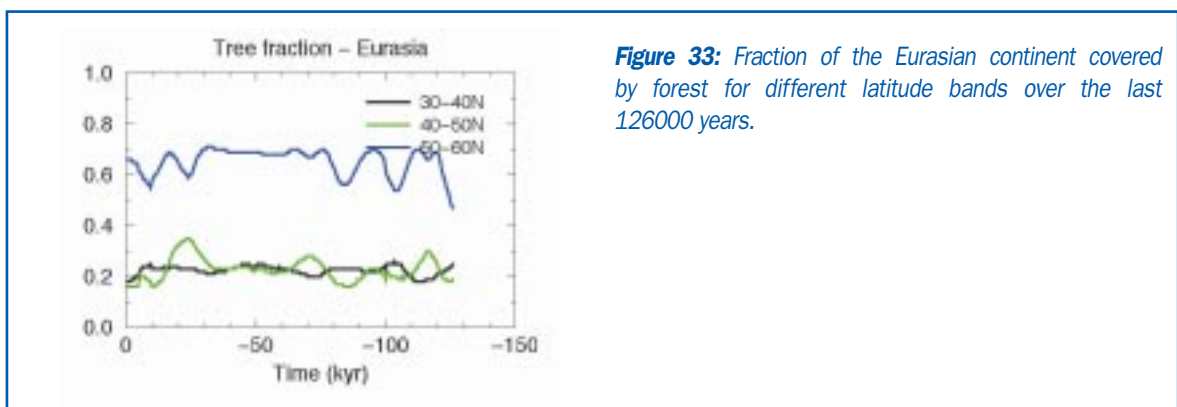
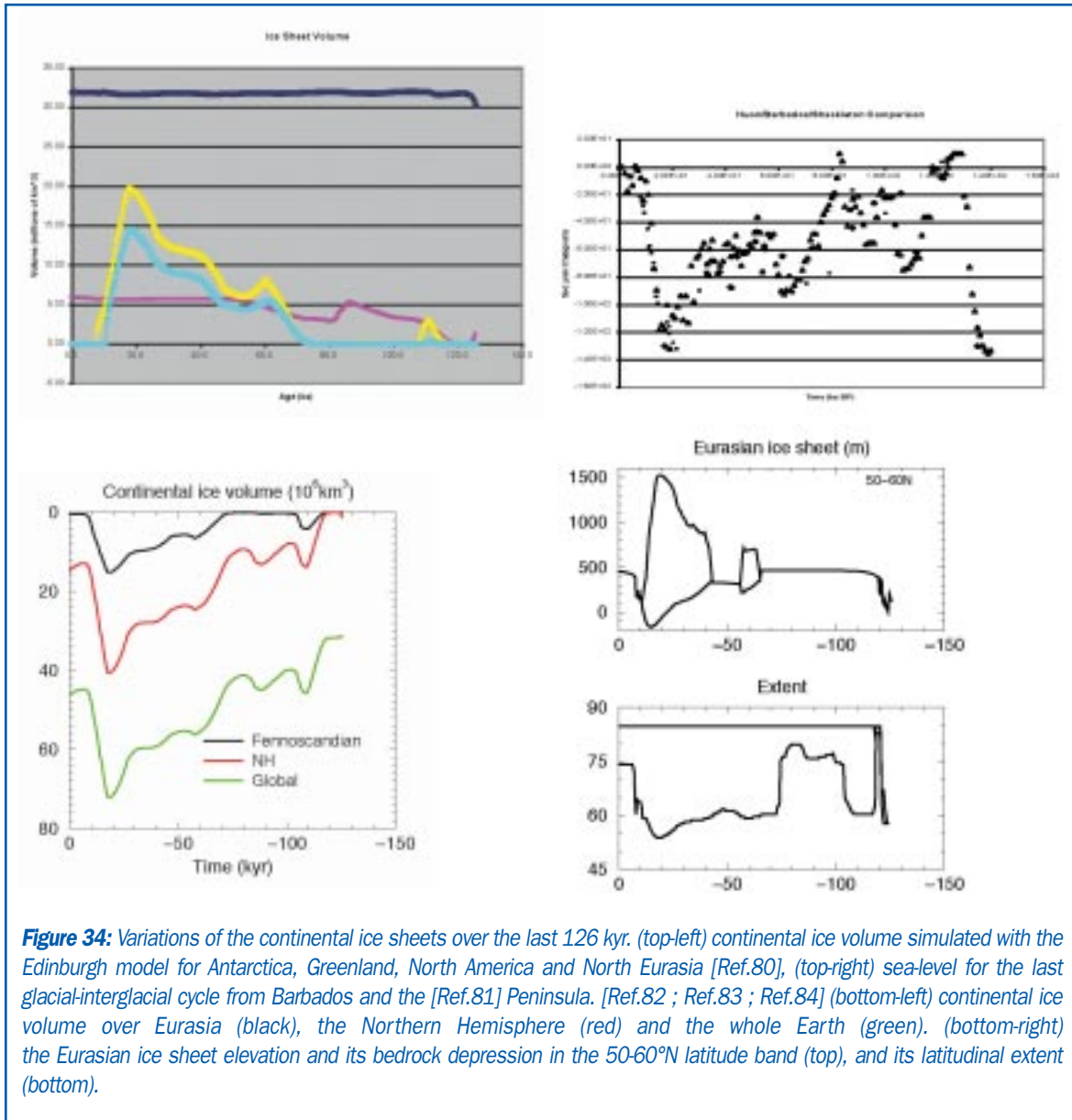


Figure 33: Fraction of the Eurasian continent covered by forest for different latitude bands over the last 126000 years.

Ice sheets

There is a generally increasing trend in continental ice volume from the last interglacial until the last glacial maximum (Figure 34). The maximum continental ice in the Northern Hemisphere is simulated at 18 kyr BP with a volume of more than 40×10^6 km³. This value is probably slightly underestimated, compared to empirical reconstructions and other simulations

[Ref.80]. Over Eurasia, an ice sheet briefly built up around 110 kyr BP (volume 4×10^6 km³ at the maximum). It only starts to rebuild towards the LGM at about 75 kyr BP. It reaches its maximum at 18 kyr BP (15×10^6 km³). At its maximum extent its southern boundary reaches 53.75°N. Its altitude was higher than 1500m in the 50-60°N band.



Precipitation

Variations in the hydrological cycle (precipitation, evaporation and snow fraction as shown on Figure 35 are not very large throughout the simulation, especially at the end of the simulation when the insolation forcing is weaker. Summer precipitation and evaporation are the variables that show the largest amplitude of variability on the orbital timescale and it is of the order of less than 1 mm.day⁻¹ for the evaporation, and less for the precipitation. Precipitation and evaporation seem to vary in the same way, and when temperature

is at its maximum, precipitation and evaporation appear to be at their maximum and vice versa. This is surprising since higher temperatures should favour larger evaporation. This behaviour can be explained by a weakening of the meridional temperature gradient when high latitude temperatures are high, which would weaken equator-to-pole moisture transport, and therefore precipitation at high latitudes. Evaporation would be smaller because of reduced precipitation levels.

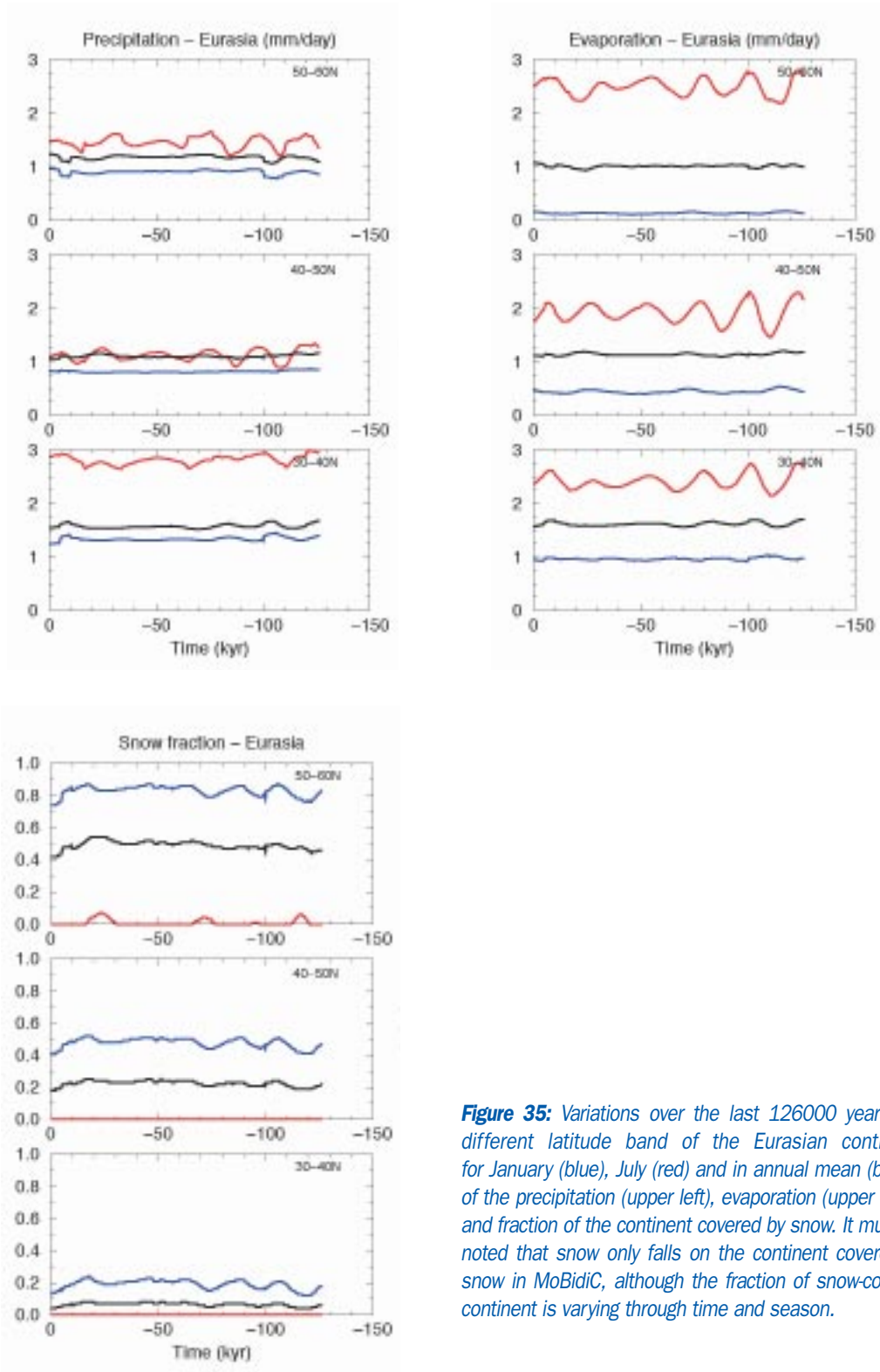


Figure 35: Variations over the last 126000 years, for different latitude band of the Eurasian continent, for January (blue), July (red) and in annual mean (black), of the precipitation (upper left), evaporation (upper right), and fraction of the continent covered by snow. It must be noted that snow only falls on the continent covered by snow in MoBidiC, although the fraction of snow-covered continent is varying through time and season.



4. BIOCLIM experiments for the next 200 kyr

4.1. - Brief description

Several simulations covering the next 200 kyr were performed using both CLIMBER-GREMLINS and MoBidiC. Rule-based downscaling of the MoBidiC simulations has been applied to provide regional climate estimates for the different regions of interest [Ref.33], while statistical downscaling has been used with CLIMBER-GREMLINS output [Ref.85].

The orbital forcing, the CO₂ forcing, and the initial conditions were identified by the BIOCLIM partners on the basis of preliminary experiments performed by the LLN 2D NH climate model. All these experiments have been forced with the same insolation distribution (Figure 36). The insolation varies in time and in latitude according to Berger [Ref.42]. The major feature of the insolation over the next few tens of thousands of years is the small amplitude of its variations (Figure 36, top). For example, the amplitude of the long-term variations of the mid-month insolation at 65°N in June is less than

30 Wm⁻² from 0 to 50 kyr AP. The variation rises to 90 Wm⁻² at the end of the study interval. The model is also forced by the atmospheric CO₂ concentration. Three scenarios for the future CO₂ concentration were selected from amongst those presented in BIOCLIM Report D3 [Ref.1] (Figure 36, bottom). They correspond to a natural scenario (A4a), a scenario including a low fossil fuel contribution in addition to the natural CO₂ variations (B3) and a scenario including a high fossil fuel contribution (B4). The simulations start with the present-day ice sheets and the ice sheets evolve according to climate change. For MoBidiC, the thermohaline circulation for the initial ocean is slightly reduced compared with the equilibrium experiment for the present climate (section 3.1.1). The southward transport of NADW at 27.5°S amounts to 9.5Sv. For CLIMBER-GREMLINS, the initial conditions are those of an equilibrium control experiment (5000 years under 280 ppmv CO₂).

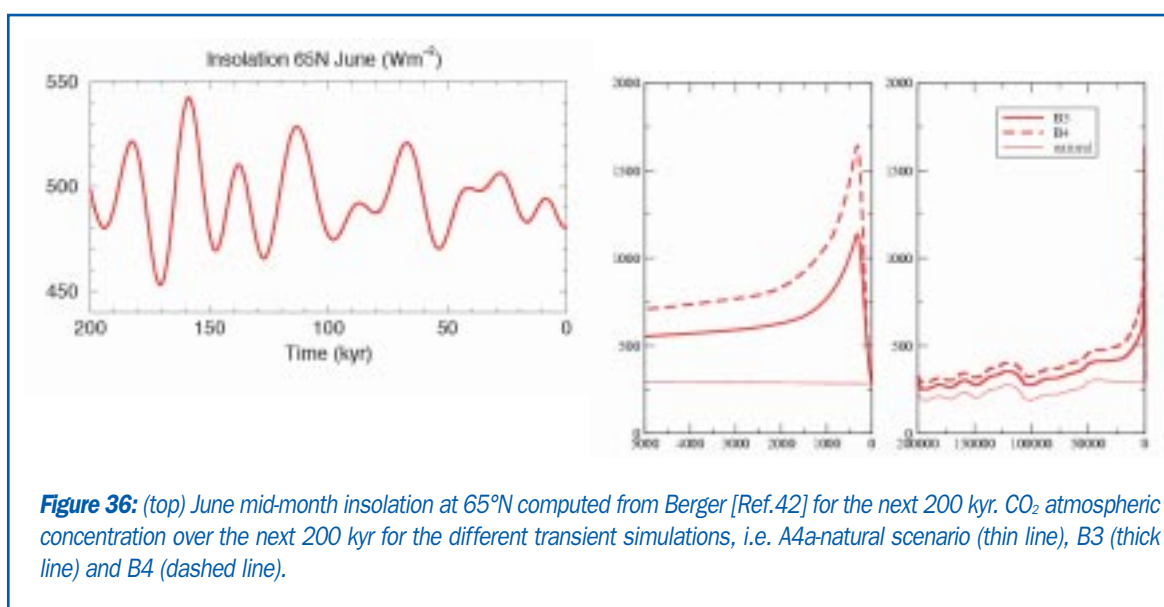


Figure 36: (top) June mid-month insolation at 65°N computed from Berger [Ref.42] for the next 200 kyr. CO₂ atmospheric concentration over the next 200 kyr for the different transient simulations, i.e. A4a-natural scenario (thin line), B3 (thick line) and B4 (dashed line).

Simulation A4a, outlined in BIOCLIM Report D3 [Ref.1], can be considered as a reference scenario for the next 200 kyr. It includes both dates selected for the snapshot, although the CO₂ concentration is lower. It could serve as a basis for the statistical downscaled future climate because the A4a simulated climate will not be drastically different from the climate that

occurred over the last few glacial-interglacial cycles. Scenario B3 allows assessment of the effect of human activities on climate during transient simulations. It also allows a comparison to be made between snapshot and transient climate simulation. Simulations forced with scenario B4 address the question of a more drastic impact of human activities on climate.

Insolation	computed for 0 to 200 kyr AP	
CO ₂ concentration	A4a - Paillard's model a B3 - Paillard's model a + low fossil fuel contribution B4 - Paillard's model a + high fossil fuel contribution	
Initial conditions	CLIMBER-GREMLINS MoBidiC	End of equilibrium experiment at present (see Table 2) From equilibrium experiment at present (see Table 2) + reduced NADW compared to snapshot at present. Present-day ice-sheets

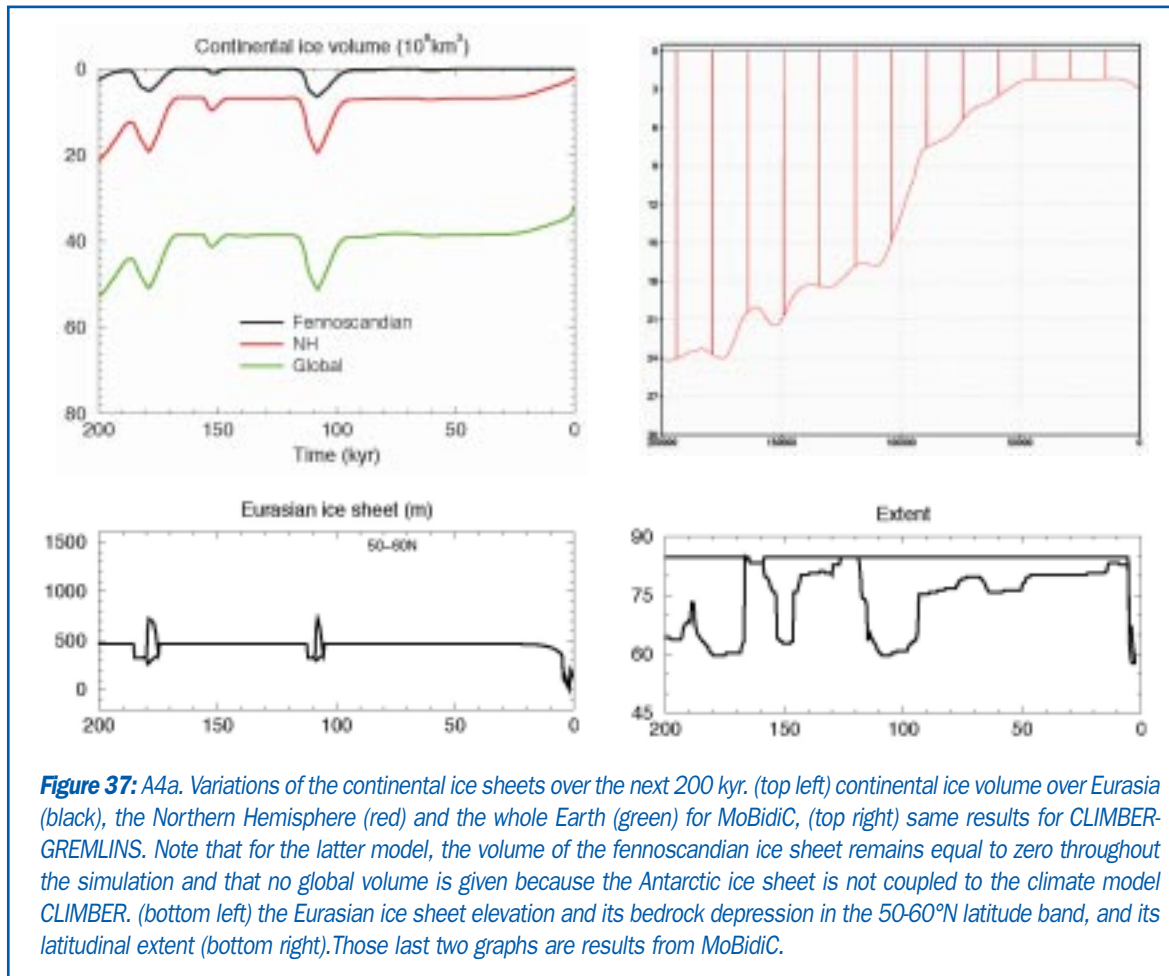
Table 4: Summary table of the experiment undertaken

4.2. - The natural scenario – A4a

The CO₂ scenario used in this simulation is characterised by relatively high values (larger than 290 ppmv) over the next 50 kyr. Then atmospheric CO₂ concentrations decrease regularly towards a minimum value of 190 ppmv reached at

100 kyr AP. The next maximum (276 ppmv) is reached at 122 kyr AP. Atmospheric CO₂ concentrations then show a general decreasing trend, on which some variations of small amplitude are superimposed (Figure 36).

4.2.1 - Ice sheets



The Northern Hemisphere continental ice volume simulated with MoBidiC (Figure 37) shows maximum of ice volume similar in magnitude and timing to the equivalent simulation with the LLN 2-D NH model [Ref.1]. However the Greenland ice sheet is more stable than in the previous simulation. Its volume remains at $\sim 6.6 \cdot 10^6 \text{ km}^3$ during most of the simulation. This is clearly a shortcoming of the model, although it does not prevent it simulating glacial inception. Maxima of ice occur at 108 kyr AP ($19.5 \cdot 10^6 \text{ km}^3$), 152.5 kyr AP ($9.6 \cdot 10^6 \text{ km}^3$) and 179 kyr AP ($19.1 \cdot 10^6 \text{ km}^3$). This is hardly the amount of continental ice simulated during MIS3, far from the maximum amount of continental ice simulated at the LGM ($\sim 40 \cdot 10^6 \text{ km}^3$). The Eurasian ice sheet rarely extends south of 60°N (Figure 37). It happens only twice over the next 200 kyr, i.e. from

105.5 kyr AP to 109 kyr AP and from 175 kyr AP to 180 kyr AP.

The results from CLIMBER-GREMLINS are quite different: glaciation on the American continent starts shortly after 50 kyr AP and continues until the end of the simulation. At the times that ice sheets appear in MoBidiC, the ice sheet grows faster in CLIMBER-GREMLINS, but the difference is that it never melts completely in the latter model. At the end of the simulation, the ice volumes over America are comparable in both models. In CLIMBER-GREMLINS, no ice grows over the Eurasian continent. This shortcoming is linked to relatively warm temperatures in the north Atlantic off Scandinavia.

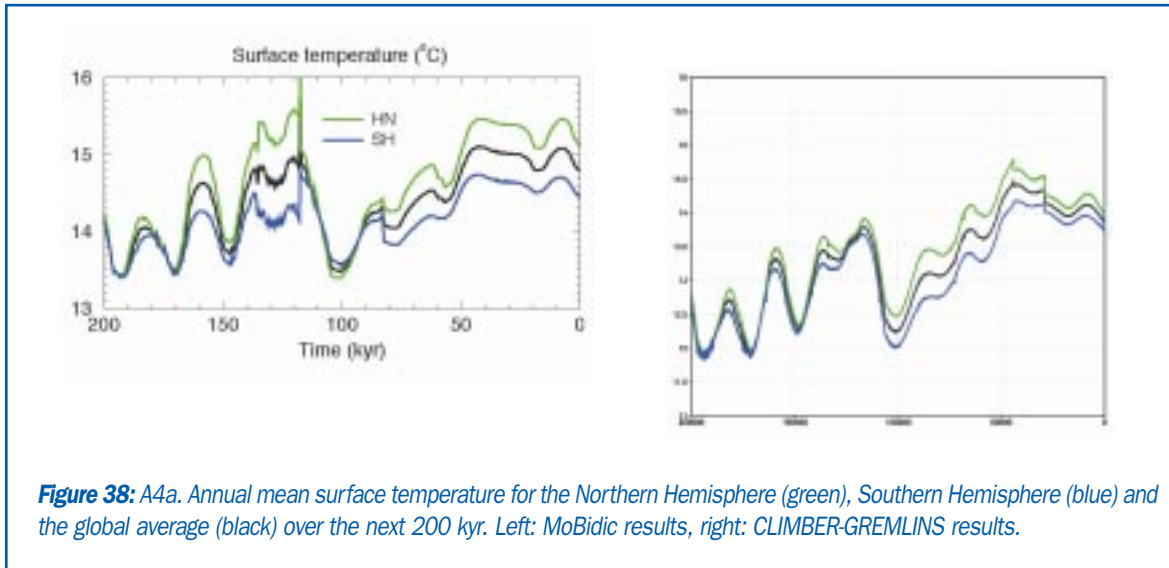
4.2.2 - Surface temperature

In MoBidiC, the surface temperature over the next 200 kyr is always higher than 13.4°C in annual mean (for each hemisphere as well as in global mean) (Figure 38). As for the past, the annual mean surface temperature exhibits larger variations in the Northern Hemisphere (2.8°C) than in the Southern Hemisphere (1.4°C). In term of the global mean, the amplitude of these variations is 2.1°C. The coldest temperatures are similar to the coldest temperatures simulated during Marine Oxygen Isotope Stage 4 (MIS4) and early MIS3. Except for an abrupt event, at 117.5 kyr AP, the warmest temperature over the next 200 kyr is 15.6°C (NH), 14.8°C (SH), 15.1°C(global). These warmest temperatures are of the same order as for the last glacial-interglacial cycle. Both continental ice volume and temperatures tend to show that the climate of the next 200 kyr is globally warmer than the climate of the last glacial-interglacial cycle. The reason for this behaviour should be looked for in the forcings. Over the next 50 kyr the variations in insolation are small. Therefore the impact of CO₂ on climate is reinforced at that time, which is characterised by high CO₂ concentration. Consequently, the model is driven towards a warm climate. Simultaneously with the decrease in CO₂ concentration, summer insolation increases. In other words the forcings are acting against each other and the climate remains in a warm state. When CO₂ concentration reaches its minimum, insolation is still large and the climate cannot be forced towards strong glaciation, although the impact of the reduction in CO₂ concentration can be recognised through a global cooling of ~ 1.3°C from 50 kyr AP to 100 kyr AP and a weak glaciation. Then both insolation and CO₂ increase, leading to a rapid warming. The following coolings occur with the simultaneous minimum in summer insolation and CO₂ concentration. It must be kept in mind that atmospheric CO₂ concentration is prescribed and taken as an external forcing of the model, although it is part of the climate

system. Therefore some inconsistencies could have been introduced and the phase relationship between insolation and CO₂ concentration could be artificial.

CLIMBER-GREMLINS simulates a different temperature evolution for the next 200 kyr. The global average, as well as the Northern and Southern Hemisphere averages, show a decreasing trend over the length of the simulation. This is due to the fact that shortly after 50 kyr AP, contrary to MoBidiC, CLIMBER-GREMLINS simulates the start of a glaciation. So, the models do not react to the competing factors of increasing insolation and decreasing CO₂ in the same way: for MoBidiC, the insolation factor prevents a durable glaciation, whereas in CLIMBER-GREMLINS it does not – except over Scandinavia. Moreover CLIMBER-GREMLINS is more sensitive to CO₂ concentration changes than MoBidiC. Therefore, the decrease in CO₂ concentration starting at 50 kyr AP has a larger impact on temperature in CLIMBER-GREMLINS than in MoBidiC. From then on, as the ice builds up in the CLIMBER-GREMLINS simulation, temperatures decrease. We can recognise similar variabilities on the Milankovitch time scales in the simulations from both models (cold periods around 100 kyr AP, shortly before 150 kyr AP, and at 170 and 190 kyr AP, warm periods between 120 and 140 kyr AP, around 160 kyr AP and 185 kyr AP) but a decreasing trend is added to the CLIMBER-GREMLINS results. This results in the maximum temperatures being reached at around 40 kyr AP in the CLIMBER-GREMLINS simulation, whereas they are reached at 120 kyr AP in the MoBidiC run.

We can also note that in the CLIMBER-GREMLINS simulation, as in the MoBidiC simulation, there also is an “abrupt” event in the 200 kyr run, at around 30 kyr AP (and therefore not at the same time as in the MoBidiC run). These events are discussed later in the section.



In both models, the summer temperature variations over the Eurasian (Figure 40) continent are closely related to the insolation variations. In particular, the variations are smaller over the next 100 kyr than after 100 kyr AP. For example, in MoBidiC in the 40-50°N latitude band, the continental July temperature variations are 5.6°C over the next 100 kyr; the amplitude of these variations reaches 10°C over the next 200 kyr. In annual mean, the zonally averaged temperature is showing behaviour similar to the global temperature, i.e. first a rather constant temperature over the next 50000 years, then a general decreasing trend until 100 kyr AP (~1.9°C in 50 kyr in the 40-50°N latitude band). From 100 kyr AP to 200 kyr AP, these temperatures experience larger oscillations (1.9°C in 26 kyr in the 40-50°N latitude band). This behaviour, described for MoBidiC, is also found in CLIMBER-GREMLINS results. Although the Northern Hemisphere average shows a marked decreasing trend as the simulation progresses, this is mainly caused by the

glaciation of America and cannot be found in the evolution of temperatures over Eurasia.

The abrupt event identified in the MoBidiC global and hemispheric annual mean temperatures shows up very clearly in Atlantic temperatures, especially in the 50-60°N latitude band (Figure 40). In these latitudes, there is a jump from an annual mean temperature of 4.5°C before 100 kyr AP to 6.5°C after 120 ky AP. A jump of similar amplitude appears at every month of the year. In fact, this event is characterised by a gradual winter cooling, which has already started at 50 kyr AP. From 100 to 110 kyr AP, summer temperatures slightly increase and then suddenly drop by 3°C at 112 ky AP. Then summer and annual mean temperatures start again to increase, first slowly over the next 5 kyr, and then rapidly (more than 5°C in less than 1000 years between 117 and 118 kyr AP). Winter ocean temperature shows an even stronger warming of more than 7°C.

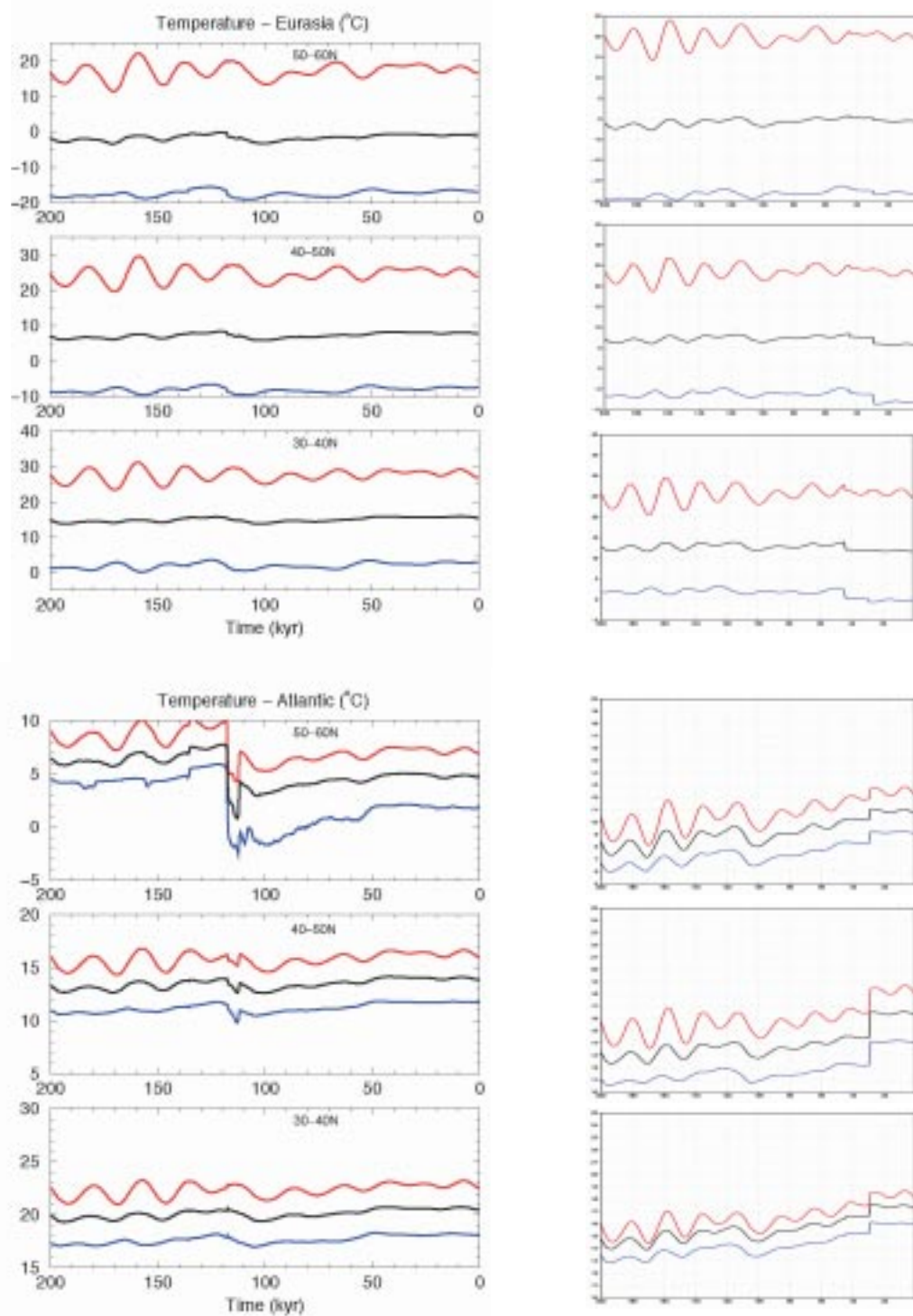


Figure 39: A4a. Variations over the next 200 kyr of the simulated temperature for the Eurasian continent (top) and the Atlantic Ocean (bottom), for three latitude bands, in January (blue), in July (red) and in annual mean (black). Results for MoBidiC on the left, for CLIMBER-GREMLINS on the right.

The abrupt temperature changes in the high latitudes of the Northern Atlantic Ocean are associated with a change in the thermohaline circulation (Figure 42). The export of NADW is almost stable over the next 100 kyr (~9 Sv). At 112.5 kyr AP there is a nearly complete collapse of the thermohaline circulation (export of NADW = 4 Sv) followed by an increase (export of NADW = 18 Sv from 117 to 135 kyr AP) and at last a stabilisation at 12 Sv, this last value being slightly higher than in the first part of the simulation. These changes in the strength of the thermohaline circulation are also accompanied by changes in the convection sites. At the beginning of the simulation, the northward convection sites are located in the 50-55°N latitude band. Simultaneously with the cooling and the reduction of the thermohaline circulation (THC) the convection site in the 50-55°N band is suppressed. When THC resumes, convection sites are located up to 65-70°N. These northern sites of convection are suppressed after 135 kyr AP. Different causes can be put forward to explain these abrupt events. Changes in THC can be related to changes in the density of the water masses (either through salinity or temperature). The large amount of fresh water discharged from the melting ice sheets strongly modifies the density in the Northern Atlantic, where deep water forms. In turn, this

can lead to a disruption of the THC. However in this simulation, the ice sheets are small and the fresh water discharge is probably not large enough to induce large changes in THC. Another candidate is related to the sea ice cover. It appears that long before the abrupt event the winter SSTs decrease, leading to an increase of sea-ice cover, especially in winter when deep convection takes place. If the ocean is largely covered by ice, convection is disabled and THC can be strongly affected.

CLIMBER-GREMLINS also simulated such an abrupt event, which shows as 0.3°C warming in the Northern Hemisphere mean temperature (Figure 38), as a small warming in the Eurasian temperatures in the 40-50N belt (Figure 40), but as a marked cooling in the North Atlantic SSTs (Figure 40, cooling of about 2°C in the 40-50°N belt). One can relate such abrupt changes to a jump in the North Atlantic overturning circulation (Figure 42), but the decrease in the North Atlantic SSTs is counterintuitive. In fact, the sea ice extent over this area increases and this appears to favour deep convection and therefore an increase of the THC. Thus, a decrease in the North Atlantic SSTs occurs at the same time as an increase in the temperature average for the Northern Hemisphere.

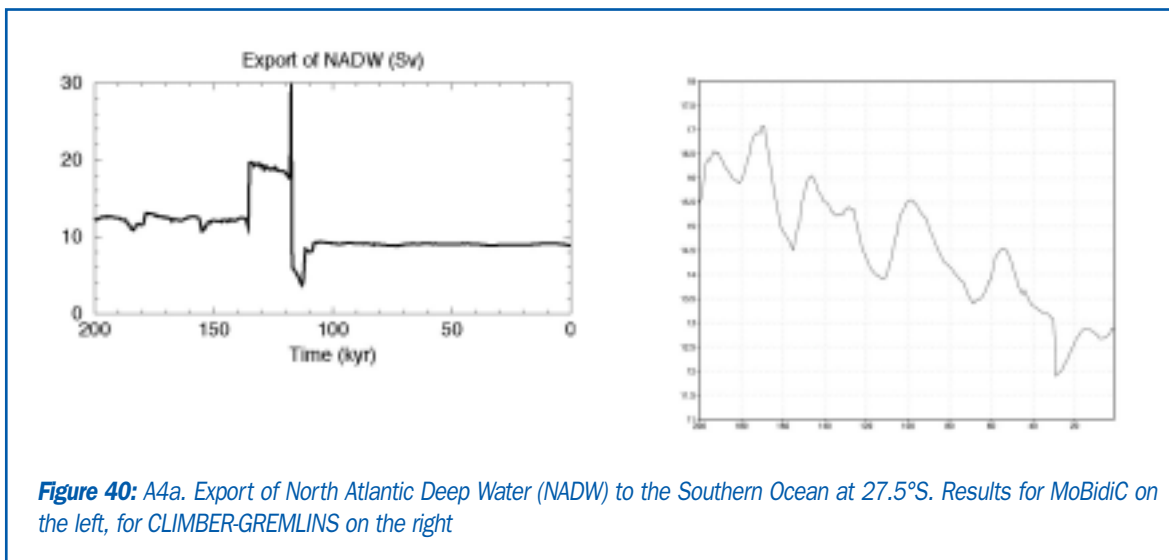


Figure 40: A4a. Export of North Atlantic Deep Water (NADW) to the Southern Ocean at 27.5°S. Results for MoBidiC on the left, for CLIMBER-GREMLINS on the right

4.2.3 - Vegetation

In the MoBidiC simulation, vegetation undergoes large variations over the next 200 kyr (Figure 44), especially in the northern latitudes. In contrast, vegetation changes over the next 100 kyr in mid latitudes (30-50°N latitude band) are much smaller. In the 50-60°N latitude band, vegetation changes are controlled by both temperature and precipitation. In mid-latitudes precipitation constrains vegetation much more than temperature.

In CLIMBER-GREMLINS, there are abrupt changes in the vegetation cover, at 30 kyr AP for the 40-50°N and 50-60°N belts, and at around 45 kyr AP for the 30-40°N belt. It is not very easy to explain these step-like changes. However, they seem to be connected to precipitation changes more than to temperature changes, because the former are much larger than the latter. However, changes in precipitation and evaporation are also caused by these changes in vegetation cover, which is obvious from Figure 46 and Figure. So, rather than inputting vegetation changes to precipitation or temperature, or evaporation and precipitation changes to changes in vegetation, one can say that at the time of these abrupt changes, the model jumps into a different state that is characterised by slightly higher temperatures, increased evaporation (favoured by the larger forest area) and increased precipitation (by local recycling, increased evaporation

is directly connected to increased precipitation).

After these large and abrupt changes, one can easily see the imprint of orbital variations in the vegetation of the northernmost belt, as is the case in MoBidiC. As for the latter model, there are virtually no variations in forest cover in the 30-40°N band after the change of climatic state. The variations of forest cover on orbital variation timescales are actually in opposite senses in the two models. This is particularly obvious from the curves for the 40-50°N latitude belt in the second half of the simulation. This appears to be linked to variations in the hydrological cycle (next section), which exhibit similar behaviour.

The vegetation cover is a good way to assess the differences between the two models because it is computed in exactly the same way in both models (using the VECODE module, developed in Potsdam). By comparing vegetation cover, one can compare the impact of temperature and precipitation changes. In CLIMBER-GREMLINS, from the timing of the changes compared to insolation variations, one can see that it is changes in the hydrological cycle that are closely related to tree fraction changes. In MoBidiC, both changes in the hydrological cycle and in temperatures can be related to tree fraction variations.

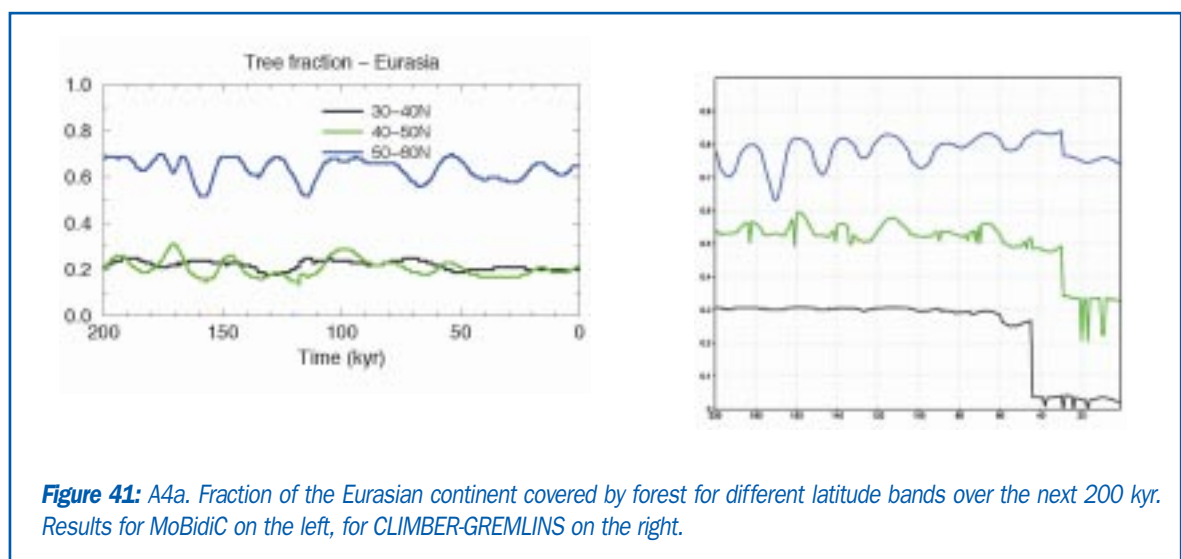


Figure 41: A4a. Fraction of the Eurasian continent covered by forest for different latitude bands over the next 200 kyr. Results for MoBidiC on the left, for CLIMBER-GREMLINS on the right.

4.2.4 - Precipitation, evaporation and snow cover

In both models, and apart from the abrupt changes in the CLIMBER-GREMLINS simulation, changes in precipitation (Figure 46) and evaporation (Figure 47) are very small in winter, and the global mean is determined by the summer changes. However, the hydrological cycle does not vary in the same way in both models. In the last 100 kyr of the simulations, when variations are largest, they appear to be inversely correlated. In CLIMBER-GREMLINS, variations in evaporation appear to be directly linked to variations in temperature (there is more evaporation when it is warmer) and variations in precipitation follow those in

evaporation, as if they were determined by available moisture from the underlying surface. In contrast, in MoBidiC, there is more precipitation when it is colder. In this case, it could be that the changes are controlled by an increase in the meridional temperature gradient, which would force more diffusion of heat and water from the Equator toward the North Pole. Evaporation varies in the same way as precipitation. Its variations can be seen as a consequence of the precipitation variations, since they cannot be related to temperature variations in a simple way.

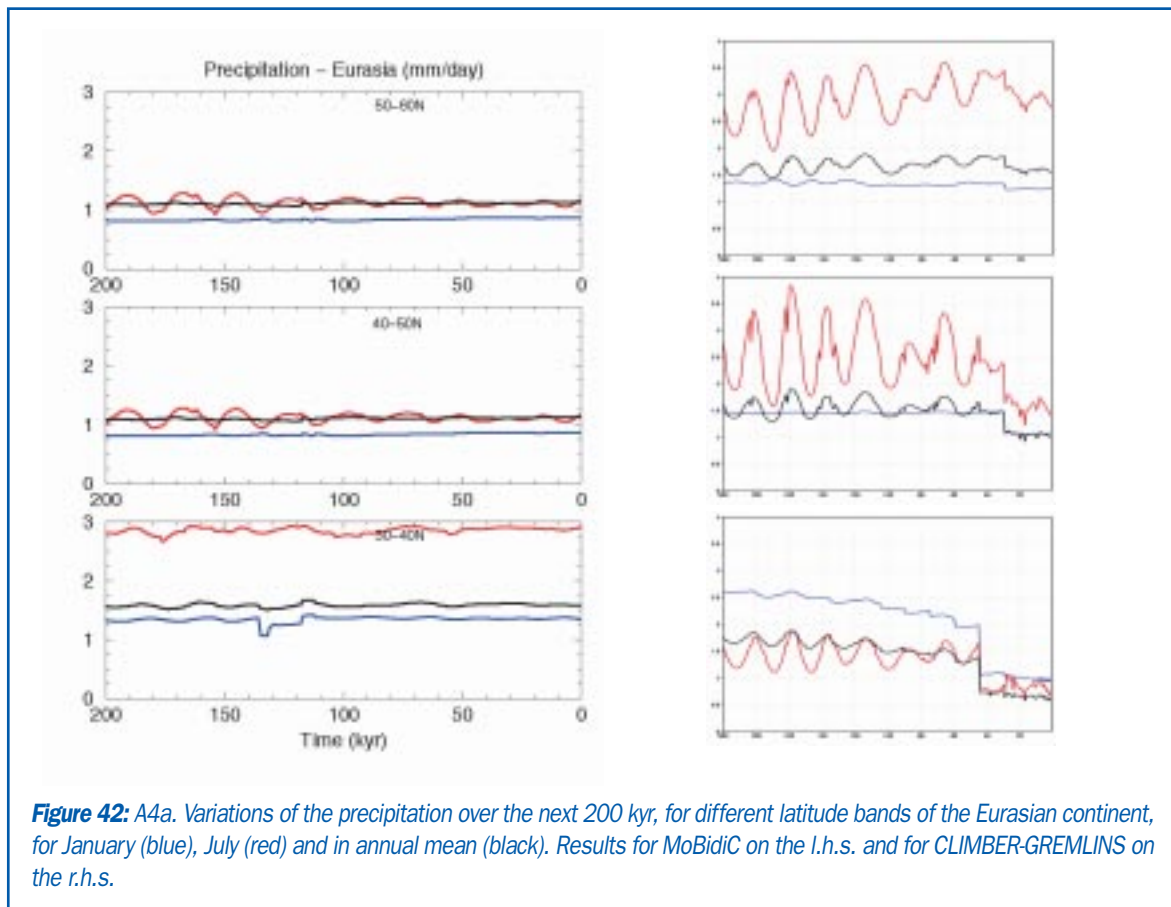


Figure 42: A4a. Variations of the precipitation over the next 200 kyr, for different latitude bands of the Eurasian continent, for January (blue), July (red) and in annual mean (black). Results for MoBidiC on the l.h.s. and for CLIMBER-GREMLINS on the r.h.s.

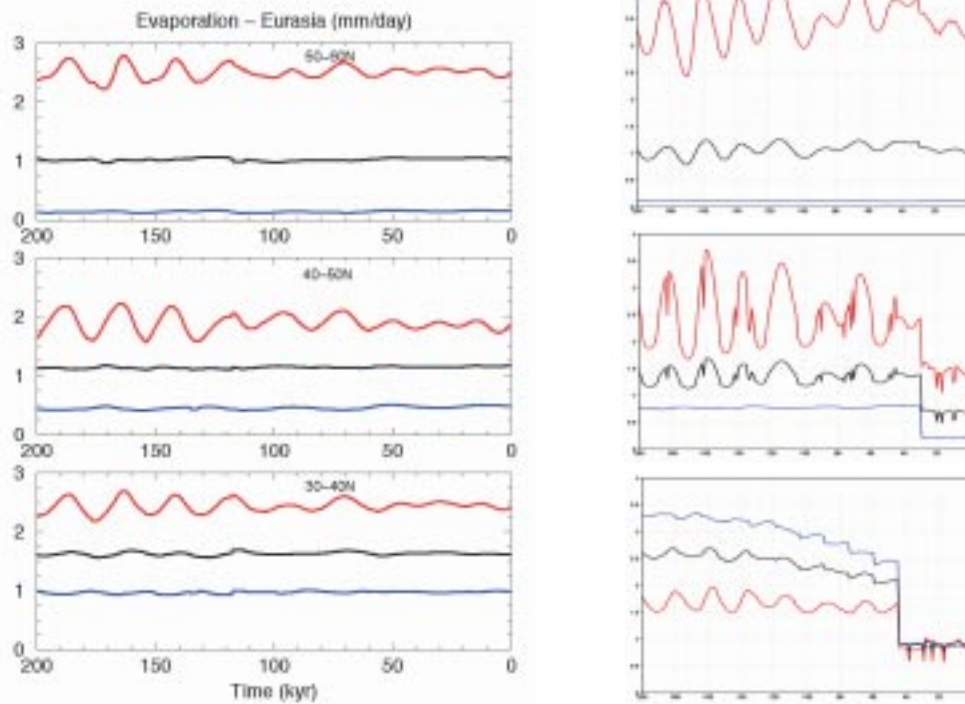


Figure 43: A4a. Variations of the evaporation over the next 200 kyr, for different latitude bands of the Eurasian continent, for January (blue), July (red) and in annual mean (black). Results for MoBidiC on the l.h.s. and for CLIMBER-GREMLINS on the r.h.s.

The larger amplitude precipitation variations in CLIMBER-GREMLINS play a role in the larger variations in the snow cover. However, the temperature variations are also important, since more precipitation falls as

snow when it is colder. Both reasons link the snow cover to orbitally induced variations. These are much less visible in the results from MoBidiC, probably because the variations in precipitation are not so large.

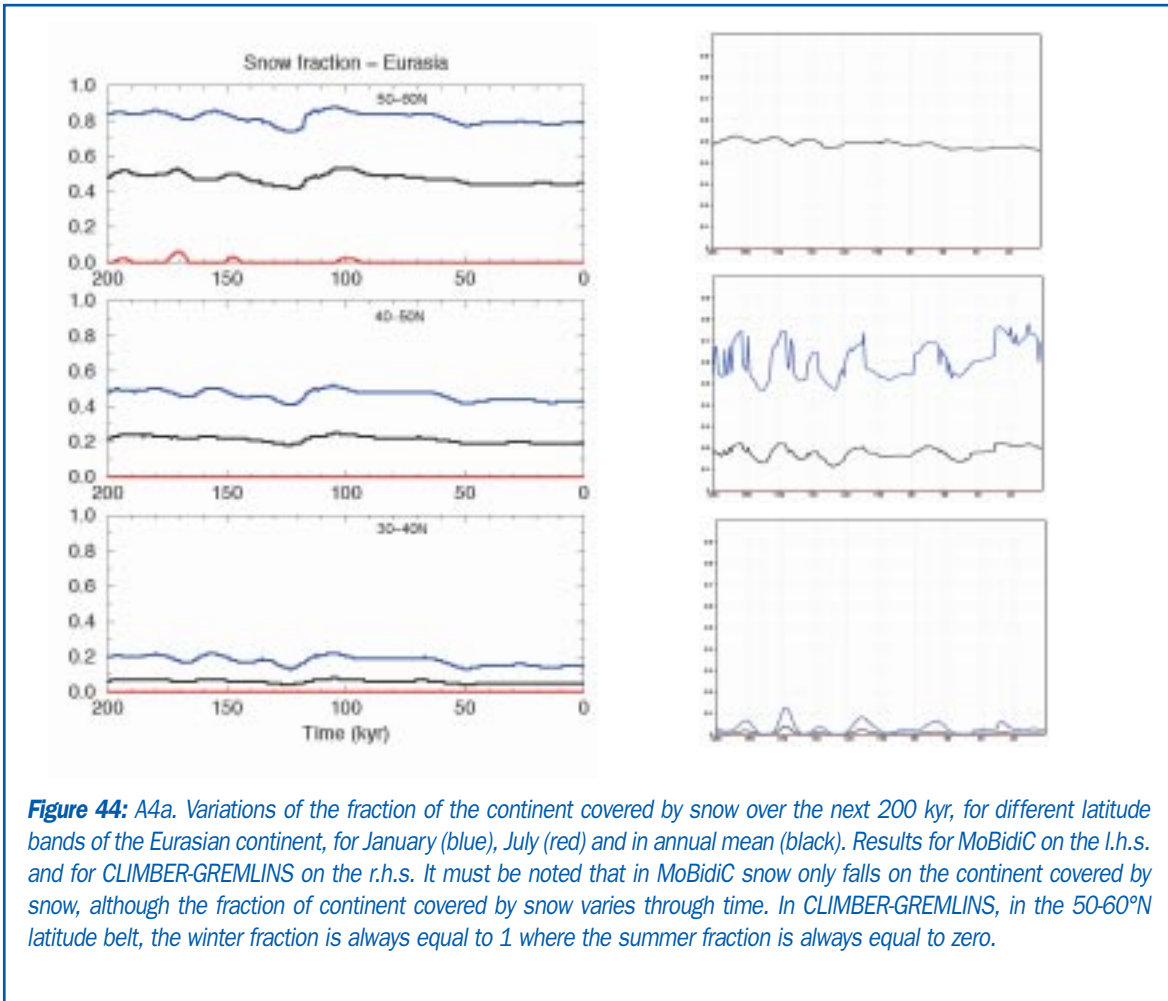


Figure 44: A4a. Variations of the fraction of the continent covered by snow over the next 200 kyr, for different latitude bands of the Eurasian continent, for January (blue), July (red) and in annual mean (black). Results for MoBidiC on the l.h.s. and for CLIMBER-GREMLINS on the r.h.s. It must be noted that in MoBidiC snow only falls on the continent covered by snow, although the fraction of continent covered by snow varies through time. In CLIMBER-GREMLINS, in the 50-60°N latitude belt, the winter fraction is always equal to 1 where the summer fraction is always equal to zero.

4.3. - Simulation “B3”

In addition to the natural CO₂ scenario described above, the B3 scenario (Figure 36, bottom) assumes that fossil fuel burning will contribute to an increase in the natural CO₂ concentration in the atmosphere. The B3 simulation assumes a 'low' fossil fuel contribution. Nevertheless, this anthropogenic contribution will add 850 ppmv at 325 yr AP to the natural concentration. Moreover, there is still a non-natural contribution of 50 ppmv at 200 kyr AP. Therefore, it is expected that the simulated climate will

be warmer than the A4a climate throughout the simulation. Nevertheless the impact of the fossil fuel contribution should be larger at the beginning of the simulation than towards its end. On the other hand, the system also retains a memory of its past. So, the climate after 100 kyr AP could be warmer than a climate simulated with a small increase (~60 ppmv) in atmospheric CO₂ concentration from the present to 200 kyr AP.

4.3.1 - Ice sheets

In accordance with the discussion above, the Northern Hemisphere remains free of continental ice most of the time during the next 200 kyr (Figure 50) in the simulations made using both models. However, in CLIMBER-GREMLINS, Greenland melts more slowly (in about 40 kyr) than in MoBidiC (a few thousand years). Some ice accumulates over Greenland at 108 kyr AP ($1.6 \times 10^6 \text{ km}^3$ for MoBidiC, $4 \times 10^4 \text{ km}^3$ for CLIMBER-GREMLINS) and at 151 kyr AP ($0.7 \times 10^6 \text{ km}^3$ for MoBidiC, $7 \times 10^4 \text{ km}^3$ for CLIMBER-GREMLINS). Moreover, starting from 167 kyr AP, the different Northern Hemisphere continental ice sheets start to accumulate. However, in MoBidiC the amount of continental ice at 175.5 kyr AP is smaller ($11.2 \times 10^6 \text{ km}^3$) than in A4a ($18.9 \times 10^6 \text{ km}^3$ at 179.5 kyr AP) and the Eurasian ice sheet never extends

southward of 60°N over the next 200 kyr. In CLIMBER-GREMLINS, the ice volume reached at 200 kyr AP is much smaller than in MoBidiC and no ice grows over Fennoscandia. Although this has not been shown through the experiments of Section 3., we have noticed that although the model “keeps” the Fennoscandian ice sheet when it is given as an initial condition in an LGM equilibrium simulation, it is very difficult for the model to build this ice sheet by itself. We are currently examining why this is the case. However, we see this as a deficiency of the version of the model that has been used for BIOCLIM, a deficiency that has not been resolved at the time of writing. It is noteworthy that even though the simulated ice volumes are different in the two models, the time evolution of the ice sheets is the same, corresponding to the orbital forcing.

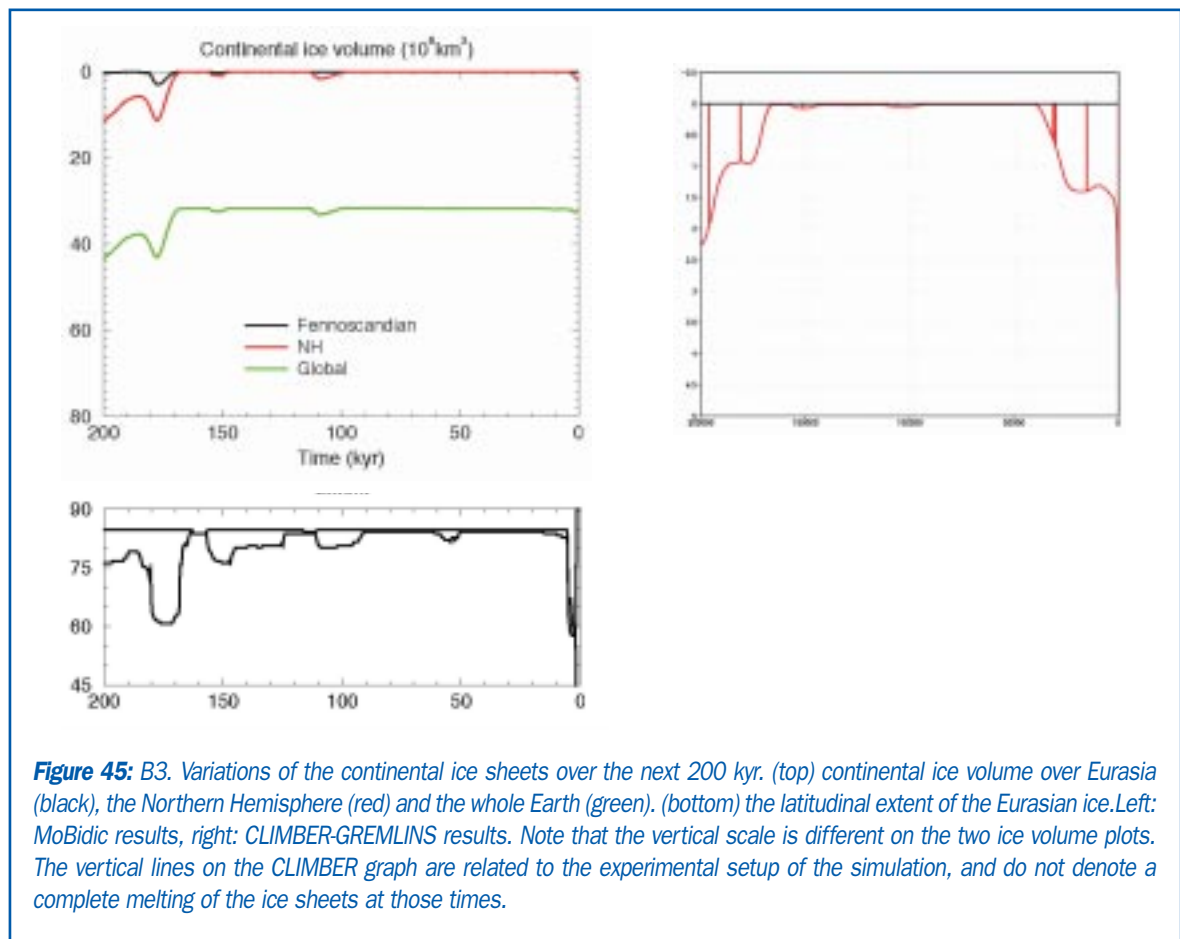


Figure 45: B3. Variations of the continental ice sheets over the next 200 kyr. (top) continental ice volume over Eurasia (black), the Northern Hemisphere (red) and the whole Earth (green). (bottom) the latitudinal extent of the Eurasian ice. Left: MoBidiC results, right: CLIMBER-GREMLINS results. Note that the vertical scale is different on the two ice volume plots. The vertical lines on the CLIMBER graph are related to the experimental setup of the simulation, and do not denote a complete melting of the ice sheets at those times.

Thus, an initial peak in CO₂ concentration results in drastic changes in the Northern Hemisphere ice cover over a time interval longer than the perturbation itself. Moreover, atmospheric CO₂ concentration remains above its natural values for the next 200 kyr (still 60 ppmv

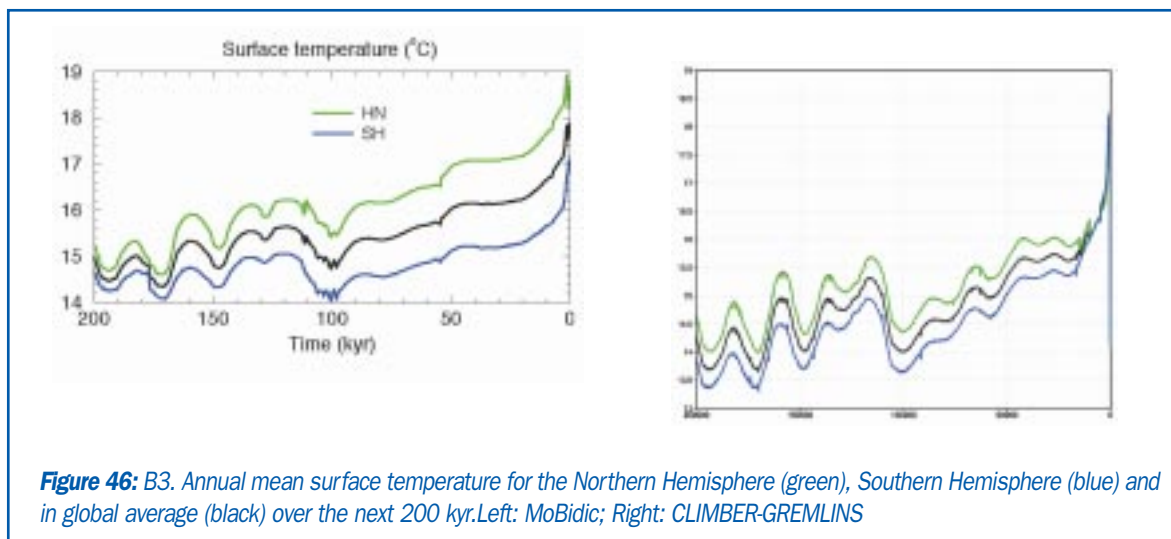
at 200 kyr AP). Both factors impact on the climate response. This is particularly the case in the CLIMBER-GREMLINS simulation, but it is also the case in the MoBidiC run, in which the ice sheet that initially melts takes almost 170 kyr to recover.

4.3.2 - Surface temperature

In MoBidiC, the large fossil fuel contribution to the natural CO₂ concentration induces an annual mean warming (with respect to A4a) of 3.0°C, 3.8°C, 2.2°C for the global average, over the Northern Hemisphere and over the Southern Hemisphere, respectively, over the next 1500 years (Figure 52). CLIMBER-GREMLINS simulates a warming of similar amplitude: 3.7°C in global average, 3.7°C for the Northern Hemisphere and 3.6°C in the Southern Hemisphere. The warming is slightly larger in CLIMBER-GREMLINS than in MoBidiC, this is in agreement with the larger sensitivity of CLIMBER-GREMLINS compared to MoBidiC to a doubling of the atmospheric CO₂ concentration. In MoBidiC, the larger response in the Northern Hemisphere than in the Southern Hemisphere is related to a sensitivity different over continents and oceans (see below).

still rapid cooling (0.013°C per kyr for MoBidiC, about 0.03°C/kyr for CLIMBER-GREMLINS) until 100 kyr AP. Temperatures reach a first minimum at 100.5 kyr AP. By that time, CLIMBER-GREMLINS has reached a mean annual temperature of 14°C, one degree cooler than MoBidiC, a difference that is maintained until the end of the simulations. In MoBidiC, this temperature minimum at 100 kyr AP is still 1.2°C warmer than in A4a. In CLIMBER-GREMLINS it is 1.6°C warmer than the A4a global average. After 100 kyr AP, any clear decreasing temperature trend becomes difficult to identify. Thus, global annual mean temperature is still 0.8°C warmer than in A4a at 200 kyr AP in MoBidiC, and 1.5°C warmer in CLIMBER-GREMLINS. Note that in both simulations, the Northern Hemisphere remains warmer than the southern one, and that whereas the temperature difference between the two hemispheres decreases with time in MoBidiC, it remains roughly constant in CLIMBER-GREMLINS, contrary to what happens in the A4a simulation (Figure 52).

Subsequently, surface temperatures show a very fast decrease (0.082°C per kyr for MoBidiC, even faster in CLIMBER-GREMLINS). This is followed by a slower but



In MoBidiC, the cooling trend over the next 200 kyr is larger in the Northern Hemisphere than in the Southern Hemisphere. This reflects the fact the Northern Hemisphere responds more strongly to changes in the climate forcing than the Southern Hemisphere. Indeed, there are large continental areas in the Northern Hemisphere, in particular in the northern latitudes, which are subject to different feedbacks, able to amplify the initial forcing. Ocean covers a major part of Southern Hemisphere, and there are only very small continental areas in high southern latitudes, with the exception of the Antarctic ice sheets. Therefore, climate changes are dampened, mostly because of the thermal inertia of the ocean. CLIMBER-GREMLINS does not seem to be so sensitive to this process, as the temperature trends in the Northern and the Southern Hemispheres are comparable.

Figure 54 shows the temperature evolution over latitudinal bands of the Atlantic and Eurasia. The initial peak in temperature does not appear on those figures because the data were not saved with the same frequency as the data shown on Figure 52. In CLIMBER-GREMLINS, the data is saved every 1000 years. In MoBidiC, most of the data are saved every 500 years. They are the mean over the last 500 years. But continental ice volume, global, Northern and Southern Hemisphere annual mean temperature, NADW export are saved every year although they are displayed with a 500 year step. In both models the cooling trend is slightly larger at high latitudes than at low latitudes

(Figure 54. In MoBidiC, it is $0.013^{\circ}\text{C}/\text{kyr}$ ($0.0075^{\circ}\text{C}/\text{kyr}$) in the $30\text{-}40^{\circ}\text{N}$ latitude band and it rises to $0.017^{\circ}\text{C}/\text{kyr}$ ($0.013^{\circ}\text{C}/\text{kyr}$) in the $50\text{-}60^{\circ}\text{N}$ latitude band over the Eurasian continent (Atlantic Ocean). In CLIMBER-GREMLINS, it is nearly 0 in the $30\text{-}40^{\circ}\text{N}$ and $40\text{-}50^{\circ}\text{N}$ latitude belts, and $0.017^{\circ}\text{C}/\text{kyr}$ in the $50\text{-}60^{\circ}\text{N}$ band over the Eurasian continent. Over the Atlantic, the cooling trend is larger than over the Eurasian continent: $0.026^{\circ}\text{C}/\text{kyr}$ for the two northernmost belts and $0.020^{\circ}\text{C}/\text{kyr}$ in the southernmost one. Despite the fact that CLIMBER-GREMLINS simulates colder SSTs than MoBidiC, the temperatures over Eurasia are remarkably similar for both models.

Except for this general cooling trend, the pattern of temperature change over Eurasia and the North Atlantic is similar to A4a (Figure 54). Moreover the mean values over the 200 kyr interval are larger in B3 than in A4a. This difference depends on both the latitude and the time in the year. In annual mean over the Eurasian continent, the warming related to the additional contribution of fossil fuel to the CO_2 concentration (B3 compared with A4) 1.5°C (1.2°C), 1.8°C (1.8°C), 2.0°C (1.9°C) respectively in the $30\text{-}40^{\circ}\text{N}$, $40\text{-}50^{\circ}\text{N}$ and $50\text{-}60^{\circ}\text{N}$ latitude band for MoBidiC (CLIMBER-GREMLINS). Moreover the difference is much larger at the beginning (3.0°C , 3.2°C , 3.0°C for MoBidiC, 1.8°C , 2.0°C , 2.5°C for CLIMBER-GREMLINS) than at the end (0.9°C , 1.1°C , 1.1°C for MoBidiC, 1.3°C , 1.7°C , 2.2°C for CLIMBER-GREMLINS) of the simulations.

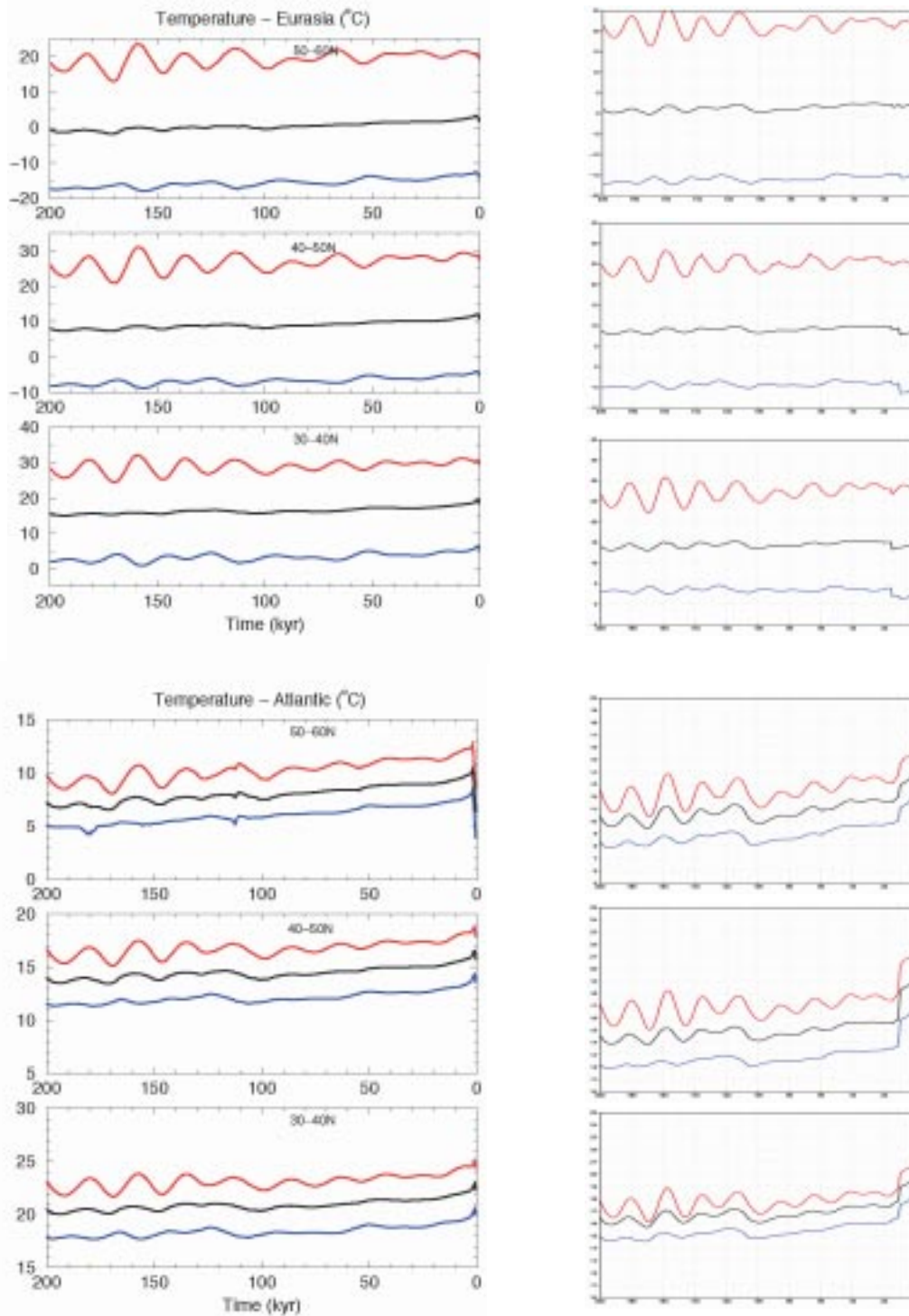
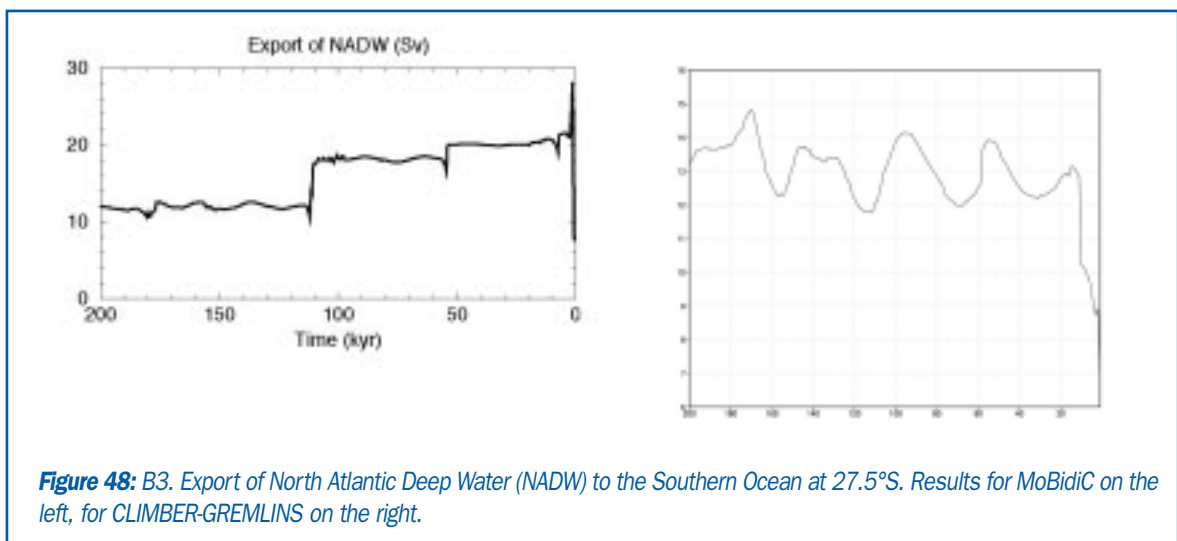


Figure 47: B3. Variations over the next 200 kyr of the simulated temperature for the Eurasian continent (top) and the Atlantic Ocean (bottom), for three latitude bands, in January (blue), in July (red) and in annual mean (black). Left: MoBidiC; right: CLIMBER-GREMLINS. Note: the vertical scales are not the same for both models

The behaviour of the thermohaline circulation is very different in the two models. In MoBidiC, the export of NADW is first increasing to 28 Sv, before experiencing a stepwise decrease over the next 200 kyr (Figure 56): over the next 54 kyr it remains stable at about 20 Sv. Then it decreases very slightly to ~18 Sv. At about 111 kyr AP, it undergoes a second decrease to a lower value of ~12 Sv. These changes in the thermohaline circulation cannot be recognised in Atlantic SSTs south of 50°N. In the 50-60°N latitude band, these epochs are marked by a very small cooling in the SST (0.2°C at 54 kyr AP and 0.4°C at 111 kyr AP). At 111 kyr AP, the cooling is stronger at the higher latitudes. This cooling is related to the southward shift of the convection sites. In CLIMBER-GREMLINS, the consequence of the large warming due to the initial CO₂ forcing is a significant decrease in NADW export. This was already documented by Rahmstorf and Ganopolski [Ref.86]. This export then starts to recover, first gradually and then abruptly, at around 15 kyr AP. Contrary to the results in MoBidiC, it then varies slowly on orbital time

scales but the amplitude of these variations is not very large (around 2 Sv). The relationship between the North Atlantic sea surface temperatures shown on Figure 54 and the thermohaline circulation variations shown on Figure 56 is not straightforward. In the early years of the simulation, while the thermohaline circulation decreases, the temperatures between 30 and 60°N are quite high, and when the thermohaline circulation recovers, the sea surface temperatures decrease very quickly to a value lower by up to several degrees Celsius. The decrease in SSTs expected during a slow down of the thermohaline circulation actually occurs at higher latitudes in the North Atlantic. When the thermohaline circulation slows down, the heat which is no longer brought to the high latitudes by the ocean is released in the 30-60°N region. This region is additionally warmed by the atmosphere. When the thermohaline circulation starts again, those latitudes suffer from a deficit of heat that is brought to higher latitudes again.



4.3.3 - Vegetation

In MoBidiC, in the 50-60°N latitude band the climate change related to the increase in atmospheric CO₂ concentration induces a reduction of the tree fraction (Figure 58, compared to Figure 44). It is about 10% at the beginning of the simulation but becomes much smaller after 110 kyr AP. Nevertheless, it

averages about 5% during the warmest phases. In the 40-50°N latitude band, the tree fraction remains almost unchanged over the next 100 kyr. There is a small increasing trend but the oscillations identified in the A4a simulation hardly appear. In the second half of the simulation, these oscillations reappear. However their

amplitude is smaller than in A4a and the tree fraction remains smaller than in A4a. The time evolution of the tree fraction in the 30-40°N latitude band is very similar in the A4a and B3 simulations, although the tree fraction is smaller (by ~5%) in the B3 simulation.

The results are quite different for CLIMBER-GREMLINS. As for the A4a scenario, there is a step-like variation at the beginning of the simulation that indicates a change in the climatic-vegetation state. This jump occurs much earlier in A4a than in B3. Contrary to MoBidiC, the tree fraction increases both in the 50-60°N and in the 40-50°N bands. It remains stable in the southernmost belt. The variations on orbital timescales are dampened

in the 50-60°N latitude band and amplified in the 40-50°N band, which appears to be much more sensitive than in the A4a scenario. These changes can be associated with the precipitation changes shown in the next section. Both models simulate an increase in precipitation in the two northernmost belts and nearly no change in the southernmost one, but the increase is much larger in CLIMBER-GREMLINS, which already had larger precipitation in the A4a simulation. In our opinion, this explains the differences between the tree fractions simulated by the two models, since temperatures are quite similar over Eurasia in the A4a as well as in the B3 scenario.

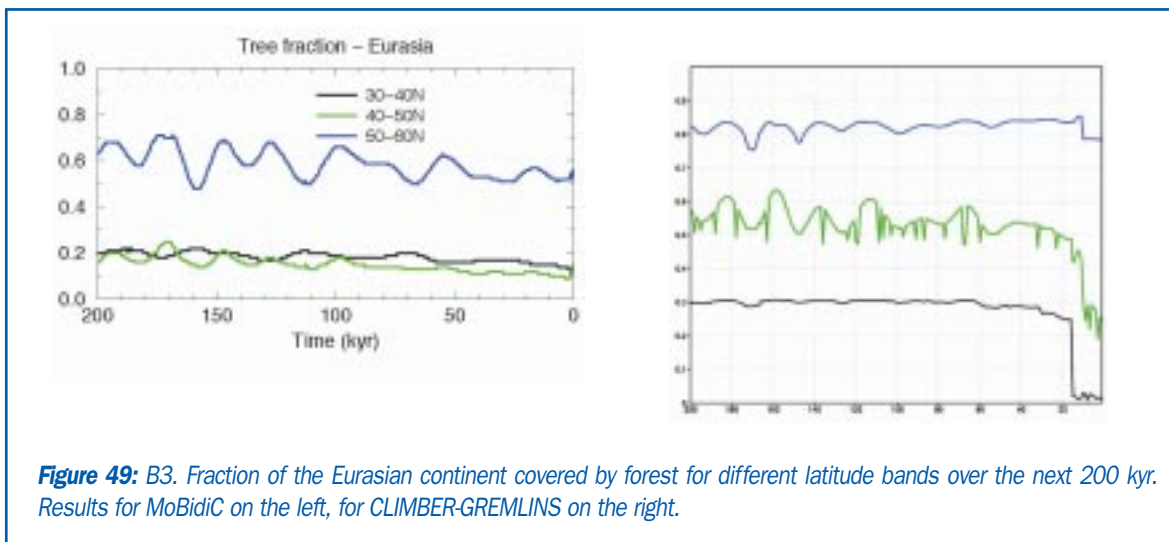


Figure 49: B3. Fraction of the Eurasian continent covered by forest for different latitude bands over the next 200 kyr. Results for MoBidiC on the left, for CLIMBER-GREMLINS on the right.

4.3.4 - Vegetation

As pointed out in the previous section, the changes in hydrological cycle are quite different in the two models. Whereas there is a slight increase, in B3 compared to A4a, in the precipitation simulated by MoBidiC, especially in the 50-60°N latitude belt, the increase is much larger in CLIMBER-GREMLINS in the 40-50°N and in the 50-60°N latitude

bands. We already noticed in the A4a simulation that the amplitudes of the orbital timescale variations are much larger in CLIMBER-GREMLINS than in MoBidiC. The fact that the increase in precipitation for increased CO₂ is larger in CLIMBER-GREMLINS is therefore not surprising. It confirms that the hydrological cycle in this model is more sensitive than the one in MoBidiC.

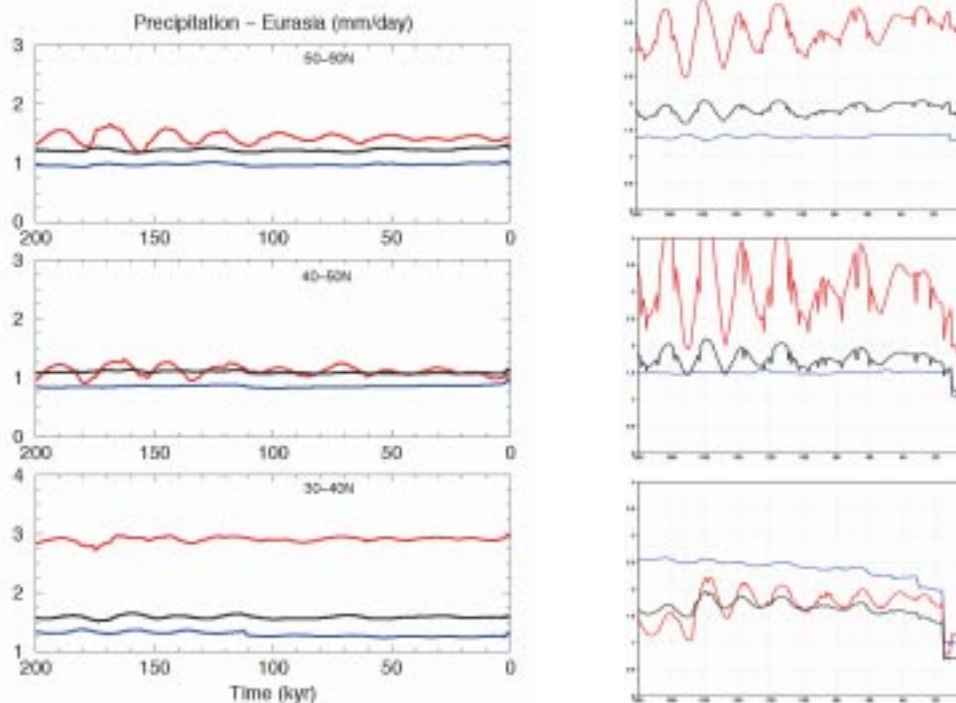


Figure 50: B3. Variations in precipitation over the next 200 kyr in the B3 scenario, for different latitude bands of the Eurasian continent, for January (blue), July (red) and in annual mean (black). Results for MoBidiC on the l.h.s. and for CLIMBER-GREMLINS on the r.h.s.

Like the precipitation, the evaporation is not very different in MoBidiC compared with the A4a scenario. In contrast, it increases between 40 and 60°N in CLIMBER-GREMLINS, like the precipitation. In the latter model, it is therefore the full hydrological cycle which is amplified in the anthropogenic scenario. As was explained for the variations in the A4a scenario, the

parameterisations of the hydrological cycle in the two models are very different and precipitation is sensitive to different variables in both models. The same distinction in mechanisms could explain the differences in the behaviour of the two models as far as the differences between the B3 and the A4a scenarios are concerned.

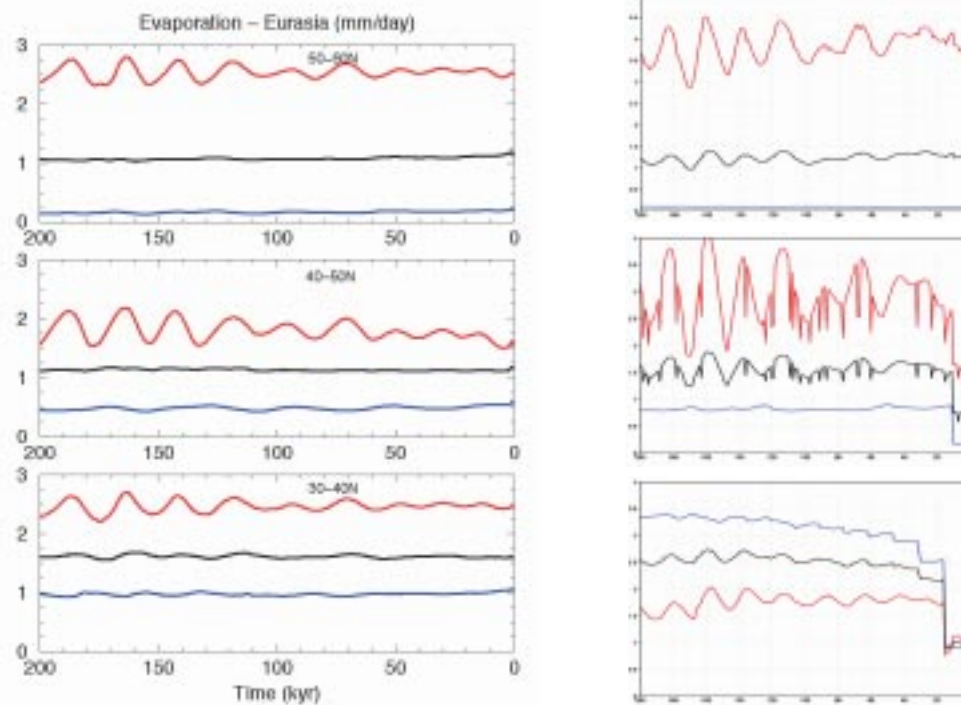


Figure 51: B3. Variations of the evaporation over the next 200 kyr, for different latitude bands of the Eurasian continent, for January (blue), July (red) and in annual mean (black). Results for MoBidiC on the l.h.s. and for CLIMBER-GREMLINS on the r.h.s.

The snow fraction, as expected from the forcing, decreases in the B3 simulation, compared with A4a, in both models. This is particularly the case at the beginning of the simulation, when the CO₂ forcing is largest. However, even by the end of the simulation, the

difference in snow fraction between B3 and A4a is small, except in the 40-50°N latitude belt in CLIMBER-GREMLINS, which we already noted to be the most sensitive latitude band in the B3 simulation.

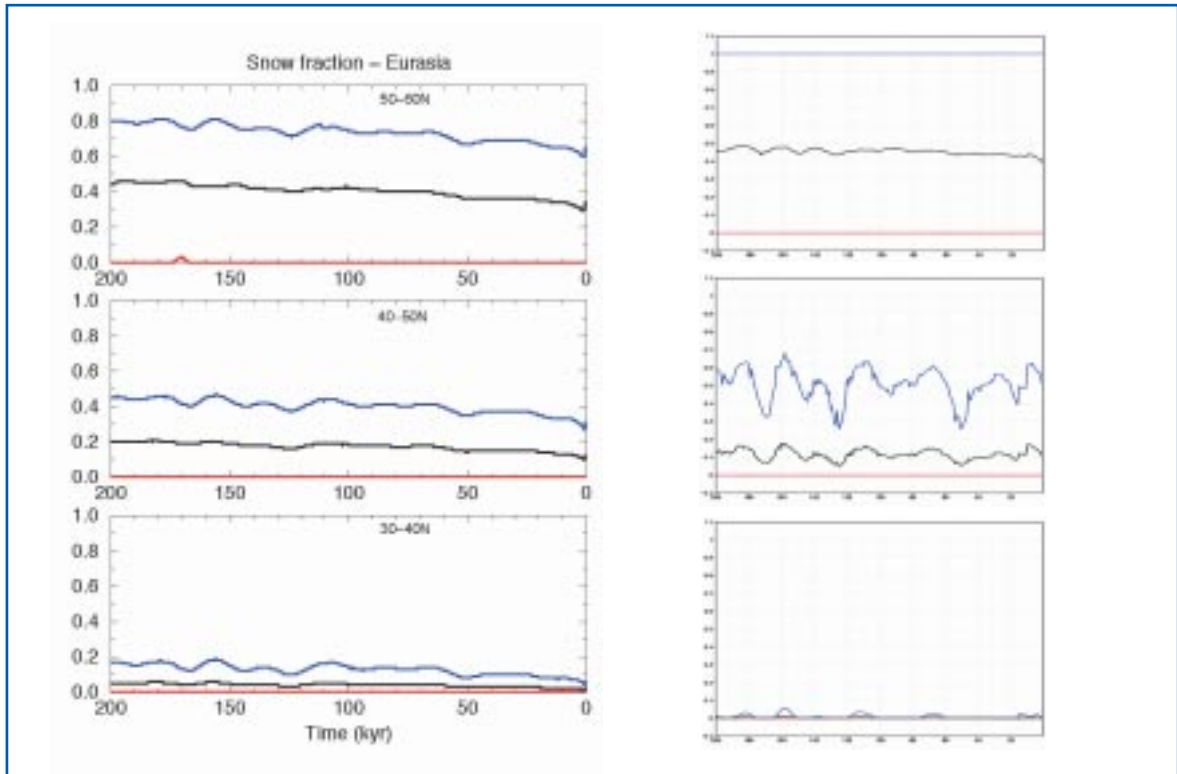


Figure 52: B3. Variations of the fraction of the continent covered by snow over the next 200 kyr, for different latitude band of the Eurasian continent, for January (blue), July (red) and in annual mean (black). Results for MoBidiC on the l.h.s. and for CLIMBER-GREMLINS on the r.h.s. It must be noted that in MoBidiC snow only falls on the continent covered by snow, although fraction of the continent covered in snow varies through time. In CLIMBER-GREMLINS, in the 50-60°N latitude belt, the winter fraction is always equal to one whereas the summer fraction is always equal to zero.

4.4. - Simulation “B4”

Similarly to the B3 scenario, the B4 scenario assumes that fossil fuel burning will contribute to an increase in the natural atmospheric CO₂ concentration (Figure 36, bottom). However B4 assumes a 'high' fossil fuel contribution. Indeed, this anthropogenic contribution will add 1350 ppmv at 325 Kyr AP to the natural concentration. Moreover,

there is still a non-natural contribution of 85 ppmv at 200 kyr AP. Therefore it is expected that the simulated climate will not only be warmer than the A4a climate but also than the B3 climate. Moreover, the fossil fuel contribution at the end of the simulation is still large enough to have a significant impact at that time.

4.4.1 - Ice sheets

In both models, the Northern Hemisphere continental ice sheets (Figure 63) fully melt after a few millennia. In MoBidiC, they do not significantly reappear before 168 kyr AP (there is a small accumulation, smaller than $0.02 \times 10^6 \text{ km}^3$ over the Eurasian ice sheet around 105 kyr AP). At 200 kyr AP, there is more than $5 \times 10^6 \text{ km}^3$ of continental ice in the

Northern Hemisphere, mostly over Greenland. In CLIMBER-GREMLINS, the ice sheets start reappearing by 170 kyr AP but never reach the present day volume before the end of the simulation. The climatic system therefore “remembers” the high peak of CO_2 at the beginning of the simulation for a very long time.

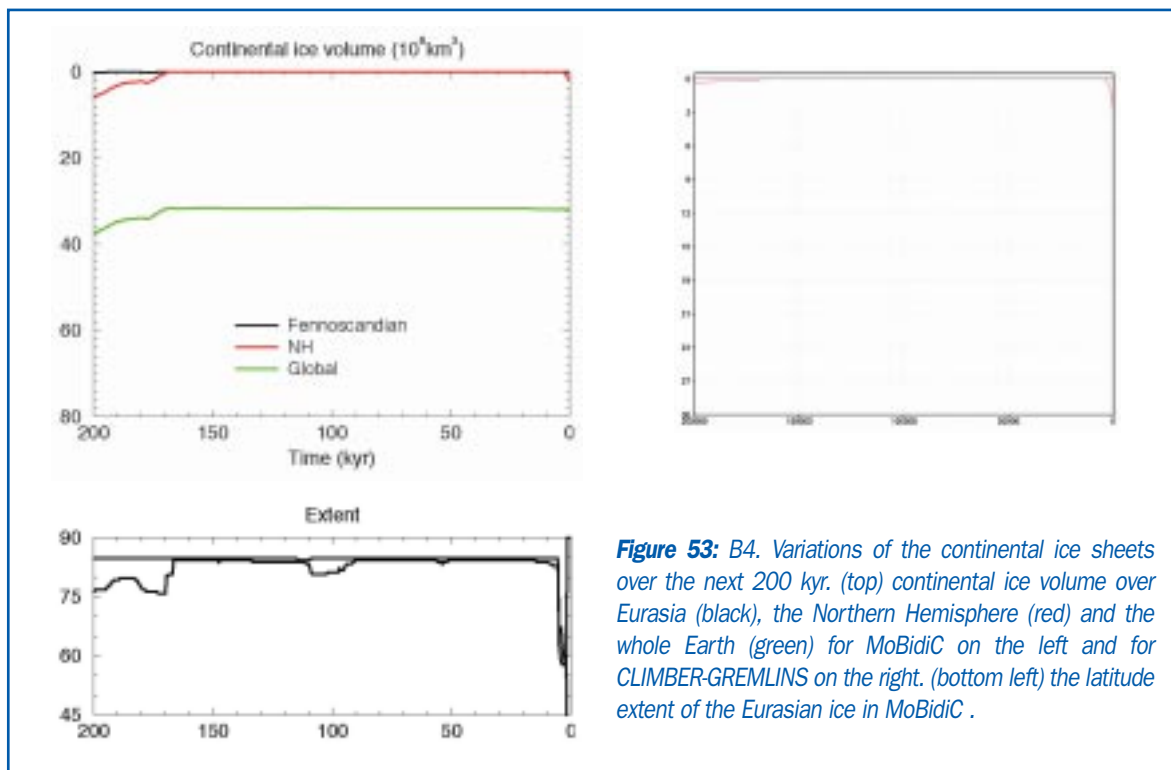


Figure 53: B4. Variations of the continental ice sheets over the next 200 kyr. (top) continental ice volume over Eurasia (black), the Northern Hemisphere (red) and the whole Earth (green) for MoBidiC on the left and for CLIMBER-GREMLINS on the right. (bottom left) the latitude extent of the Eurasian ice in MoBidiC .

4.4.2 - Surface temperature

After 1500 years, the temperature increase in MoBidiC, with respect to the A4a simulation, amounts to 3.7°C, 4.6°C, 2.9°C in the global average, over the Northern Hemisphere and Southern Hemisphere, respectively (Figure 65). After 1000 years, the figures for CLIMBER-GREMLINS are as follows: 4.9°C, 4.9°C and 5.0°C in global average, Northern Hemispheric average, Southern Hemisphere average. This represents an additional warming to the B3 simulation of 0.7°C, 0.8°C and 0.7°C respectively for MoBidiC, 1.2°C, 1.1°C, 1.3°C for CLIMBER-GREMLINS.

In MoBidiC, as for the B3 simulation, temperature undergoes a rapid decrease until 90 kyr AP. The first minimum of temperature at 100.5 kyr AP is reached with a value of 15.4°C in global mean. This is 2°C warmer than without any fossil fuel contribution, and 0.7°C warmer than with a low contribution. At 200 kyr AP, the global annual mean temperature is still warmer in B4 than in A4a (by 1.1°C) and B3 (by 0.4°C). Moreover the gradient of temperature between the Northern and the Southern Hemisphere is larger in B4 than in B3. In CLIMBER-GREMLINS, the temperature

decreases even more rapidly. After the initial peak, the globally averaged temperature falls to around 16.5°C shortly after 20 kyr AP and from then on progressively decreases until 100 kyr AP. Then and until the end of the simulation, the orbital variations are more obvious,

superimposed on a small decreasing trend. The difference between the Northern and the Southern Hemisphere remains constant from 20 kyr AP to 200 kyr AP, and is much smaller than in MoBidiC.

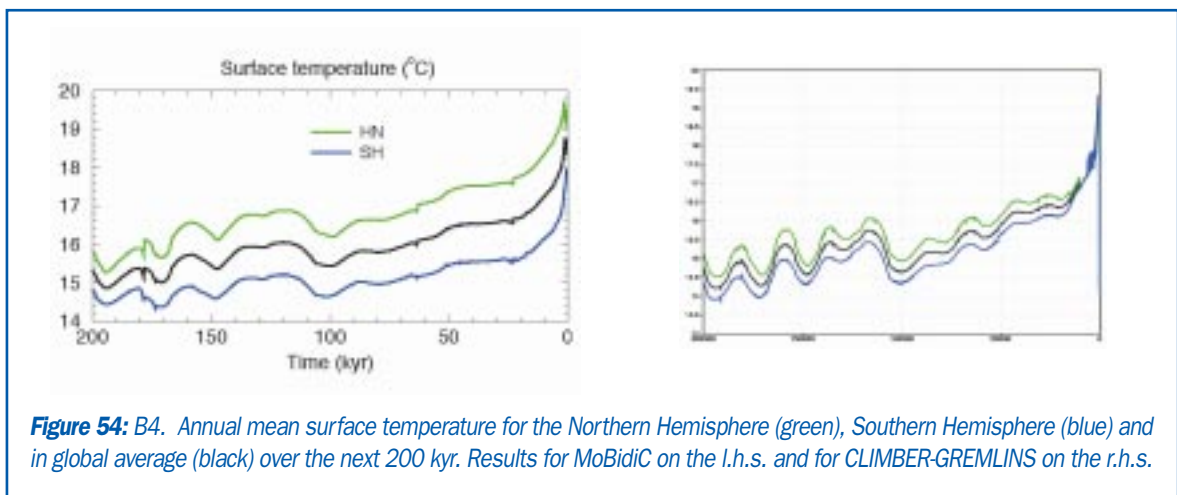


Figure 54: B4. Annual mean surface temperature for the Northern Hemisphere (green), Southern Hemisphere (blue) and in global average (black) over the next 200 kyr. Results for MoBidiC on the l.h.s. and for CLIMBER-GREMLINS on the r.h.s.

In both MoBidiC and CLIMBER-GREMLINS, the general pattern of temperature change over Eurasia and the North Atlantic is similar to that in A4a and B3, except for the cooling trend related to the decrease in time of the fossil fuel contribution to the CO₂ concentration. Moreover, the mean values over the 200-kyr interval are higher in B4 than in A4a and B3. This difference depends on both the latitude and the time in the year. For MoBidiC, in annual mean over the Eurasian continent, the additional warming simulated in B4

compared with B3 is 0.6°C, 0.8°C, 0.8°C respectively in the 30-40°N, 40-50°N and 50-60°N latitude bands. For CLIMBER-GREMLINS, the respective figures are 0.8°C, 0.6°C and 0.6°C. Moreover, the difference decreases only slightly from the beginning (0.7°C, 0.6°C, 0.6°C for MoBidiC, 0.9°C, 0.9°C, 0.8°C for CLIMBER-GREMLINS) to the end (0.5°C, 0.6°C, 0.6°C for MoBidiC, 0.5°C, 0.6°C, 0.7°C for CLIMBER-GREMLINS) of the simulations.

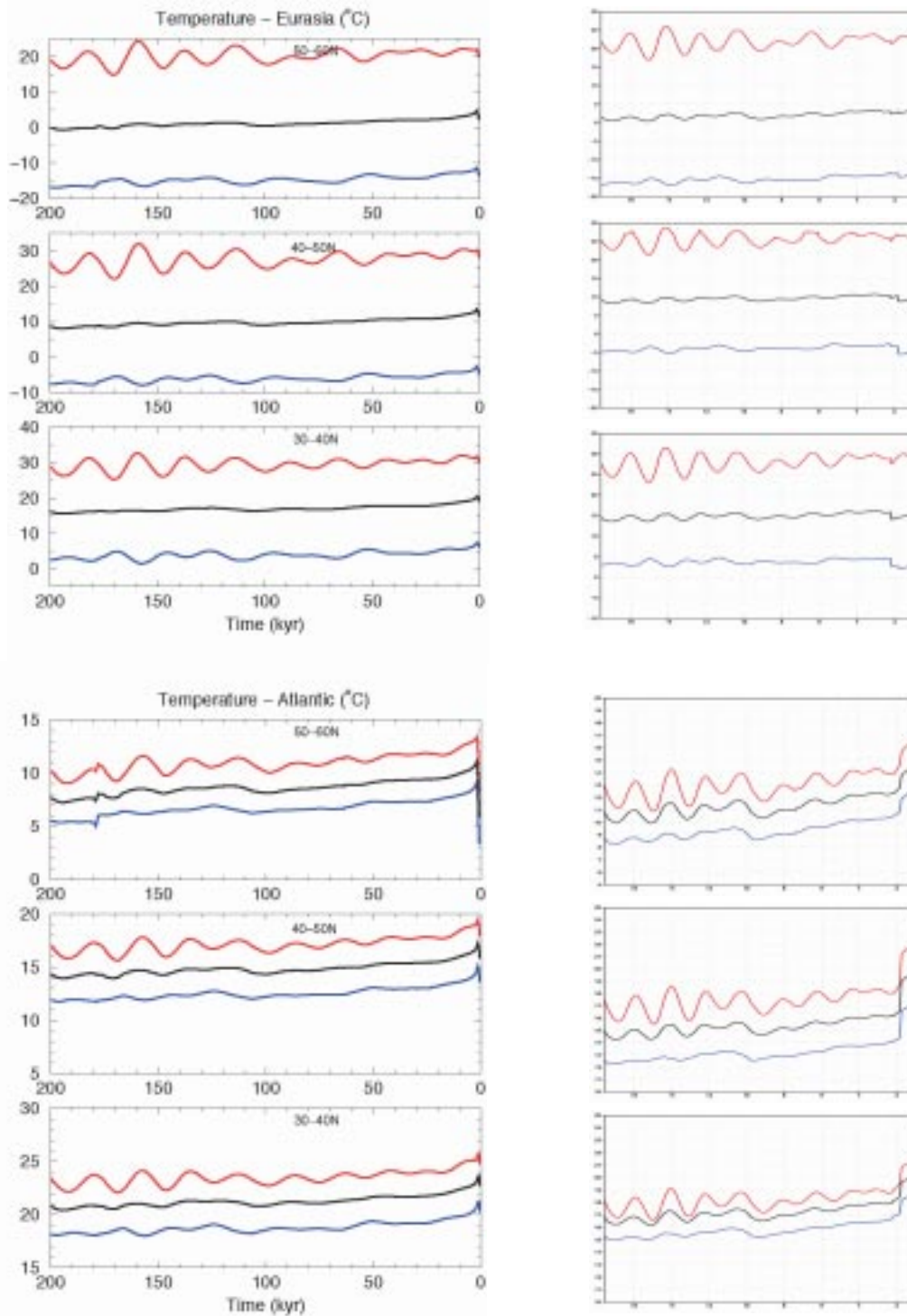
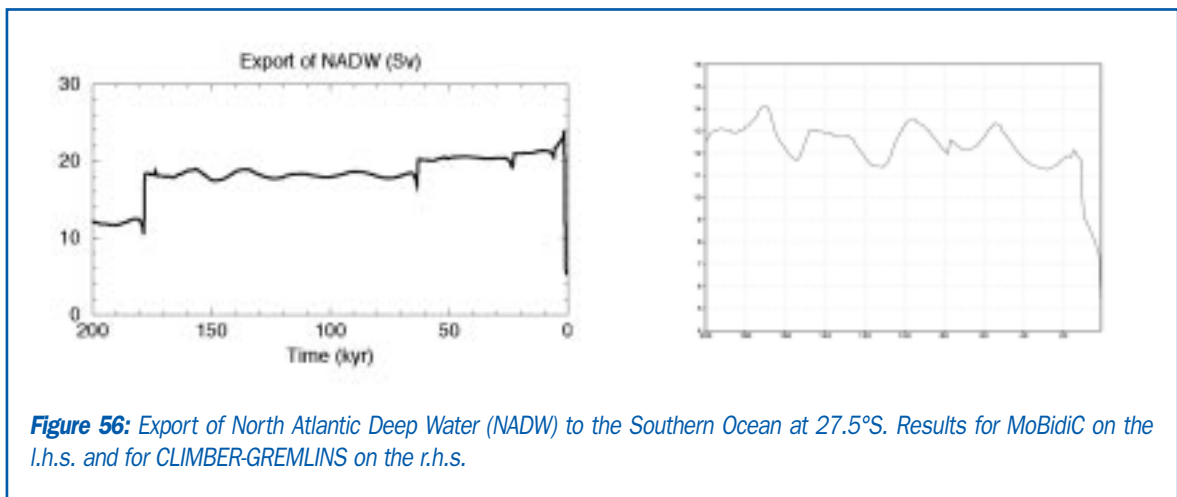


Figure 55: B4. Variations over the next 200 kyr of the simulated temperature for the Eurasian continent (top) and the Atlantic Ocean (bottom), for three latitude bands, in January (blue), in July (red) and in annual mean (black). Results for MoBidiC on the l.h.s. and for CLIMBER-GREMLINS on the r.h.s.

In MoBidiC, as in B3, the export of NADW experiences a two step decrease (Figure 68), first from ~20 Sv to ~18 Sv and then from ~18 Sv to ~12 Sv. However the timing of these two steps is different. They occur at 63.5 kyr AP and 178.5 kyr AP. Again, these reductions

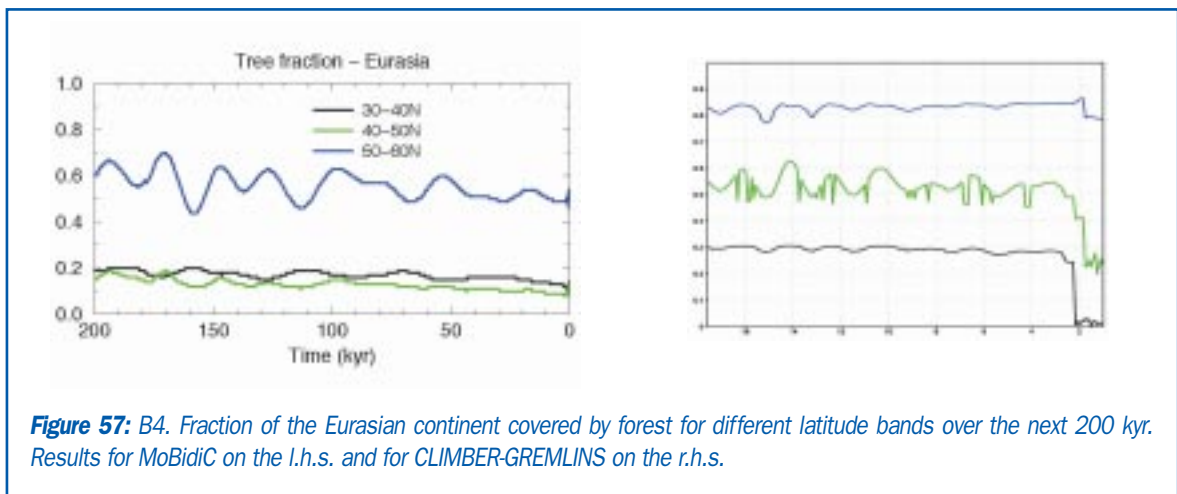
in the export of NADW are correlated with a cooling in high latitude SSTs (larger for the second step than for the first). In CLIMBER-GREMLINS, the evolution of the NADW export is very similar to the B3 scenario one.



4.4.3 - Vegetation

In MoBidiC, the vegetation changes are very much similar to the vegetation changes in the B3 simulation (Figure 70). In the 50-60°N latitude band, the climate change related to the increase in atmospheric CO₂ concentration induces a reduction of the tree fraction. The tree fraction in B4 is very close to the tree fraction in B3 until 110 kyr AP. Then, whereas

B3 tends to recover its unperturbed state, B4 shows significant differences from B3 and its unperturbed state up to 160 kyr AP. The time evolution of the tree fraction in the 30-40°N latitude band is very similar to the A4a and B3 simulations although the tree fraction is smaller (~5%) in the B4 simulation.



As for the B3 simulation compared with the A4a one, the tree fraction in CLIMBER-GREMLINS does not follow the same behaviour as in MoBidiC. The behaviour of the vegetation in the B4 CLIMBER-GREMLINS scenario is very similar to what occurs in the B3 scenario. As far as the vegetation is concerned, whereas in A4a the sensitive latitudes were between 50-60°N, in B3 and B4, it is the 40-50°N band which is most sensitive. As

noted for the other two simulations, the forest cover variations are mainly related to precipitation: there is more forest when it rains more, and this effect counterbalances the effect of increasing temperatures. This effect cannot enter into action in MoBidiC because it does not simulate an increase of precipitation at the times of a decrease in temperature.

4.4.4 - Precipitation, evaporation and snow cover

The hydrological cycle in MoBidiC is not very different from that in the B3 simulation. This is also the case for CLIMBER-GREMLINS. The

differences between the two models are therefore larger than the difference between the two anthropogenic scenarios for each model.

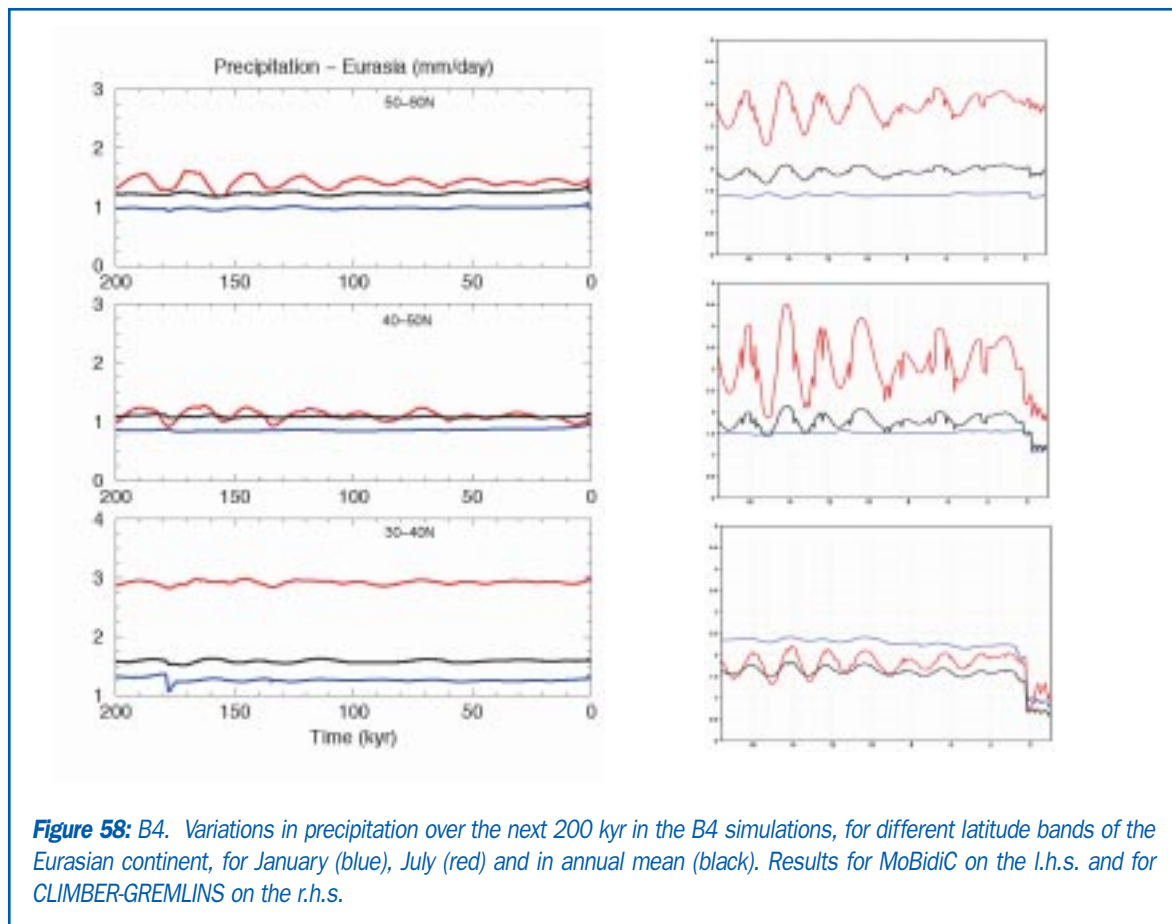
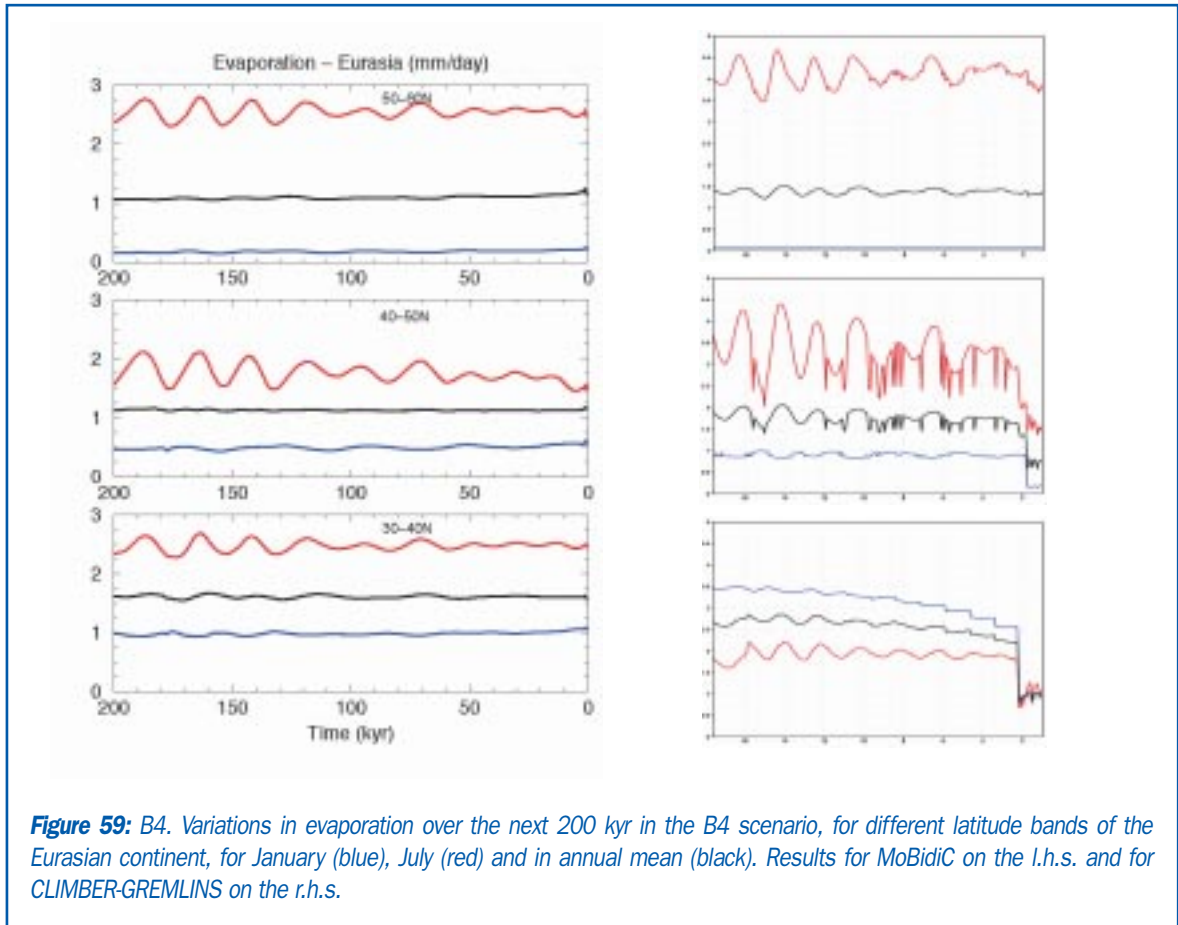


Figure 58: B4. Variations in precipitation over the next 200 kyr in the B4 simulations, for different latitude bands of the Eurasian continent, for January (blue), July (red) and in annual mean (black). Results for MoBidiC on the l.h.s. and for CLIMBER-GREMLINS on the r.h.s.



In MoBidiC, the snow fraction decreases compared with B3, especially at the beginning of the simulation. However, the changes are not very large. In CLIMBER-GREMLINS, as for the vegetation and the hydrological

cycle, to which it is linked, the snow fraction changes most in the 40-50°N band compared with B3 simulation, particularly during the warm periods, but these changes are not very large.

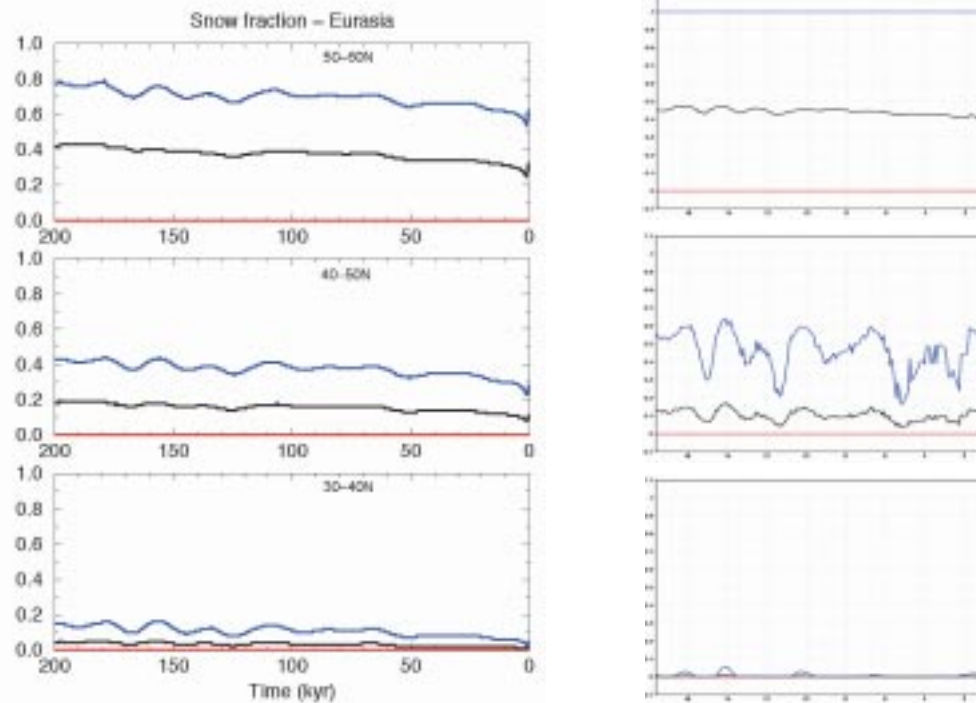


Figure 60: B4. Variations of the fraction of the continent covered by snow over the next 200 kyr, for different latitude bands of the Eurasian continent, for January (blue), July (red) and in annual mean (black). Results for MoBidiC on the l.h.s. and for CLIMBER-GREMLINS on the r.h.s. It must be noted that in MoBidiC snow only falls on the continent covered by snow, although the fraction of the continent covered in snow varies through time. In CLIMBER-GREMLINS, in the 50-60°N latitude belt, the winter fraction is always equal to 1 where the summer fraction is always equal to zero.



5. Uncertainties and limitations

5.1. - Uncertainties on the CO₂ scenarios

(A post scriptum of deliverable D3 [Ref.1] written by Didier Paillard)

The objectives of the BIOCLIM project are to provide reasonable long term scenarios for the climatic evolution of the Earth, and more specifically for the European area, on time scales of several hundreds of thousands of years. Such scenarios can be built on existing theories of Quaternary climate evolution, and more specifically on the theory of glacial-interglacial cycles. The fundamental ideas behind this theory were suggested by Milutin Milankovitch in the first half of the XXth century. Specifically, the orbital parameters of the Earth are slowly changing, and the amount of energy received at a given latitude and at a given time of the year will change accordingly on time scales of thousands to hundreds of thousands of years. Since large ice-sheets develop quasi-periodically over Canada and Fennoscandinavia, a critical parameter should be the summer insolation received at high northern latitudes. Indeed, the evolution of glaciers and ice-sheets is mostly governed by the ability of the snow, falling during the winter to accumulate over the years. The changing insolation of the Earth, and in particular the summer insolation at high northern latitudes should control climate over the multi-thousand-year time scales. This theory was beautifully demonstrated in the 1970s [Ref.87] through advances in geochemistry, geochronology and micropaleontology, and in the following decades some simplified models of the Earth were used to test, in a more detailed fashion, the physical mechanisms involved in this astronomical theory of paleoclimates. Clearly, along these lines, it is reasonable to hope to make some prediction of the long-term future of the climate of the Earth.

However, it has become quite clear, in particular during the last ten years, that the Milankovitch theory, as outlined above, is not sufficient to explain many features of the past evolution of climates (see e.g.

Ref.88). Some paradoxes of the theory were noted already from the beginning:

- there is almost no insolation forcing at the 100 kyr periodicity, whereas this is the frequency of the largest glacial-interglacial oscillations;
- there is some small forcing at 100 kyr, due to eccentricity variations, that could be invoked, but the 400 kyr changes in eccentricity are much larger, but without a counterpart in the climate record;
- the largest climatic transitions, like the stage 12 to stage 11 deglaciation, are associated with the smallest changes in insolation;
- the pacing of the glacial-interglacial oscillations has changed throughout the Pliocene from 23 kyr, to 41 kyr to 100 kyr in the Late Pleistocene, without any comparable changes in the astronomical forcing.

To this traditional list, some new paradoxes have been added more recently:

- the earliest responses to the insolation forcing appear to be in the Southern Hemisphere, or in the tropics, but probably not at high northern latitudes;
- there are large and unexplained changes in the atmospheric carbon dioxide concentration that are amazingly parallel to the temperature records of the Southern Hemisphere;
- there is climatic variability with a much higher frequency, from one to seven thousand years (Dansgaard-Oeschger events and Heinrich events), which is clearly linked to insolation changes, but to internal climatic reorganisations.

All these problems are still mainly unsolved, and therefore they give us some idea of the limitations of current climate models on these time scales. The most likely explanation for these problems is the still unexplained variations in atmospheric CO₂. Indeed, if CO₂ changed with a 100 kyr periodicity (which is the case for the last 400 kyr), this could provide a possible answer for most of the problems enumerated above. The missing piece of the puzzle is an understanding of the atmospheric CO₂ concentration and glacial cycles

interactions but the mechanisms behind the lower $p\text{CO}_2$ during glacial times are still very speculative and such a connection has not been possible yet.

To circumvent this problem, but also to take into account the present day anthropogenic forcing, some scenarios for the future evolution of atmospheric CO_2 concentration were chosen at the beginning of the BIOCLIM project [Ref.1]. These scenarios clearly have very substantial limitations:

1 - the natural CO_2 changes have been computed using a simple model of glacial-interglacial cycles. We obtained a CO_2 concentration from a very crude climate, or ice-sheet, model, and have used this output to force several much more sophisticated climate and ice-sheet models. The whole construction therefore stands quite heavily on top of a rather weak starting point;

2 - the natural CO_2 variations and the anthropogenic CO_2 have been linearly superimposed to provide a scenario for the expected future « non-natural » evolution of CO_2 . This assumes that there is no interaction between the additional fossil fuel CO_2 , and the cyclic evolution of natural CO_2 concentration. Since the models used in BIOCLIM have shown that the anthropogenic carbon does affect the evolution of the ice-sheets, we should expect that it should also affect the balance between the oceanic and atmospheric carbon distribution and therefore it should alter the CO_2 variations themselves (following point 1). In other words, we have demonstrated that this « linear superposition » is not valid. However, in the absence of a theory for glacial CO_2 changes, we had no other possible choice but these crude assumptions. Nevertheless we need to keep in mind that they may have considerable implications for the model results.

During the course of the BIOCLIM project, some new ideas have emerged concerning the oceanic circulation during glacial times. These ideas could have fundamental consequences on the sequestration of CO_2 in the glacial ocean, and therefore on the theory of glacial-interglacial cycles. Though still quite speculative, these ideas have the ability to provide a foundation for a renewed astronomical theory, in which the atmospheric CO_2 changes have a critical role. This

presents the advantage of potentially solving most (if not all) of the paradoxes enumerated above concerning the « traditional » astronomical theory, and also to offer the possibility of representing explicitly and consistently the interaction between CO_2 and ice-sheets, even for the anthropogenic case.

This new theory is based on the idea that the glacial deep ocean is both very cold and very salty, whereas during interglacial times, as today, it is cold and rather fresh. Keeling and Stephens [Ref.89] probably made the first mention of such a cold and salty glacial deep ocean. In such a state, very cold and salty waters are formed around Antarctica by brine rejection during sea-ice formation. Adkins et al. [Ref.90] have since provided experimental data that support the idea of a very salty glacial deep ocean. In the present day configuration, the vertical stratification of water masses is rather weak, since the temperature (colder below) and the salinity (saltier above) are acting in opposite ways on the vertical density gradient. In the glacial case, (colder below and saltier below) they would both act together to strengthen the vertical stratification. The deep vertical mixing could therefore be much less than it is today, and would help to keep the carbon in the deep ocean, away from the atmosphere. If this is indeed the mechanism that explains lower glacial CO_2 concentrations in the atmosphere, then the atmospheric CO_2 concentration should be controlled, to first order, by the formation of these very dense (cold and salty) bottom waters around Antarctica. This is in full agreement with the extraordinary similarity of the Vostok CO_2 and temperature records. More precisely, the formation of dense waters around Antarctica should be controlled by the formation of sea-ice, and thus influence the climate of the Southern Ocean. In other words, the Southern Hemisphere has a critical role in this new theory. Another critical parameter will be the extent of the Antarctic ice-sheet : when it reaches maximum extension, it will invade most of the continental shelves, where shallow water conditions favour the continuous formation of sea-ice and therefore the formation of salty bottom waters. Consequently, when the Antarctic ice-sheet extends to its maximum, it will stop the formation of these very dense waters, and switch the deep ocean into an interglacial mode. The CO_2 will outgas and warm the

atmosphere, and at the next favourable orbital configuration, a rapid melting of the Northern Hemisphere ice-sheets will then be possible.

This scenario can be written in a more mathematical form:

We define F, the efficiency of formation of salty bottom waters, by:

$$F = a V - b A - c I_{60} + d + k t$$

with V = Northern Hemisphere ice volume; A = Antarctic ice sheet extent; I_{60} = the daily insolation at 60°S, 21st February; a, b, c and d constant coefficients ; with t being the time and k a small constant. It is assumed here that the rapidity of the melting of the sea-ice late in the Austral summer could play an important role for the Southern Ocean heat budget, in particular through the ice-albedo feedback, and therefore for the switching of the oceanic mode, hence the February insolation at 60°S. When F is negative, the ocean is in "interglacial" mode, and when F is positive, it is in "glacial" mode. The model equations for A, V and C (the atmospheric CO₂ concentration) are:

$$dV/dt = (V_R - V)/\tau_V$$

$$dA/dt = (V - A)/\tau_A$$

$$dC/dt = (C_R - C)/\tau_C$$

with $V_R = -x C - y I_{65} + z$; $C_R = \alpha I_{65} - \beta V + \gamma H(-F) + \delta$; H is the Heaviside function (H=1 if F<0 ; H=0 otherwise) ; I_{65} = insolation 65°N, 21st June; τ_V , τ_A , τ_C are time constants ; x, y, z, α , β , γ , δ are constants. The contribution of Antarctica to changes in global ice volume V is neglected, and V is therefore assumed to represent the Northern Hemisphere ice volume only. It is limited by a minimum zero value.

The results are extremely good for the last 3 MyrBP (see Figure 75). In particular, it is possible to reproduce the transition from 23 kyr around 3 Myr BP, to 41 kyr to 100 kyr oscillations around 1Myr BP. It is also possible to extrapolate these results for the future (Figure 62).

When compared with the scenarios defined at the beginning of the BIOCLIM project, there are some substantial differences. The largest change is the smaller variability in these new future CO₂ scenarios. Indeed, this « natural » variability was prescribed in the assumptions made at the beginning of the BIOCLIM project [Ref.1]. But there are reasons to believe that, in a warmer climate, the glacial-interglacial cyclicality should be different. This is what paleoclimatic data tells us when looking at pre-Quaternary climates. It is also what is reproduced with this new conceptual theory of glacial-interglacial cycles, where the largest variations, occurring every 100-kyr during the Quaternary, are linked to Antarctic ice-sheet extent and the formation of brines on the continental shelves. According to this new concept, the anthropogenic perturbation on the long term climate evolution has a larger impact than previously thought, since the 100-kyr cyclicality and the associated large Northern Hemisphere ice-sheet changes do not occur anymore before the second half of the next million year time interval.

In any case, one result of the BIOCLIM exercise is probably to emphasize the long term impact of the anthropogenic forcing on the glacial-interglacial time scale, and to highlight that a simple extrapolation of Quaternary climate variability may not be sufficient to provide a range of possible future changes. Our proposed new statistical model suggests that anthropogenic CO₂ will affect seriously the natural 100-kyr cyclicality of atmospheric CO₂ due to changes in ocean circulation. Another question to be addressed would be the weathering time constant used here (200 kyr, from Ref.91) for the long term sequestration of CO₂. There are many reasons to believe it should also be affected by large and durable climatic changes.

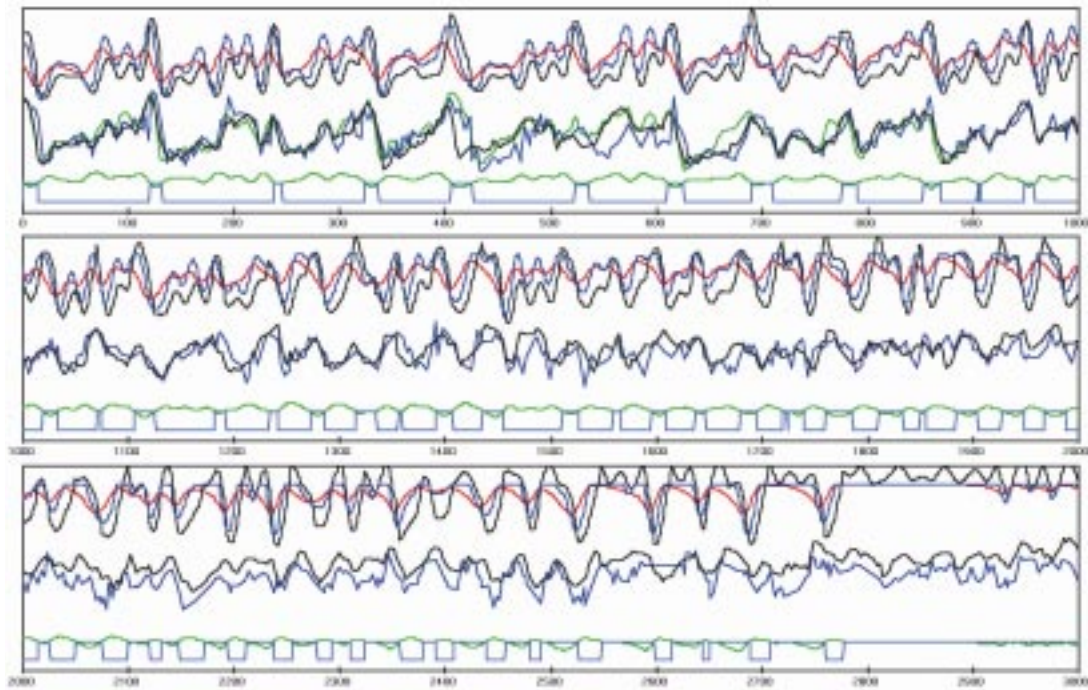
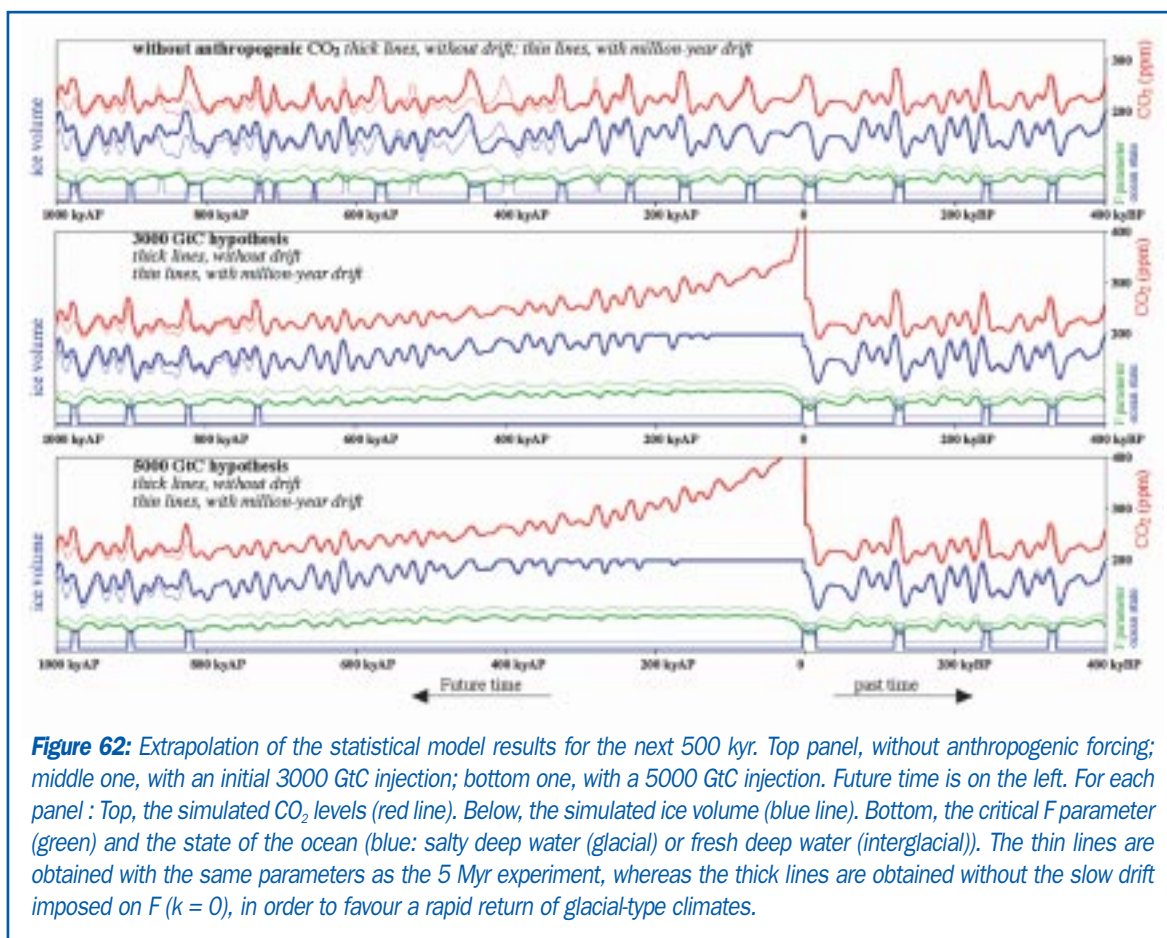


Figure 61: Model results over the last 3 Myr. Top panel : between 0 and 1 MyrBP, middle panel : between 1 and 2 MyrBP, bottom panel : between 2 and 3 MyrBP..For each panel : Top, the simulated CO₂ levels (black line), the simulated ice volume (blue line), the Antarctica area (red line). Middle, sea-level curves (green: Ref.92 ; blue : Ref.93; black : Ref.94). Bottom, the critical F parameter (green) and the state of the ocean (blue: glacial or interglacial).



5.2. - Model and experimental setup limitations

As noted in the introduction, both climate models are still under development. The CLIMBER-GREMLINS model has been developed in the framework of the present project and many aspects of the coupling procedure between the climate model and the ice sheet model will be improved and tested in the near future. It has taken much more time than initially planned to develop the coupling between CLIMBER and GREMLINS and, as can be seen from the missing transient simulations of past climate evolution for the last glacial-interglacial cycle, the model has not been tested as much as was desirable before starting to run the BIOCLIM experiments.

One particular missing process in the coupling procedure between CLIMBER and GREMLINS is the fresh water flux that results from melting an ice sheet. In the present version of the model, no corresponding

flux is given to the ocean. For the past climate simulations, the observed global eustatic sea level change is given to the model. Obviously for the future scenarios this was not possible, so global eustatic sea level was kept constant. So were some parameterisations such as the one dealing with gyre transport in the North Atlantic, which was kept at its present value.

A major drawback in the present version of the CLIMBER-GREMLINS model is that we have not seen any situation yet in which the model spontaneously built a Fennoscandian ice sheet. This has to be taken into account when reading about the BIOCLIM results, it is a known bias of the model that we will try to correct in the future.



6. Summary

	MoBidiC				CLIMBER-GREMLINS			
	Past	A4a	B3	B4		A4a	B3	B4
Ice vol. (10⁶km³)								
Max	40.6	21.1	11.4	5.8		24.0	2.8 (0kyr)	2.8 (0kyr)
Mean	17.9	8.6	1.3	0.5		11.9	0.4	0.05
Std	10.3	4.1	2.9	1.2				
Global surf. T. (°C)								
Min	12.9	13.4	14.3	14.9		11.8	13.6	14.2
Max	15.0	15.5	17.9	18.7		14.5	18.0	19.2
Mean	14.0	14.4	15.5	16.0		13.3	14.9	15.4
Std	0.5	0.5	0.6	0.7				

Table 5: Summary of some features of the long term (past and future) climate simulations

Three simulations of the future climate have been performed with MoBidiC and CLIMBER-GREMLINS. The natural simulation takes into account the natural variations of atmospheric CO₂ concentration through a prescribed scenario. It does not take into account the additional CO₂ from fossil fuel burning. Two other simulations are taking into account this additional CO₂. Global features of these simulations are displayed in

Table 5. Depending on the scenario, the anthropogenic CO₂, induces a maximum warming of 3.0 to 3.7°C (MoBidiC), 4.2 to 5.4°C (CLIMBER-GREMLINS) in global average (Figure 77). Moreover a warming related to the contribution of fossil fuel is still present after 200 kyr. It amounts to 0.7 to 1.1°C in MoBidiC and 1.6 to 2.1°C in CLIMBER-GREMLINS.

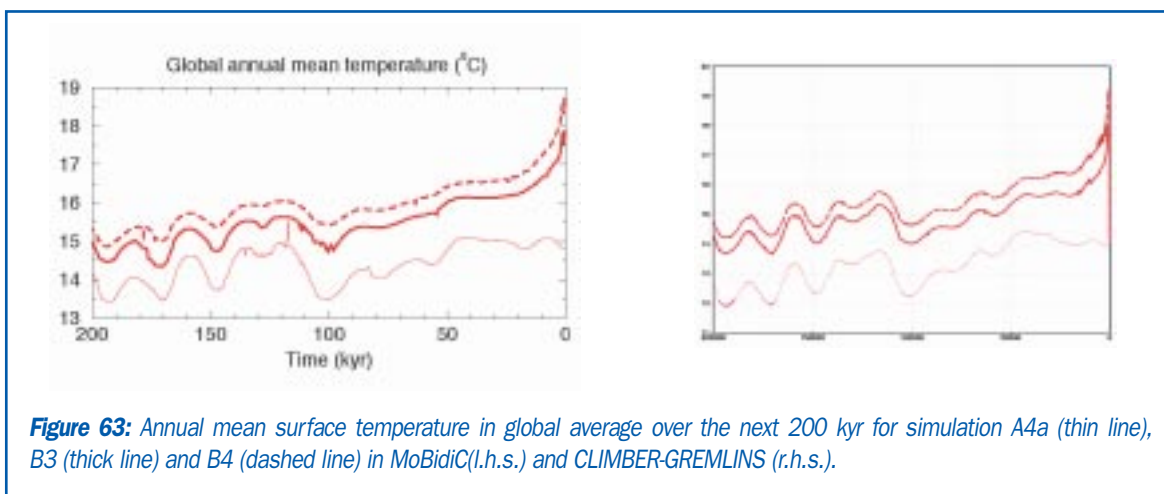


Figure 63: Annual mean surface temperature in global average over the next 200 kyr for simulation A4a (thin line), B3 (thick line) and B4 (dashed line) in MoBidiC(l.h.s.) and CLIMBER-GREMLINS (r.h.s.).

The warming related to the human induced contribution to atmospheric CO₂ concentration can also be recognised at the more regional scale, both for the continent and the ocean (Figure 78). Moreover MoBidiC is displaying an important change in the THC at about

115 kyr AP in the natural simulation and at the early stage of the perturbed simulations. The consequence of this change in THC can be identified mostly in the high northern latitudes through a rapid increase of the temperature.

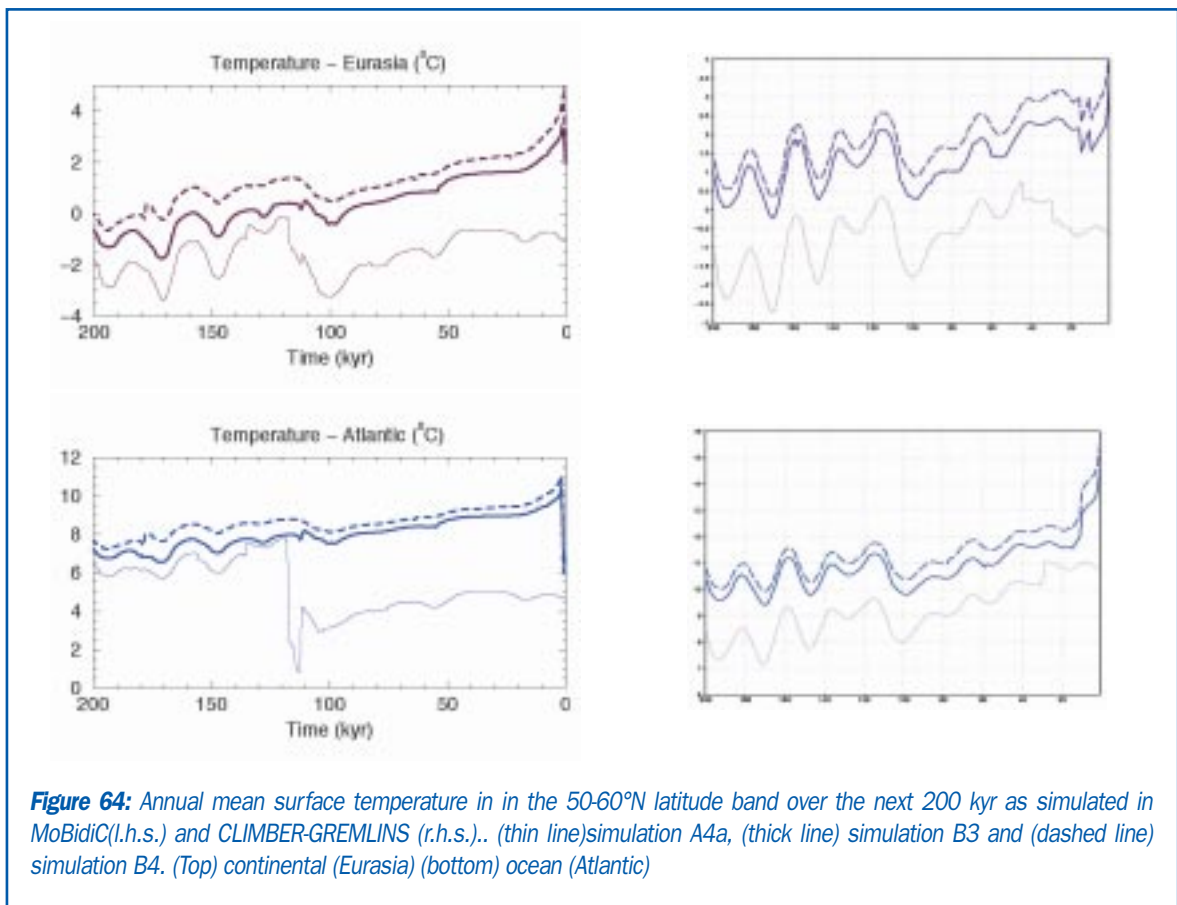


Figure 64: Annual mean surface temperature in in the 50-60°N latitude band over the next 200 kyr as simulated in MoBidiC(l.h.s.) and CLIMBER-GREMLINS (r.h.s.).. (thin line)simulation A4a, (thick line) simulation B3 and (dashed line) simulation B4. (Top) continental (Eurasia) (bottom) ocean (Atlantic)

Due to the increase in atmospheric CO₂ concentration and the subsequent warming the tree fraction in the 50-60°N latitude band slightly decreases in MoBidiC (Figure 79). In fact, the water availability has not increased enough to meet the new demand related to

warming. Contrarily to MoBidiC, the tree fraction simulated by CLIMBER-GREMLINS is larger in the perturbed experiments than in the natural simulation. In all three simulations it is also significantly larger in CLIMBER-GREMLINS than in MoBidiC.

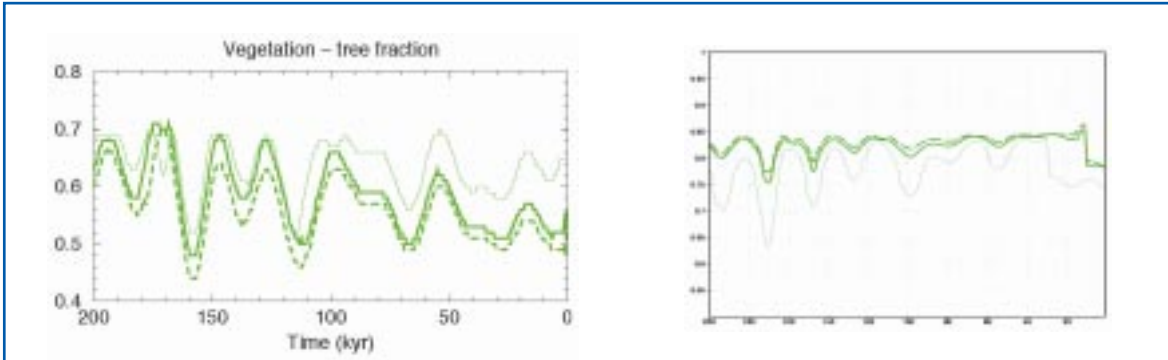


Figure 65: Fraction of the Eurasian continent covered by forest in the 50-60°N latitude band over the last 200 kyr as simulated in MoBidiC(l.h.s.) and CLIMBER-GREMLINS (r.h.s.). (thin line)simulation A4a, (thick line) simulation B3 and (dashed line) simulation B4

The time evolution of the THC during the next 200 kyr is very different in MoBidiC and CLIMBER-GREMLINS (Figure 80). In MoBidiC there are mostly two modes; the THC is either strong (about 20 Sv) or slightly reduced (about 10 Sv). The transition between these two modes is characterised by abrupt changes, that can also be recognised in the evolution of temperature. The changes in THC are related to change in the location of the convection sites, in the density of the water at these

sites, to the modification in the sea-ice extent and to fresh water fluxes from the melting ice sheets. The export of NADW to the Southern Ocean is larger for a warmer climate. A strong 40-kyr signal is present in the export of NADW simulated by CLIMBER-GREMLINS. The amplitude of this oscillation is about 2 Sv. In the natural simulation, it is superimposed on an increasing trend of about 4 Sv over the next 200 kyr. The export of NADW to the Southern Ocean is smaller for a warmer climate.

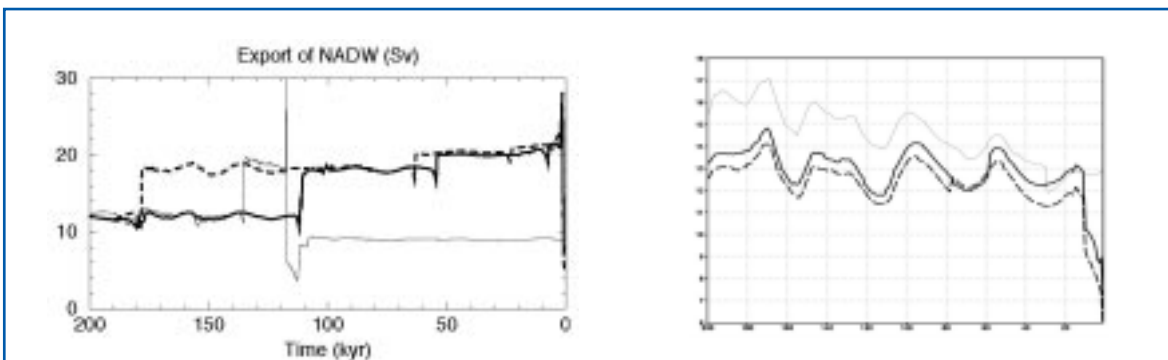


Figure 66: Export of the NADW to the Southern Ocean simulated in MoBidiC(l.h.s.) and CLIMBER-GREMLINS (r.h.s.). (thin line)simulation A4a, (thick line) simulation B3 and (dashed line) simulation B4



7. References

- Ref. 1:** BIOCLIM Report D3 (2001) Global climatic features over the next million years and recommendation for specific situations to be considered. Available on www.andra.fr/bioclim.
- Ref. 2:** Holton, J. R., 1992. An introduction to Dynamic Meteorology, 3rd Edition, Academic Press (San Diego), 507pp.
- Ref. 3:** Jaeger, L., 1976. Monatskarten des Niederschlags für die ganze Erde. Tech.Rep. 139. Ber. Dtsch. Wetterdienstes 38pp.
- Ref. 4:** Gallée, H., van Ypersele, J. P., Fichefet, T., Tricot, C., and Berger, A., 1991. Simulation of the last glacial cycle by a coupled, sectorially averaged climate-ice sheet model. Part I: The climate model., *J. Geophys. Res.*, 96, 13,139–13,161.
- Ref. 5:** Bryan, K., 1969. A numerical method for the study of the circulation of the world ocean, *J. Comp. Phys.*, 4, 347–376.
- Ref. 6:** Semtner A.J., 1976. A model of thermodynamic growth of sea ice in numerical investigation of climate, *J.Phys.Oceanogr.*, 6, 379-389.
- Ref. 7:** ETOPO5, Global 5'x5' depth and elevation. Available from National Geophysical Data Center, NOAA US Dept of Commerce, Code E/GC3, Boulder, CO80303.
- Ref. 8:** Hovine, S., and Fichefet, T., 1994. A zonally averaged, three-basin ocean circulation model for climate studies, *Clim. Dyn.*, 10, 313–331.
- Ref. 9:** Hirsch, C., 1988. Numerical Computation of Internal and External Flows. Vol.I: Fundamentals of Numerical Discretization, Numerical Methods in Engineering. Wiley & Sons, 515 pp.
- Ref. 10:** Campin, J.-M., 1997. Modélisation tridimensionnelle de la circulation générale océanique lors du dernier maximum glaciaire, Ph.D. thesis, Institut d'Astronomie et de Géophysique G. Lemaître, Université catholique de Louvain, 342 pp.
- Ref. 11:** Goosse, H., and Fichefet, T., 2000. Open-ocean convection and polynya formation in a large-scale ice-ocean model, *Tellus*, 53(1), 94–111.
- Ref. 12:** Campin, J.-M., and Goosse, H., 1999. Parameterization of density-driven downsloping flow for a coarse-resolution ocean model in z-coordinate, *Tellus*, 51A, 412–430.
- Ref. 13:** Beckmann, A., and Döscher, R., 1997. A method for improved representation of dense water spreading over topography in geopotential-coordinate models, *J. Phys. Oceanogr.*, 27, 581–591.
- Ref. 14:** Crucifix, M., Tulkens, P., and Berger, A., 2001. Modelling abrupt climatic change during the last glaciation, in *The Oceans and Rapid Climate Changes: Past, Present and Future*, edited by D. Seidov, B. J. Haupt, and M. Maslin, vol. 126 of AGU Monograph Series, pp. 117–134. American Geophysical Union
- Ref. 15:** Ganopolski, A., and Rahmstorf, S., 2001. Rapid changes of glacial climate simulated in a coupled climate model, *Nature*, 409(6817), 153–158.

- Ref. 16:** Held, I. M., and Hou, A. Y., 1980. Non-linear axially symmetric circulations in a nearly inviscid atmosphere, *J. Atmos. Sci.*, 37, 515–533.
- Ref. 17:** Peng, L., Chou, M. D. , and Arking, A., 1987. Climate warming due to increasing atmospheric CO₂ : Simulations with a multilayer coupled atmosphere-ocean seasonal energy balance model, *J. Geophys. Res.*, 92, 5505–5521.
- Ref. 18:** Crucifix, M., Loutre, M. F., Tulkens, P., Fichet, T., and Berger, A., 2002. Climate evolution during the Holocene: A study with an Earth system model of intermediate complexity, *Clim. Dyn.*, 19, 43-60 (DOI 10.1007/s00382-001-0208-6).
- Ref. 19:** Brovkin, V., Ganopolski, A., and Svirezhev, Y., 1997. A continuous climate-vegetation classification for use in climate-biosphere studies, *Ecol. Modell.*, 101, 251–261.
- Ref. 20:** Harvey, L.D.D., 1988. On the role of high latitude ice, snow and vegetation feedbacks in the climatic response to external forcing changes. *Climatic Change*, 13, 191-224.
- Ref. 21:** Petoukhov, V., Ganopolski, A., Brovkin, V., Claussen, M., Eliseev, A., Kubatzki, C., Rahmstorf, S., 2000. CLIMBER-2: a climate system model of intermediate complexity. *Climate Dynamics*, 16, 1-17.
- Ref. 22:** Dickinson, R.E., Henderson-Sellers, A. and Kennedy, P.J., 1993. Biosphere-atmosphere transfer scheme (BATS) version 1e as coupled to the NCAR community climate model, NCAR Technical Note TN-387+STR, Boulder, Colorado, 72 pp..
- Ref. 23:** Ritz, C., Fabre, A. and Letréguilly, A., 1997. Sensitivity of a Greenland ice sheet model to ice flow and ablation parameters: consequences for the evolution through the last climatic cycle. *Climate Dynamics*, 13, 11-24.
- Ref. 24:** Tulkens, P. N., 1998. A zonally averaged model of the coupled atmosphere-ocean-sea ice system for climate studies, Ph.D. thesis, Université catholique de Louvain, Louvain-la-Neuve, 163 pp.
- Ref. 25:** Gallée, H., van Ypersele, J. P., Fichet, T., Marsiat, I., Tricot, C., and Berger, A., 1992. Simulation of the last glacial cycle by a coupled, sectorially averaged climate-ice sheet model. Part II: Response to insolation and CO₂ variation, *J. Geophys. Res.*, 97, 15,713–15,740.
- Ref. 26:** Dutrieux, A., 1997. Etude des variations à long terme du climat à l'aide d'un modèle global à deux dimensions du système climatique, Ph.D. thesis, Institut d'Astronomie et de Géophysique G. Lemaître, Université catholique de Louvain, 274 pp.
- Ref. 27:** Teller, J. T., 1990. Meltwater and precipitation runoff to the North Atlantic, Arctic, and Gulf of Mexico from the Laurentide ice sheet and adjacent regions during the Younger Dryas, *Paleoceanogr.*, 5(6), 895–905.
- Ref. 28:** Crucifix, M., and Berger, A., 2002. Simulating ocean-ice sheets interactions during the deglaciation, *Paleoceanogr.*, 17(4), 1054, doi:10.1029/2001PA000702.

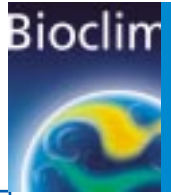
- Ref. 29:** Oerlemans, J., 1980. Model experiments on the 100,000-yr glacial cycle, *Nature*, 287(2), 430–432.
- Ref. 30:** Nakada, M., and Lambeck, K., 1987. Glacial rebound and relative sea-level variations : a new appraisal, *Geophys. J. Roy. Astron. Soc.*, 90, 171–224.
- Ref. 31:** Crucifix, M., Loutre, M. F., Lambeck, K., and Berger, A., 2001b. Effect of isostatic rebound on modelled ice volume variations over the last 200 kyr, *Earth Planet. Sci. Lett.*, 184, 623–633.
- Ref. 32:** Braconnot, P., Joussaume, S., de Noblet, N., and Ramstein, G., 2000. Mid-Holocene and last glacial maximum African monsoon changes as simulated within the Paleoclimate Modeling Intercomparison project, *Global and Planetary Change*, 26, 51-66.
- Ref. 33:** BIOCLIM Report D8a (2003a) Development of the rule-based downscaling methodology for BIOCLIM Workpackage 3. Available on www.andra.fr/bioclim
- Ref. 34:** Monnin, E., Indermühle, A., Dällenbach, A., Flückiger, J., Stauffer, B., Stocker, T. F., Raynaud, D., and Barnola, J.-M., 2001. Atmospheric CO₂ concentrations over the last termination, *Science*, 291, 112–114.
- Ref. 35:** Indermühle, A., Stocker, T. F., Joos, F., Fisher, H., Smith, H., Wahlen, M., Deck, B., Mastroianni, D., Tschumi, J., Blunier, T., Meyer, R., and Stauffer, B., 1999. Holocene carbon-cycle dynamics based on CO₂ trapped in ice at Taylor Dome, Antarctica, *Nature*, 398, 121–125.
- Ref. 36:** IPCC, 2001: *Climate Change 2001: The Scientific Basis*. Contribution of Working Group 1 to the Third Assessment Report of Intergovernmental Panel for Climate Change. [Houghton, J. T., Ding, Y., Griggs, D. J., Nogueur, M., van der Linden, P. J., Dai, X., Raskell, K., and Johnson, C. A.] Cambridge University Press, Cambridge, United Kingdom and New York, USA, 881 pp.
- Ref. 37:** Warren, S.G., and Schneider, S.H., 1979. Seasonal simulation as a test for uncertainties in the parameterizations of a Budyko-Sellers zonal climate model, *J. Atmos. Sci.*, 36, 1377-1391.
- Ref. 38:** Trenberth, K.E., 1992. *Climate system modeling*, Cambridge University Press, 788pp.
- Ref. 39:** IPCC, 1990 : *Climate Change, The IPCC Scientific Assessment*. [Houghton, J. T., Jenkins G.J., Ephraums J.J.] Cambridge University Press, Cambridge, United Kingdom and New York, USA, 365 pp.
- Ref. 40:** IPCC, 1996 : *Climate Change 1995: The Science of Climate Change*. Contribution of Working Group 1 to the Second Assessment Report of Intergovernmental Panel for Climate Change. [Houghton, J. T., Meira Filho L.G., Callander B.A., Harris N., Kattenberg A. and Maskell K.] Cambridge University Press, Cambridge, United Kingdom and New York, USA, 572 pp.
- Ref. 41:** Ganopolski A, Petoukhov, V., Rahmstorf, S., Brovkin, V., Claussen, M., Eliseev, A., Kubatzki, C, 2001. CLIMBER-2: a climate system model of intermediate complexity. Part II: model sensitivity, *Clim. Dyn.*, 17 (10), 735-751.
- Ref. 42:** Berger, A., 1978. Long-term variations of daily insolation and Quaternary climatic changes, *J. Atmos. Sci.*, 35, 2362–2367.

- Ref. 43:** Texier, D., de Noblet, N., Harrison, S.P., Haxeltine, A., Jolly, D., Joussaume, S., Laarif, F., Prentice, I.C., and Tarasov, P., 1997. Quantifying the role of biosphere-atmosphere feedbacks in climate change: coupled model simulations for 6000 years BP and comparison with paleodata for northern Eurasia and northern Africa, *Climate Dynamics*, 13, 865-881.
- Ref. 44:** Prentice, I.C., Webb III, T., 1998. BIOME 6000: reconstructing global mid-Holocene vegetation patterns from palaeoecological records, *J. Biogeogr.*, 25, 997-1005.
- Ref. 45:** MacDonald, G.M., Velichko, A.A, Kremenetski, C.V., Borisova, O.K., Goleva, A.A., Andreev, A.A., Cwynar, L.C., Riding, R.T., Forman, S.L., Edwards, T.W.D., Aravena, R., Hammarlund, D, Sziecz, J.M., Gataulin, V.N., 2000. Holocene treeline history and climate change across Northern Eurasia, *Quat Res.*, 53, 302-311.
- Ref. 46:** Harrison, S.P., Jolly, D., Laarif, F., Abe-Ouchi, A., Dong, B., Herterich, K., Hewitt, C., Joussaume, S., Kutzbach, J.E, Mitchell, J., de Noblet, N., and Valdes, P., 1998. Intercomparison of simulated global vegetation distributions in response to 6 kyr BP orbital forcing, *Journal of Climate*, 11, 2721-2742, 1998.
- Ref. 47:** Peltier, W. R., 1994. Ice age paleotopography, *Science*, 265, 195-201.
- Ref. 48:** Hewitt, C.D., and Mitchell, J.F.B., 1997. Radiative forcing and response of a GCM to ice age boundary conditions: cloud feedbacks and climate sensitivity, *Clim. Dyn.*, 13, 821-834.
- Ref. 49:** Dong, B., and Valdes, P.J., 1998. Simulations of the last glacial maximum climate using a general circulation model: prescribed versus computed sea surface temperatures, *Clim. Dyn.*, 14, 571-591.
- Ref. 50:** Hansen, J.E., Lacis, A., Ruedy, R., Sato, M., Wilson, H., 1993. How sensitive is the world's climate? *Nat. Geogr. Explor.*, 9, 143-158.
- Ref. 51:** Peyron, O., Guiot, J., Cheddadi, R., Tarasov, P., Reille, M., de Beaulieu, J.L, Bottema, S., and Andrieu, V., 1998. Climatic reconstruction in Europe for 18,000 years B.P. from pollen data, *Quaternary Research*, 49, 183-196.
- Ref. 52:** Tarasov, P. E., Peyron, O., Guiot, J., Brewer, S., Volkova, V. S., Bezusko, J. G., Durofeyuk, N. I., Kvavadze, E. V., Osipova, I. M. and Panova, N. K, 1999. Last Glacial Maximum climate of the former Soviet Union and Mongolia reconstructed from pollen and macrofossil data, *Climate Dynamics*, 15, 227-240.
- Ref. 53:** Farrera, I., Harrison, S.P., Prentice, I.C., Ramstein, G., Guiot, J., Bartlein, P.J., Bonnefille, R., Bush, M., Cramer, W., von Grafenste, U., 1999. In, K. Holmgren, H. Hooghiemstra, G. Hope, D. Jolly, S.-E. Lauritzen, Y. Ono, S. Pinot, M. Stute, and G. Yu, Tropical climates at the last glacial maximum: a new synthesis of terrestrial palaeoclimate data. I. Vegetation, lake-levels and geochemistry, *Climate Dynamics*, 15, 823-856.
- Ref. 54:** BIOCLIM Report D2 (2002) Consolidation of needs of the European waste management agencies and the regulator of the consortium. Available on www.andra.fr/bioclim.

- Ref. 55:** Lehman, SJ, Sachs, JP, Crotwell, AM, Keigwin, LD, Boyle, EA, 2002. Relation of subtropical Atlantic temperature, high-latitude ice rafting, deep water formation, and European climate 130,000-60,000 years ago, *Quat. Sci. Rev.*, 21 (18-19), 1917-1924.
- Ref. 56:** Crucifix, M., and Loutre, M. F., 2002. Transient simulations over the last interglacial period (126-115 kyr BP) : forcing and feedback analysis, *Clim. Dyn.*, 19, 417-433 (DOI 10.1007/s00382-002-0234-z).
- Ref. 57:** Petit, J. R., Jouzel, J., Raynaud, D., Barkov, N. I., Barnola, J.-M., Basile, I., Bender, M., Chappellaz, J., Davis, M., Delaygue, G., Delmotte, M., Kotlyakov, V. M., Legrand, M., Lipenkov, V. Y., Lorius, C., Pépin, L., Ritz, C., Saltzman, E., and Stievenard, M., 1999. Climate and atmospheric history of the past 420,000 years from the Vostok ice core, Antarctica, *Nature*, 399, 429–436.
- Ref. 58:** Sánchez Goñi M.F., Turon, J.L., Eynaud, F., Shackleton, N.J., Cayre, O., 2000. Direct land/sea correlation of the Eemian, and its comparison with the Holocene: a high-resolution palynological record off the Iberian margin. *Geologie en Mijnbouw- Netherlands Journal of Geosciences*, 79 (2-3), 345-354.
- Ref. 59:** Imbrie, J., Hays, J.D., Martinson, D.G., McIntyre, A., Mix, A.C., Morley, J.J., Pisias, N.G., Prell, W.L., Shackleton, N.J., 1984. The orbital theory of Pleistocene climate : support from a revised chronology of the marine $\delta^{18}O$ record. In : A.L. Berger, J. Imbrie, G. Kukla, B. Saltzman (eds), D.Reidel publishing Company, *Milankovitch and Climate, Part I*, 269-305.
- Ref. 60:** Otterman, J., Chou, M.-D., and Arking, A., 1984. Effects of nontropical forest cover on climate. *J. Appl. Meteor.*, 23, 762-767.
- Ref. 61:** Cheddadi R, Mamakowa, K., Guiot, J., de Beaulieu, J.L., Reille, M., Andrieu, V., Granoszewski, W., Peyron, O., 1998. Was the climate of the Eemian stable? A quantitative climate reconstruction from seven European pollen records, *Palaeogeog.Palaeoclimatol. Palaeoecol.*, 143 (1-3), 73-85.
- Ref. 62:** Cortijo, E, Lehman, S., Keigwin, L., Chapman, M., Paillard, D., Labeyrie, L., 1999. Changes in meridional temperature and salinity gradients in the North Atlantic Ocean (30 degrees-72 degrees N) during the last interglacial period, *Paleocenography*, 14 (1), 23-33.
- Ref. 63:** Heusser, L.E., 2000. Rapid oscillation in western North America vegetation and climate during oxygen isotope stage 5 inferred from pollen data from Santa Barbara Basin (Hole 893A). *Palaeogeogr., Palaeoclimatol., Palaeoecol.*, 407-421.
- Ref. 64:** Brovkin, V., Levis, S., Loutre, M.F., Crucifix, M., Claussen, M., Ganopolski, A., Kubatzki, C., Petoukhov, V., 2003. Stability Analysis of the Climate-Vegetation System in the Northern High Latitudes. *Climatic Change*, 57 (1), 119-138. (Article ID: 5097671)
- Ref. 65:** Boyle, E. A. and Keigwin, L. D., 1982. Deep circulation in the North Atlantic over the last 200,000 years: Geochemical evidence, *Science*, 218, 784-787.
- Ref. 66:** Duplessy, J. C., and Shackleton, N. J., 1985. Response of global deep-water circulation to earth's climatic change 135,000-107,000 years ago, *Nature*, 316, 500-507.

- Ref. 67:** Wang, Z., and Mysak, L. A., 2001. Ice sheet-thermohaline circulation interactions in a climate model of intermediate complexity, *Journ. Oceanog.*, 57(4), 481–494.
- Ref. 68:** Jansen, E., and Veum, T., 1990. Evidence for two step deglaciation and its impact on North Atlantic deep water circulation, *Nature*, 343, 612–626.
- Ref. 69:** Charles, C. D., and Fairbanks, R. G., 1992. Evidence from Southern Ocean sediments for the effect of North Atlantic deep-water flux on climate, *Nature*, 355.
- Ref. 70:** Keigwin, L. D., and Lehman, S. J., 1994. Deep circulation change linked to Heinrich event 1 and Younger Dryas in a middepth North Atlantic core, *Paleoceanography*, 9, 185–194.
- Ref. 71:** Sarnthein, M., Jansen, E., Weinelt, M., Duplessy, J.-C., Labeyrie, L., Erlenkeuser, H. and Ganssen, G., 1994. Changes in east Atlantic deep-water circulation over the last 30,000 years: Eight time slice reconstructions, *Paleoceanography*, 9, 209–267.
- Ref. 72:** Zahn, R., Schönfeld, J., Kudrass, H.-R., Park, M.-H., Erlenkeuser, J., and Grootes, P., 1997. Thermohaline instability in the North Atlantic during meltwater events: Stable isotope and ice-rafted detritus records from core S075-26KL, Portuguese margin, *Paleoceanography*, 12(5), 696–710.
- Ref. 73:** Vidal, L., Schneider R. R., Marchal, O., Bickert, T., Stocker, T., and Wefer, G., 1999. Link between the North and South Atlantic during the Heinrich events of the last glacial period, *Clim. Dyn.*, 15, 909–919.
- Ref. 74:** Stuiver, M., Grootes, P. M., and Berziunas, T. F., 1995. The GISP2 delta O-18 climate record of the past 16,500 years and the role of the sun, ocean, and volcanoes, *Quat. Res.*, 44(3), 341–354.
- Ref. 75:** Maslin, M. A., and Shackleton, N. J., 1995. Surface water temperature, salinity, and density changes in the northeast Atlantic during the last 45,000 years: Heinrich events, deep water formation, and climatic rebounds, *Paleoceanography*, 10(3), 527–544.
- Ref. 76:** Vidal, L., Labeyrie, L., Cortijo, E., Arnold, M., Duplessy, J. C., Michel, E., Becqué, S., and van Weering, T. C. E., 1997. Evidence for changes in the North Atlantic Deep Water linked to meltwater surges during the Heinrich events, *Earth. Planet. Sci. Lett.*, 146, 13–27.
- Ref. 77:** Thompson, L., Mosley-Thompson, E., Davis, M., Lin, P.-N., Henderson, K., Cole-Dai, J., Bolzan, J., and Liu, K.-B., 1995. Late glacial stage and Holocene tropical ice core records from Huscarán, Peru, *Science*, 269, 46–50.
- Ref. 78:** Thompson, L., et al., 1998. A 25,000 year tropical climate history from Bolivian ice cores, *Science*, 282, 1858–1864.
- Ref. 79:** Baker, P. A., Rigsby, C. A., Seltzer, G. O., Fritz, S. C., Lowenstein, T. K., Bacher, N. P., and Veliz, C., 2001. Tropical climate changes at millennial and orbital timescales on the Bolivian Altiplano, *Nature*, 409, 698–701.
- Ref. 80:** Haggdorn, M. K. M., Ice Sheet Modelling, PhD Thesis, University of Edinburgh, In preparation.

- Ref. 81:** Guilderson, T.P., Fairbanks, R.G., Rubenstone, J.L., 2001. Tropical Atlantic coral oxygen isotopes: glacial-interglacial sea surface temperatures and climate change, *Marine Geology*, 172, 75-89.
- Ref. 82:** Chappel, J., Omura, A., Esat, T., McCulloch, M., Pandolfi, J., Ota, Y., Pillans, B., 1996. Reconciliation of late Quaternary sea levels derived from coral terraces at Huon Peninsula with deep sea oxygen isotope records, *Earth and Planetary science letters*, 141, 227-236.
- Ref. 83:** Ota, Y, Chappell, J, 1999. Holocene sea-level rise and coral reef growth on a tectonically rising coast, Huon Peninsula, Papua New Guinea, *Quat. Int.*, 55, 51-59.
- Ref. 84:** Yokoyama, Y, Esat, TM, Lambeck, K, 2001. Last glacial sea-level change deduced from uplifted coral terraces of Huon Peninsula, Papua New Guinea, *Quat. Int.*, 83-5, 275-283.
- Ref. 85:** BIOCLIM Report D8b (2003b) Development of the statistical/physical downscaling methodology and application to climate model CLIMBER for BIOCLIM Workpackage 3. Available on www.andra.fr/bioclim
- Ref. 86:** Rahmstorf, S. and Ganopolski, A., 1999. Long-term global warming scenarios computed with an efficient coupled climate model, *Climatic Change*, 43, 353-367.
- Ref. 87:** Hays, J.D., Imbrie, J., and Shackleton, N.J., 1976. Variations in the earth's orbit: pacemakers of the ice ages: *Science*, 194, 1121-1132.
- Ref. 88:** Paillard, D., 2001. Glacial cycles: Toward a new paradigm: *Reviews of Geophysics*, v. 39, p. 325-346.
- Ref. 89:** Keeling, R.F., and Stephens, B.B., 2001. Antarctic sea ice and the control of Pleistocene climate instability, *Paleoceanography*, 16, p. 112-131.
- Ref. 90:** Adkins, J.F., McIntyre, K., and Schrag, D.P., 2002. The salinity, temperature and $\delta^{18}O$ of the glacial deep ocean: *Science*, 298, 1769-1773.
- Ref. 91:** Archer, D., Kheshgi, H., and Maier-Raimer, E., 1997. Multiple timescales for neutralization of fossil fuel CO_2 : *Geophysical Research Letters*, 24, 405-408.
- Ref. 92:** Bassinot, F.C., Labeyrie, L.D., Vincent, E., Quidelleur, X., Shackleton, N.J., and Lancelot, Y., 1994. The astronomical theory of climate and the age of the Brunhes-Matuyama magnetic reversal, *Earth and Planetary Science Letters*, 126, 91-108.
- Ref. 93:** Tiedemann, R., Sarnthein, M., and Shackleton, N.J., 1994. Astronomic timescale for the Pliocene Atlantic $\delta^{18}O$ and dust records of Ocean Drilling Program site 659, *Paleoceanography*, 9, 619-638.
- Ref. 94:** Shackleton, N.J., Berger, A., and Peltier, W.R., 1990. An alternative astronomical calibration of the lower Pleistocene timescale based on ODP site 677, *Trans. R. Soc Edinburgh Earth Sci.*, 81, 251-261.



8. Appendix 1

Several variables have been archived on a monthly mean basis (MoBidiC) and are available on www.andra.fr/bioclim :

Temperature over Eurasia (i.e. continent (snow free and snow covered)), for the zonal belts 30-40N, 40-50N, 50-60N (CLIMBER) or for 5° latitudinal belts from 30N to 60N for MoBidiC.

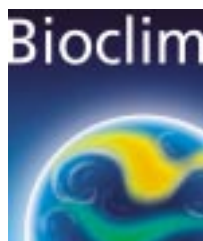
Total precipitation over Eurasia, for the zonal belts 30-40N, 40-50N, 50-60N or for 5° latitudinal belts from 30N to 60N for MoBidiC.

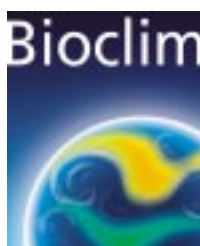
Total evaporation over Eurasia, for the zonal belts 30-40N, 40-50N, 50-60N or for 5° latitudinal belts from 30N to 60N for MoBidiC.

Snowfall over Eurasia, for the zonal belts 30-40N, 40-50N, 50-60N or for 5° latitudinal belts from 30N to 60N for MoBidiC.

Snow fraction over Eurasia (continent free of ice), for the zonal belts 30-40N, 40-50N, 50-60N or for 5° latitudinal belts from 30N to 60N for MoBidiC.

Each variable is stored in an ASCII file. Values are provided as 500-year averages, every 500 years.





For further information contact:

BIOCLIM project co-ordinator, **Delphine Texier**

ANDRA, DS/MG (Direction Scientifique - Service Milieu Géologique)

Parc de la Croix Blanche - 1/7, rue Jean-Monnet - 92298 Châtenay-Malabry Cedex - FRANCE

Tél.: +33 1 46 11 83 10

e-mail: delphine.texier@andra.fr

web site: www.andra.fr/bioclim/